COMPRESSIVE AND FLEXURAL PERFORMANCE OF MASONRY STRENGTHENED WITH ECO-FRIENDLY DUCTILE CEMENTITIOUS COMPOSITES (EDCC)

by

Matthew Erin Lynch

A Thesis submitted to the Faculty of Graduate Studies of

The University of Manitoba

in partial fulfilment of the requirements of the degree of

MASTER OF SCIENCE

Department of Civil Engineering

University of Manitoba

Winnipeg

This page intentionally left blank

Abstract

The behaviour of masonry prisms and beams strengthened with eco-friendly ductile cementitious composite (EDCC), which is a form of engineered cementitious composite (ECC), was investigated in this thesis. Compression and out-of-plane bending tests were performed to measure compressive resistance, modulus of elasticity, and flexural capacity. It was concluded that the compressive resistance of strengthened masonry prisms remained similar in load, while ultimate stress decreased due to the increased cross-sectional area. In out-of-plane bending, the strengthened concrete masonry unit (CMU) beams showed a strength increase from 11 to 26 times and the strengthened brick showed an increase from 4 to 8 times versus the beams plain counterparts. The linear strength increase was dependent on EDCC thickness, although doubling the EDCC thickness did not double the strength. Overall, masonry strengthened with EDCC is a viable alternative to ECC strengthening due to the performance and reduction in cement content.

This page intentionally left blank

Thank you to the support of my mother Leslie and father Gary. I will be forever grateful for the love and support I have always received. You have taught me how to be strong in both the good times and the bad times. I will always strive to make you as proud as you make me.

Thanks to Saeed Gerami and David Amorim for all the help in the lab and keeping the office fun; and a big thanks to Sarah Stevenson for supporting me through the various aspects of my degree.

Thank you.

This page intentionally left blank

Acknowledgements

Thank you to my advisor Dr. Aftab Mufti and my co-advisor Dr. Dagmar Svecova for their continued support and guidance; and to Dr. Basheer AlGohi for advising me on the finite element method, for always making time for me, and for showing excitement in my work. Thanks to the staff of the W.R. McQuade structures lab for helping me with all aspects of my project and giving me the chance for hands on learning. I look back on my time in the lab fondly.

I would like to acknowledge the financial support of NSERC, the John Glanville Memorial Scholarship, and the Antenbring Graduate Scholarship in Engineering.

Thank you to NSERC for providing the NSERC CRD grant, which allowed for me to be involved in a collaborative project with Professor Nemkumar Banthia and his team at the University of British Columbia, Professor Nigel Shrive and his team at the University of Calgary, and Professor Aftab Mufti and his team at the University of Manitoba, as well as the industry collaboration with Brxton.

This page intentionally left blank

Front Matter

Contents

1 Introduction 1

1.1 Background 1

1.2 Research Objectives 4

1.3 Scope of Work 5

1.4 Structure of Thesis 7

2 Literature Review 8

2.1 What Are Eco-friendly Ductile Cementitious Composites? 8

2.2 Parameters of Ternary Binder Concrete 8

2.3 Parameters of Fiber Reinforced Concrete 10

2.4 Parameters of ECC 12

2.4.1 Mix Proportions 14

2.4.2 Workability 15

2.4.3 Permeability 15

2.4.4 Cohesion 16

2.4.5 Cracking 16

2.4.6 Strength 17

2.4.7 Placement 18

2.4.8 Air Content 18

2.4.9 Heat of Hydration 19

2.4.10 Setting Time 19

2.4.11 Shrinkage 19

2.4.12 Curing 20

2.4.13 Durability 21

2.5 Applications of ECC 21

2.5.1 Spalling Prevention of Concrete 21

2.5.2 Flexural Applications 22

2.5.3 Earthquake Applications 23

2.5.4 Masonry Strengthening Applications 23

2.6 Review of Materials and Properties 24

2.6.1 Brick Properties 24
2.6.2 Concrete Block Properties 25
2.6.3 Mortar Properties 25
2.6.4 Prism Properties 26
2.6.5 Modulus of Elasticity and Modulus of Rupture 29
2.6.6 Retrofit Material / Strengthened Masonry 30
2.6.7 Prisms Retrofitted with ECC 31
2.6.8 Beams Retrofitted with ECC 33
3 Experimental Program 38
3.1 Test Specimens 38
3.2 Construction of Specimens 39
3.3 Test Setup, Instrumentation, and Test Procedures 48
3.3.1 Plain and Strengthened Masonry Prisms in Axial Compression 48
3.3.2 Individual CMUs and Bricks in Axial Compression 52
3.3.3 Mortar Cubes in Axial Compression 54
3.3.4 EDCC Cylinders in Axial Compression 54
3.3.5 Plain and Strengthened Masonry Beams in Four-Point Bending 56
3.3.6 EDCC Cylinders in Split Tension 62
3.3.7 EDCC Beams in Four-Point Bending 62
3.3.8 EDCC Ultrasonic Modulus of Elasticity Measurements 64
4 Experimental Results 67
4.1 Compression Test 67
4.1.1 Practice Compression Test 67
4.1.2 Compression Tests on Plain and Strengthened Specimens 68
4.2 Flexure Test 85
4.3 Materials Testing 96
4.3.1 Mortar Cubes 96
4.3.2 EDCC Prisms 97
4.3.3 Bricks 100
4.3.4 Concrete Blocks 101
4.3.5 Sand 102
4.3.6 EDCC Cylinders 103

5 Finite Element Modelling 108
6 Data Analysis / Discussion 109
6.1 Compression Test Analysis 109
6.2 Flexural Test Analysis 110
7 Conclusion and Recommendation 112
References 115
Appendix A: Theoretical Analysis of Flexural Specimen 118
Appendix B: Finite Element Modelling of Flexural Tests 123

List of Tables

Table 2-1: Typical plain concrete and FRC mix adapted from (Carnovale, 2013) 12
Table 2-2: Mix design comparison between plain concrete and ECC (Wang & Li, 2007) 14
Table 2-3: Kim et al mix design* 15
Table 2-4: Strength properties of polyethylene (PE) fiber ECC and polyvinyl alcohol (PVA) fiber ECC (Li, Fukuyama, & Mikame, 1998) 17
Table 2-5: Mix design for sprayable ECC (Kanda, Saito, Sakata, & Hiraishi, 2003) 22
Table 2-6: Compressive strength of mortar used for prisms (Kyriakides, 2011) 32
Table 2-7: Compression strength and elastic modulus of ECC used for prisms (Kyriakides, 2011) 32
Table 2-8: Average compressive strength and elastic modulus of masonry prisms (Kyriakides, 2011) 32
Table 2-9: Compression strength of mortar used for beams (Kyriakides, 2011) 34
Table 2-10: Compression strength and elastic modulus of ECC used for beams (Kyriakides, 2011) 34
Table 3-1: Specimen construction 44
Table 3-2: EDCC mix design* 46
Table 3-3: Kuralon RECS15 8mm fiber properties (Kuraray Co Ltd, 2017) 47
Table 3-4: Recron 3S 6mm PET fiber properties (Yan, 2016) 47
Table 4-1: Compression test results 79
Table 4-2: Compression test modulus of elasticity results 81
Table 4-3: Flexural test results and theoretical loads 89
Table 4-4: Flexural specimen relative load ratios 90
Table 4-5: Mortar cube strength properties 97
Table 4-6: EDCC prism test results 99
Table 4-7: EDCC cylinder compressive strength results 105
Table 4-8: Instrumented EDCC cylinder results 106
Table 4-9: EDCC splitting tension cylinder results 106

List of Figures

Figure 2-1: Four-point bending test from ASTM E518/E518M – 10 (ASTM International, 2010) 34
Figure 3-1: Mixing mortar for masonry prism and beam construction 39
Figure 3-2: Fresh mortar on board 40
Figure 3-3: Construction of masonry prisms and beams by masons 40
Figure 3-4: Offset of formwork for EDCC overlay 41
Figure 3-5: Mixer used for EDCC mixing 42
Figure 3-6: Mixer information plaque 42
Figure 3-7: Adding HRWRA to the mixing bowl 43
Figure 3-8: EDCC in mixing bowl 43
Figure 3-9: EDCC application 43
Figure 3-10: Practice concrete block prism compression test 49
Figure 3-11: Strengthened masonry specimen in compression load frame 51
Figure 3-12: Individual brick in compression test machine 53
Figure 3-13: Example of brick instrumentation output 53
Figure 3-14: Mortar cube compression test in Instron 300DX Universal Testing Machine 54
Figure 3-15: EDCC cylinder mounted in Cylinder Machine 55
Figure 3-16: EDCC cylinder mounted in Instron 300DX machine 55
Figure 3-17: EDCC cylinder tested using an actuator and DAQ 56
Figure 3-18: Practice unstrengthened brick flexural test setup 57
Figure 3-19: Practice strengthened CMU flexural test setup 57
Figure 3-20 Practice strengthened CMU flexural test instrumentation 57
Figure 3-21: Practice strengthened CMU flexural test 58
Figure 3-22: CBU flexural test setup 59
Figure 3-23: BBU flexural test setup 59
Figure 3-24: Schematic view of flexural test setup 61
Figure 3-25: EDCC cylinder mounted in split tension cylinder configuration 62
Figure 3-26: EDCC beam and instrumentation in four-point bending test apparatus 63
Figure 3-27: EDCC beam in four-point bending test apparatus 64
Figure 3-28: Proceq equipment in case 65
Figure 3-29: Proceq Pundit Lab front view 65

Figure 3-30: Proceq tranducer 65
Figure 3-31: EDCC Cylinder in test setup for ultrasonic modulus of elasticity measurement 66
Figure 3-32: EDCC Cylinder being tested for ultrasonic modulus of elasticity measurement 66
Figure 4-1: Practice compression test specimen before test 67
Figure 4-2: Practice compression test specimen after test 68
Figure 4-3: Schematic drawing of compression test 69
Figure 4-4: Schematic plan view of compression test instrumentation 70
Figure 4-5: BPS10 in compression testing configuration 70
Figure 4-6: CPS10-6 strain gauge instrumentation 71
Figure 4-7: CPS30-7 LVDT instrumentation 71
Figure 4-8: CPU-4 stress-strain plot 73
Figure 4-9: CPS10-1 stress strain plot 73
Figure 4-10: CPS10-6 stress-strain plot 74
Figure 4-11: CPS20-5 stress-strain plot 74
Figure 4-12: CPS30-1 stress-strain plot 75
Figure 4-13: BPU-4 stress-strain plot 75
Figure 4-14: BPS10-1 stress-strain plot 76
Figure 4-15: BPS20-2 stress-strain plot 76
Figure 4-16: BPS30-5 stress-strain plot 77
Figure 4-17: Typical delamination of EDCC from brick prism 78
Figure 4-18: Ultimate load compression test results 80
Figure 4-19: Ultimate stress compression test results 80
Figure 4-20: CPS30-8 stress-strain plot 82
Figure 4-21: CPS30-8 stress-displacement plot 82
Figure 4-22: CPS30-7 in compression test setup 83
Figure 4-23: CPS30-7 stress-strain plot 84
Figure 4-24: CPS30-7 stress-displacement plot 84
Figure 4-25: CPS30-7 after testing 85
Figure 4-26: Strengthened brick beam in test setup 88
Figure 4-27: Example of brick beam failure at mortar joint and EDCC 88
Figure 4-28: Flexural test results and theoretical loads 89
Figure 4-29: EDCC thickness vs strength ratio of strengthened masonry beams 91

Figure 4-30: CBS10 load-deflection plots 93
Figure 4-31: CBS20 load-deflection plots 93
Figure 4-32: CBS30 load-deflection plots 94
Figure 4-33: BBS10 load-deflection plots 94
Figure 4-34: BBS20 load-deflection plots 95
Figure 4-35: BBS30 load-deflection plots 95
Figure 4-36: Mortar cube with steel cap plate 96
Figure 4-37: Mortar cube in test setup 97
Figure 4-38: EDCC prism in test setup 98
Figure 4-39: EDCC prism instrumentation 98
Figure 4-40: EDCC prism load-deflection plot (all samples) 99
Figure 4-41: Direct tension dog-bone test on EDCC at University of British Columbia (Soleimani-Dashtaki, Soleimani, Wang, Banthia, & Ventura, 2017) 100
Figure 4-42: Saw cut brick in test setup 101
Figure 4-43: Failed brick specimen 101
Figure 4-44: Failed CMU specimen 102
Figure 4-45: EDCC sand sieve gradation analysis 103
Figure 4-46: EDCC cylinder in typical compression setup 104
Figure 4-47: EDCC cylinder instrumented with strain gauges in large test setup 104
Figure 4-48: EDCC cylinder instrumented with dial gauges 105
Figure 4-49: EDCC split cylinder test 105
Figure 4-50: EDCC cylinder 1 stress-strain plot 106
Figure 4-51: EDCC cylinder 2 stress-strain plot 107
Figure 4-52: EDCC cylinder 3 stress-strain plot 107
Figure 6-1: EDCC thickness vs strength ratio of strengthened masonry beams 110
Figure 6-2: CMU load-deflection plot 111
Figure 6-3: Brick load-deflection plot 111
Figure A-1: Free body diagram, shear diagram, and bending moment diagram 118
Figure A-2: Cross section of beam at mid-height in the maximum moment region 118
Figure B-1: Idealization of finite element model 124
Figure B-2: BBS10 load-deflection plots with FEM results 125
Figure B-3: BBS20 load-deflection plots with FEM results 125

Figure B-4: BBS30 load-deflection plots with FEM results 126
Figure B-5: CBS10 load-deflection plots with FEM results 126
Figure B-6: CBS20 load-deflection plots with FEM results 127
Figure B-7: CBS30 load-deflection plots with FEM results 127

1 Introduction

1.1 Background

Brick masonry has been a common structural building material for centuries. Many older structures were designed using empirical equations that were based on construction practices. These buildings have stood the test of time with respect to gravity loads, but may be susceptible to lateral loads stemming from strong winds and earthquakes (Franklin, Lynch, & Abrams, 2001). This is due to unreinforced masonry having a lower tensile strength than compressive strength (Canadian Standards Association, 2004). Many cities are taking a proactive approach to retrofitting their masonry structures to resist the impending strong wind or seismic events. Specifically, in British Columbia the government has committed funding to "seismically upgrade or replace 213 high-risk schools" (Province of British Columbia, 2013). Many innovative strengthening techniques exist, such as fiber reinforced polymer exterior application, exterior shotcrete with exterior steel reinforcement, and interior coring with steel reinforcement and grouting, to name a few (Franklin, Lynch, & Abrams, 2001). These applications can be applied prior to wall damage or as a rehabilitation technique for post damaged walls. The goal of this thesis is to determine the modulus of elasticity, compressive strength, and flexural strength of brick and concrete block masonry that has been strengthened with eco-friendly ductile cementitious composite (EDCC) developed at the University of British Columbia. Theoretical calculations, finite element models, and laboratory tests will be utilized to determine the effect that strengthening material has on masonry prisms and beams composed of bricks and concrete blocks.

This project is a part of the Natural Sciences and Engineering Research Council (NSERC) Collaborative Research and Development (CRD) grant entitled "Development of Sustainable Masonry Rehabilitation Technology (SMART) using Eco-Friendly Ductile Cementitious Composites (EDCC)", which involved collaboration between the University of Manitoba, University of Calgary, and University of British Colombia. The University of British Columbia and the University of Calgary each have a variety of researchers participating in the NSERC CRD to research various durability, strength, and material properties of EDCC and masonry, among other things. The research at the University of Calgary is being coordinated by Dr. Nigel Shrive, the research at the University of Manitoba is being coordinated by Dr. Aftab Mufti, and the research at the University of British Columbia is being coordinated by Dr. Nemkumar Banthia, who is the innovator of EDCC.

The need for this project, and the other projects being conducted as part of the NSERC CRD, stems from the behaviour of unreinforced masonry walls in lateral loading situations, such as earthquakes and wind events. While the wall may have high axial load carrying capacity, it is likely that there is insufficient lateral strength to carry the required load, resulting in failure. The walls can be subjected to two different forms of horizontal loading, in-plane and out-of-plane.

In-plane loading can induce three different types of failures in the wall, being flexural, diagonal cracking, and sliding shear. Flexural failure consists of failure at the base of the wall, including toe crushing in the compression region and tension failure between the masonry and the mortar bed joint. Diagonal cracking consists of a diagonal compressive strut forming in the wall which leads to tensile failure along that strut due to the Poisson's

ratio effect. Sliding shear consists of a horizontal crack forming between the masonry and the mortar bed joints, first from debonding between the masonry and the mortar and then the masonry overcoming frictional forces with the mortar bed joint.

Out-of-plane failures consist of the tensile resistance between the mortar and masonry being overcome due to out-of-plane loading. The stresses occur from Equation 1, where f_t is the tensile stress (MPa), P is the axial compressive force (N), A is the cross-sectional area (mm^2), M is the bending moment (N-mm), and S is the section modulus (mm^3):

$$f_t = -\frac{P}{A} + \frac{M}{S} \qquad [1]$$

which indicates that an applied out-of-plane moment on the wall will induce tension in the wall based on the magnitude of the moment and the section modulus of the wall. Axial load without any eccentricity will induce compression across the entire cross section of the wall, counteracting the tension that will be induced from the horizontal load. If the axial load is applied to the wall with eccentricity, it could induce additional tension in the wall resulting in earlier failure. The axial loads in walls may be low, which would result in the first term of Equation 1 being negligible and therefore omitted and the wall behaving like a beam. The typical specified bond strength between masonry and mortar ranges from 0.2 to 1.3 MPa (Canadian Standards Association, 2004), depending on the type of masonry unit, the mortar type, and the direction of loading relative to the mortar bed joint. A simply supported 1 m tall modular brick column in stack bond would fail under a horizontal point load of 538 N applied in the middle, neglecting any axial load on the column. In this research program, masonry columns will be utilized as opposed to constructing full wall

segments to allow for more specimens to be tested. Similar theory should apply between the failure modes exhibited by walls and columns.

As per 2010 National Building Code of Canada Volume 2 Division B sentence 4.1.8.3.(5), for seismic loading the walls that are perpendicular to the direction of lateral loading must be able to carry their axial loads while undergoing displacements induced in them due to diaphragm displacements (Canadian Commision on Building and Fire Codes, National Research Council of Canada, 2010). This displacement would induce load into the wall as a function of the stiffness of the wall. The collapse of out-of-plane loaded walls is possible due to their relatively low strength since the walls may not be confined in the out-of-plane direction. Out-of-plane strengthening or confinement is helpful in preventing these collapses. In-plane failures may not result in collapse like out-of-plane failures. Both in-plane and out-of-plane failures will be brittle in nature, and therefore will not have high energy dissipation capabilities. A structures primary means of resisting earthquake is through energy dissipation. One of the components of energy dissipation is plastic straining. Masonry will crack under lateral load but will not exhibit continual straining under any additional load. By introducing strengthening materials that will have plastic straining behaviour, it is possible to absorb and dissipate energy put into the structure.

1.2 Research Objectives

This thesis looks to outline the following:

1) Determine the modulus of elasticity and axial capacity of unstrengthened and strengthened brick and concrete block masonry prisms through experimental testing.

2) Determine the flexural capacity of unstrengthened and strengthened brick and concrete block masonry prisms through theoretical calculations, finite element modelling by others, and experimental testing.
3) The effect of the thickness of strengthening material on the compressive and flexural strength of the masonry specimens.

The following questions will be answered:

1) How does the capacity and behaviour of the brick and concrete block masonry specimens change due to the application of the strengthening material.
2) How do the different methods of determining flexural strength compare to the test results.
3) Can the individual material properties of brick, concrete block, strengthening material and mortar be translated into a composite specimen through finite element modelling.
4) What further research is required to better quantify the applicability of the strengthening material for masonry applications.

1.3 Scope of Work

The scope of work consisted of first fabricating brick and concrete block prisms and beams by experienced masons and allowing them to cure. Mortar cube specimens were prepared at this time as well to quantify their strength at a later date. The test procedures were prepared as well using practice specimens prepared at an earlier date by the researcher to quantify the suitability of the test apparatus and instrumentation output. First, the compression test setup was evaluated. Testing then began for the specimens that had

adequately cured that didn't require strengthening. While this was ongoing the EDCC mix procedure was coordinated with the researchers at the University of British Columbia and the University of Calgary who were involved in the NSERC CRD. Once the mix procedure was deemed adequate, strengthening of the masonry prisms and beams took place. Once the EDCC reached maturity the specimens were tested. EDCC cylinders and beams were also cast to quantify the EDCC material properties.

The flexural test setup was constructed next. It was reported by other researchers that performing tests where the masonry beams were mounted horizontally and load was applied vertically caused the masonry beams to fail prior to loading under their own self weight. It was for this reason that a modified approach was taken to the test apparatus. Horizontal load and reaction frames were constructed and supports were welded into place. The actuator was horizontally mounted to the load frame and was equipped with chains and turn buckles to ensure that the load was applied horizontally. This allowed for the specimens to be lifted into the test frame and any self weight would be experienced as a negligible axial load instead of out-of-plane bending. Given that the axial capacity of masonry beams is much higher than their out-of-plane capacity this was deemed a more appropriate test configuration as premature failure would not occur. The axial load imparted on the specimen due to self weight would have a negligible impact on the flexural performance. Testing of the flexural masonry specimens that were unstrengthened and strengthened then took place.

While the testing was ongoing, individual material properties were quantified through testing clay bricks and concrete blocks in compression, testing EDCC cylinders in compression and splitting tension, and testing EDCC beams in four-point bending.

Additional tests performed consisted of taking ultrasonic modulus of elasticity measurements of EDCC cylinders, weighing EDCC cylinders and performing compression tests and weighing mortar cubes. Through these supplemental tests it was possible to quantify individual material properties to be utilized in hand calculations and finite element modelling. After all the testing was completed photos were taken of the failed specimens and they were disposed of.

Finite element modelling was performed in ABAQUS by Dr. Basheer AlGohi, who is a colleague in the research group at the University of Manitoba, utilizing experimental material properties. The outputs from the finite element models were compared against the experimental results to determine their adequacy. Once these tasks were completed the work was compiled and conclusions were drawn, and further research was identified to determine the applicability of EDCC strengthening for masonry, and other potential areas of EDCC applicability.

1.4 Structure of Thesis

This thesis is structured into seven chapters: Chapter One discusses the introduction, including the background, research objectives and scope of work; Chapter Two discusses literature review on the materials and applications; Chapter Three describes the experimental program, including the test specimens and test setups; Chapter Four describes the experimental results; Chapter Five briefly discusses the finite element modelling component of the research; Chapter Six includes data analysis and discussion on the test results; and Chapter Seven consists of conclusions and recommendations based on the results of the research program.

2 Literature Review

2.1 What Are Eco-friendly Ductile Cementitious Composites?

Concrete is composed of cement, water, and aggregate. Within the concrete field improvements have been made in the constituent materials or mixture proportions to better suit certain applications. Eco-friendly ductile cementitious composites (EDCCs) are a combination of two concrete technologies. The eco-friendly component consists of replacing a certain percentage of the cement binder with supplementary cementitious materials such as fly ash or slag. The focus of this thesis will be on fly ash as a cement replacement. The ductility component stems from the use of fibers. Assuming a consistent distribution of randomly oriented fibers in the matrix, as cracks in the matrix begin forming the fibers will become engaged in tension. At this point, a combination of frictional forces between the fiber and the matrix as well as the tensile capacity of the fiber will begin carrying tensile load. The result of this is concrete that exhibits relatively large strains, ranging from 3 to 5%, and micro cracking, typically 100 μm in crack width (Wang & Li, 2007). The composite material is referred to as an engineered cementitious composite (ECC) as it is going beyond the traditional concrete constituents. Using supplementary cementitious materials, fibers, chemical admixtures and a finely tuned mix design it is possible to create a material that surpasses conventional concrete and traditional fiber reinforced concrete with regards to certain applications that will be outlined later.

2.2 Parameters of Ternary Binder Concrete

The effect of replacing the Portland cement component of concrete with supplementary cementitious materials can have positive effects on the plastic, hardened and environmental properties of concrete. In the plastic (fresh) state of concrete, by using fly ash as a cement

replacement the workability of the concrete is improved. This can be attributed to the spherical shape of the fly ash particles, causing them to act like ball-bearings and slide over one another. Fly ash has a lower density than that of cement, so if cement is replaced with an equivalent weight of fly ash it will result in a higher binder volume resulting in more cohesion within the mix. This can be beneficial to prevent segregation within the fresh concrete. Given an improved workability, the spraying or pumping process of concrete containing fly ash is improved over regular Portland cement concrete (National Concrete Pavement Technology Center, 2014). Consolidation of concrete containing fly ash is also improved due to the increased workability. Silica fume, on the other hand, is very cohesive which results in decreased workability. Due to this cohesiveness segregation is reduced. Silica fume reacts with cement hydration products very quickly resulting in increased heat of hydration, which results in a faster setting time. Due to the fine nature of silica fume, particle packing takes place which prevents water from bleeding out of the mix. Due to the faster setting time, increased heat of hydration, and particle packing, concrete with silica fume is very susceptible to plastic shrinkage cracks. Therefore, it is necessary to provide a strict curing regiment to the surface of the concrete to prevent these cracks.

With respect to the hardened ternary binder concrete, fly ash will reduce the early age strength and increase the later age strength due to its slow reacting pozzolanic nature. Silica fume, on the other hand, has a very rapid pozzolanic reaction meaning it provides an increase in early and later age strength (National Concrete Pavement Technology Center, 2014). One of the reasons for the increase in strength is the pozzolanic reaction with calcium hydroxide present in the interfacial transition zone (ITZ), which is where micro-cracks form and propagate upon loading. Through the pozzolanic reactions the ITZ is

strengthened which helps reduce the negative impact of the ITZ. Due to the improved strength and particle packing action, which prevents capillary pores and improves the mortar matrix at the micro level, ternary binder concrete is less permeable which is beneficial. Fly ash has been known to inhibit air entrainment, so for this reason special care should be taken when using fly ash in a concrete application subjected to freeze thaw cycles. Ultimately, the replacement of cement with fly ash and the addition of silica fume provides an improved concrete product in the fresh and hardened state and reduces the environmental impact associated with the production of cement.

Typical percentages of binders reported by (National Concrete Pavement Technology Center, 2014) show that the cement content for ternary binder concrete should "be above 40%, silica fume content should be less than 10%, Class F fly ash content should be less than 30% and Class C fly ash content should be less than 40%". These percentages are based on research and practice for typical everyday applications.

2.3 Parameters of Fiber Reinforced Concrete

Fiber reinforced concrete is concrete with the addition of steel, glass, synthetic, or natural fibers, to name a few, dispersed in the mortar matrix. The purpose of the fibers is to provide additional tensile capacity and improve other mechanical and serviceability properties that will be discussed. The two main components that provide additional resistance is the fibers bond to the mortar matrix and the tensile capacity of the fiber itself. Once a crack forms in the concrete, the fiber will bridge the tensile stress between the cracked concrete. At this point, a combination of chemical and mechanical bonds holds the fiber within the mortar matrix, causing the crack width to grow at a restrained rate. If the bond between the fiber and mortar is overcome, the fiber will pull out of the mortar matrix, causing the crack width

to grow. If the bond between the mortar matrix and fiber is strong, the fiber may fail in tension within the crack opening. To create a ductile behavior, it is important to have a gradual pull out of the fiber (Li & Wang, 2007). Another advantage of fibers is their potentially random dispersion in concrete mixtures, given that the fibers must span across to the crack direction to provide tensile resistance. This provides capacity to the concrete member given any crack orientation. The tensile behavior of fiber reinforced concrete (FRC) is strain softening, in which the first crack load will be reached, and a subsequent drop in stress will occur as the specimen strains to failure. The amount of strain that occurs is much higher than that of plain concrete and is a function of the type of fibers used and the bond between the fibers and mortar. Fiber reinforced concrete may contain coarse aggregate, unlike ECC. This is because FRC is not as reliant on the micro mechanical response of the element compared to ECC.

One of the disadvantages of fiber reinforced concrete is that it may require a large percentage of fibers. Given that fibers present another source of cost and environmental impact in their production this may be detrimental to the economic and environmental performance of the concrete. Other properties of the concrete may also be impacted, such as workability which can impede placement.

A typical mix design for plain concrete (PC), as well as FRC using steel (SFRC) and synthetic fibers (PPFRC) can be seen in Table 2-1. A direct tension test was performed on both plain concrete and synthetic FRC. The plain concrete remained linear until approximately 75% of its ultimate tensile capacity, at which point it began to soften until sudden failure. The measured stress at ultimate was approximately 4.2 MPa and the measured strain at ultimate was approximately 0.00014. The synthetic FRC exhibited

similar behaviour up to ultimate stress. The difference is in the post crack response, where the synthetic FRC exhibits a tension softening behaviour. The stress drops significantly (to approximately 1.6 MPa) and the crack width continues to grow. The stress then rises to 2.4 MPa and then proceeds to fall until a crack width up to 12mm is reported at a stress of 0.4 MPa (Carnovale, 2013).

Table 2-1: Typical plain concrete and FRC mix adapted from (Carnovale, 2013)

Material	Unit	PC	SFRC	PPFRC
GU Cement	(kg)	375	500	500
Water	(kg)	139	200	200
Sand	(kg)	847	1114	1114
10mm Limestone Coarse Aggregate	(kg)	1080	792	792
HRWRA (Glenium® 7700)	(mL)	3300	3670	4000
Steel Fibers	(kg)	-	78.5	-
Macro-Synthetic Fibers	(kg)	-	-	18.2

2.4 Parameters of ECC

By combining fiber reinforced concrete with cement replacement materials that are more environmentally friendly and fine tuning the mix proportions an innovative material that poses reduced environmental impacts is created. Engineered cementitious composites exhibit a tensile strain hardening ductile behavior similar to metal, whereas regular concrete behaves like a brittle material and FRC strain softens. The ductile behavior of ECC means that in applications that require a large amount of energy absorption many benefits are posed, given that energy absorption is measured as toughness which is the area under the stress strain curve. Research into the micro and macro properties of ECC began in the early 1990s (Li & Kanda, Engineered Cementitious Composites for Structural

Applications, 1998). Studies have been conducted to determine the behavior of ECC on the macro and micro level, and given their positive results research is being done on applications and improvements and/or modifications that can be made. One area of focus is on making ECC more environmentally friendly. Given that ECC requires a large amount of cement relative to regular concrete, shown as 3 times the cement required for conventional concrete (Wang & Li, 2007), using supplementary cementitious materials as a cement replacement will help lessen the environmental impact of ECC. The principle of ECC design is to consider the mortar matrix toughness and the interface between the fiber and mortar matrix. Equations have been developed which are used to determine if ductile behavior will be exhibited by ECC. These equations are used to calculate J_{tip} and J'_b. J_{tip} is the fracture toughness of the mortar matrix, and J'_b is the complementary energy required for fiber pull out. J_{tip} represents the complementary amount of energy that is required to form cracks in the mortar matrix, and J'_b is the complementary energy to cause fiber failure. By calculating the J'_b / J_{tip} ratio it is possible to determine whether multiple cracks will occur or not, and whether the behavior of the composite system will be ductile (Wang & Li, 2007).

Using fly ash as a cement replacement for ECC was investigated by (Wang & Li, 2007) and was shown to provide a similar behavior to that of ECC with cement as the sole binder. It was reported that the tensile strain capacity ranged from 3 to 4% and the tensile strength was above 4.5 MPa. The study showed that fly ash lowered the J_{tip} value and increased J'_b, which yields a better strain hardening response. The study concluded that using fly ash as a cement replacement provides mechanical behavior similar to traditional ECC while being

more environmentally friendly with regards to greenhouse gas emissions of constituent materials.

2.4.1 Mix Proportions

To achieve the unique strain hardening characteristics of ECC, a finely tuned concrete mix is required. Regular concrete uses cement, water, coarse aggregate and fine aggregate. ECC relies on having a tough matrix, thus coarse aggregates cannot be included in the mix. Coarse aggregates typically have weak areas in their immediate vicinity, known as the ITZ. This area typically has a high content of calcium hydroxide, porosity and micro cracks. By removing coarse aggregates, it is necessary to provide additional cement to the mix. The increase in cement will also require an increase in water. Since an increase in water content means more capillary pores present in the matrix, it is necessary to limit the amount of additional water added. This can be achieved using a high range water reducing admixture (HRWRA). Table 2-2 shows three typical mix designs, that of conventional concrete, polyethylene fiber ECC (PE-ECC) and polyvinyl alcohol fiber ECC (PVA-ECC).

Table 2-2: Mix design comparison between plain concrete and ECC (Wang & Li, 2007)

	Cement (kg/m^3)	Aggregate (kg/m^3)	Water (kg/m^3)	HPMC (kg/m^3)	HRWRA (kg/m^3)	Fiber (kg/m^3)
Concrete	390	1717	166	-	-	-
PE - ECC	1205	603	314	0.6	12	17
PVA - ECC	832	832	366	1.26	17	26

Work conducted by (Li & Wang, 2007) used a constant water/binder ratio of 0.24 while varying the fly ash amount in the mix to determine if high volume fly ash replacement of cement is possible. (Kim, Kong, & Li, 2003) reported that given a lower volume of fly ash

(0.3 mass ratio of cement), with a sand/cement ratio of 0.8 and a water/cement ratio of 0.47, yielding a water/binder ratio of 0.36, was an optimal design, as seen in Table 2-3.

Table 2-3: Kim et al mix design*

Mixture	Cement	Water	Sand	Fly Ash	Hydroxypropyl-methylcellulose	HRWRA	Calcium Aluminate Cement	Fiber Volume Fraction
S-0	1	0.47	0.8	0.3	0.0005	0.02	0	0.015
S-1	0.95	0.47	0.8	0.3	0.0005	0.015	0.05	0.015
S-2	0.95	0.47	0.8	0.3	0.0005	0.015	0.05	0.02
S-3	0.95	0.46	0.8	0.3	0.0005	0.0075	0.05	0.02

*All numbers are mass ratios except for Fiber Volume Fraction (Kim, Kong, & Li, 2003)

2.4.2 Workability

Due to the low water/binder ratio used for ECC, chemical admixtures are often needed to improve workability. Using HRWRA the workability of ECC is greatly increased without sacrificing strength through the addition of water. With respect to supplementary cementing materials (SCMs), fly ash improves the workability of the mix due to the ball bearing effect, whereas silica fume reduces the workability due to its cohesiveness. To provide adequate mixing to disperse the fibers, while preventing segregation, it is important to control the quantity of previously mentioned constituent materials carefully when creating a mix design.

2.4.3 Permeability

The permeability of ECC is much lower than that of regular concrete for many reasons. The use of silica fume provides a more refined micro structure of the mortar matrix which limits the amount of harmful chemicals that can permeate into the ECC. Given that ECC relies on the formation of multiple micro-cracks the crack widths typically do not exceed 100 μm (Wang & Li, 2007), the permeation of harmful chemicals is less likely to occur through cracks.

2.4.4 Cohesion

Cohesion within the fresh ECC is present using viscosity enhancing admixtures and the use of SCMs. The use of fly ash and silica fume helps to improve the cohesion within the mix and prevent fiber segregation. Fly ash provides a higher volume of paste to coat the fibers which helps improve cohesion. Due to silica fumes fine particle size it provides an increase in cohesion. By using viscosity enhancing admixtures cohesion can also be improved. The absence of coarse aggregate also removes one of the constituent materials that typically can segregate.

2.4.5 Cracking

ECC demonstrates a unique cracking behavior relative to regular concrete. Upon first cracking under load, the fibers are engaged and immediately restrain the crack from growing (Li V. C., On Engineered Cementitious Composites (ECC) A Review of the Material and Its Applications, 2003). Due to the attention to micro mechanical behavior of the mortar matrix and fibers, multiple micro-cracks will form allowing for large straining. The mortar matrix is designed to be weaker than the fiber bridging capacity, meaning that multiple cracks will form in the matrix engaging multiple fibers and allowing them to bridge the stresses. It is not until the tensile strain becomes high, ranging from 3 to 5% (Wang & Li, 2007), that the frictional bond between the matrix and fiber is exceeded and fiber pull out occurs resulting in the micro-cracks opening and the ECC failing. Consideration must be given to the ultimate stress of the fiber during the design to limit and/or prevent fiber rupture. The difference between FRC and ECC in terms of cracking is that FRC exhibits a strain softening and relatively large cracks compared to ECC. Due to ECCs design at the micro level, it is possible to create multiple micro cracks due to stress bridging characteristics of the fibers and the correct proportioning of matrix fracture

toughness and fiber pull out stresses. Cracks in ECC are typically 100 μm (Wang & Li, 2007).

2.4.6 Strength

The strength of ECC is dependent on the age of the specimen and the type of SCMs and fibers used in the mix design. Various strength properties can be seen in Table 2-4. Tests have shown that the compression strength of ECC is similar or better in behavior to that of plain concrete (Wang & Li, 2007). In tension, ECC has a first crack stress around 4 MPa and then exhibits a strain hardening response similar to metals (Wang & Li, 2007). This response is unique to ECC versus regular concrete, which is brittle, or fiber reinforced concrete, which exhibits a strain softening response. The ultimate tensile strain reached by ECC can be up to several hundred times that of normal concrete (Li, Lepech, Wang, Weimann, & Keoleian, 2004). This ductile behavior is desirable for seismic applications which require large amounts of deformation and energy absorption. ECCs ability to excessively deform under constant stress means that more visible warning will be evident before failure of the material, in the form of plastic straining.

Table 2-4: Strength properties of polyethylene (PE) fiber ECC and polyvinyl alcohol (PVA) fiber ECC (Li, Fukuyama, & Mikame, 1998)

	Tensile				Compressive		Stiffness	Flexural	Fracture
	σ_{fc} (MPa)	ε_{fc} (%)	σ_{cu} (MPa)	ε_{cu} (%)	f_c' (MPa)	ε_c' (%)	E (GPa)	MOR (MPa)	J (kJ/m^2)
PE-ECC	2.5	0.021	4.6	5.6	68.5	0.67	22	12.5	27
PVA-ECC	2.2	-	3.1	1.5	35	0.45	16	-	-

2.4.7 Placement

Two placement techniques of ECC have been researched, those being conventional casting, and spraying. In either case, proper preparation of the substrate material is necessary to improve the bond between the substrate and ECC. Research shows that important factors contributing to bonding are contact surface area, which is controlled by the roughness of the substrate, and substrate moisture (Zhou, 2011). Conventional casting is the same that is used for regular cast in place concrete. The ECC is placed in a form and is adequately compacted using vibration. The more unique placement technique is that of spraying, similar to shotcrete. ECC differs from shotcrete in that it contains fibers and no coarse aggregate. To spray ECC, the mix needs to have a fluid nature and must also have the ability to adhere to the substrate material. This requires a properly proportioned mix design to achieve both parameters. The spraying of ECC is improved by the presence of water, HRWRA, and fly ash (which is spherical and exhibits a ball bearing effect). Research done (Li, Fischer, & Lepech, Shotcreting with ECC, 2009) showed that spraying is feasible, and that spraying and casting the same type of ECC yields similar mechanical behavior.

2.4.8 Air Content

Air content in concrete is an important parameter to control. Different types of air content are present in concrete, being entrapped air and entrained air. Entrapped air is present from the lack of proper consolidation, and entrained air comes from the use of air entraining admixtures. If a high amount of fly ash is used, it may affect the effectiveness of the air entraining admixture. Also, given that the ECC may be sprayed, the air content may vary between mixing and after spraying (Kanda, Saito, Sakata, & Hiraishi, 2003). If the ECC is being used in an area that is subjected to freeze thaw cycles it is important to provide adequate air content. An advantage of ECC to help mitigate the effects of freeze thaw is its

lower permeability and smaller crack widths due to its constituent materials and mechanical behaviour.

2.4.9 Heat of Hydration

Due to the large amount of cement content in ECC, as seen previously in Table 2-2, it is necessary to consider the amount of heat given off from the hydration of cement, which is an exothermic reaction. The use of silica fume also increases the heat of hydration at early ages. This can be controlled by using fly ash or slag as a cement replacement, as they have a delayed heat evolution response relative to cement. Another option is to provide chilled mixing water, which will lower the overall temperature of the mix. The risk in having a high heat of hydration is that the rapid hydration of cement particles will occur and can result in a coarse outer shell, which may result in lower later age strength. High heat may also increase the rate of water loss through evaporation and hydration, resulting in plastic shrinkage cracks and self-desiccation.

2.4.10 Setting Time

The setting time of ECC is highly dependent on the constituent materials. Relative to cement, silica fume has a faster setting time. Fly ash has a slower setting time and HRWRA can act as a retarder if used in large quantities. In the pursuit of a reduced environmental impact using SCMs, setting time may be delayed resulting in more precaution needed in the early stages of ECC post casting. Disrupting the specimen before adequate strength gain may have detrimental effects on the mortar-fiber interface which is a crucial component of the strain hardening behavior of ECC.

2.4.11 Shrinkage

Given the large quantity of cement in ECC, it is prone to shrinkage cracking. This does not pose a serious threat to the ECC given that it can resist large tensile strains due to its strain

hardening effect and crack width control due to the presence of fibers. This may present issues on the bond interface between the ECC and the substrate material, when using ECC in repair or strengthening applications. A study conducted (Zhou, 2011) showed that the interface between a concrete substrate material and ECC was the likely location of failure in flexural testing. Given that the substrate material has likely been in place for a sufficient time to allow for plastic and autogenous shrinkage to take place the relative movement between the substrate and newly placed ECC will be large. With special attention to curing it is possible to lessen the impact of shrinkage. This behaviour of EDCC cast over a substrate material will be evident through the testing outlined in this study.

2.4.12 Curing

ECC requires an extended amount of curing due to the large cement content and the possible use of SCMs. Despite cracking not being overly detrimental, through good curing practices it is possible to limit plastic shrinkage cracking. Due to the action of particle packing, bleed water is less likely to reach the surface of ECC. Therefore, to prevent drying of the ECC surface it is necessary to provide an external source of surface water. The presence of curing water also helps to prevent autogenous shrinkage, which in part is the act of self–desiccation of a sample. Self-desiccation occurs due to the loss of water within the concrete to chemical reaction with the cement. The products are physically smaller, resulting in voids being formed and suction forces being exerted on the capillary pores. This becomes more problematic when lower water/cement ratios are used, given that the loss of water will occur more quickly relative to high water/cement ratio concrete (Zhou, 2011).

2.4.13 Durability

ECC has many benefits from a durability standpoint due to its cracking behavior. Given that cracks allow for harmful chemicals to travel into the concrete, restricting crack width is desired. This is achieved by the fibers present in the concrete. The silica fume also prevents bleeding of water which improves the presence of capillary pores, which can be a source of chemical intrusion. At early ages, the fibers may act as a location of possible mortar delamination; therefore, careful attention should be paid to abrasive forces on the exterior face of the cast ECC.

2.5 Applications of ECC

Given that research has been carried out to determine the mechanical behavior of ECC, the next step is to evaluate various types of applications. ECC not only poses advantages from a mechanical standpoint, it also has advantages in its placement process. Several applications are examined and the performance of ECC is evaluated.

2.5.1 Spalling Prevention of Concrete

ECC has been used to prevent spalling of concrete with corroded rebar. The corrosion of rebar is an expansive reaction, resulting in internal pressures being applied to the surrounding concrete. If these pressures exceed the concretes tensile capacity, cracking can take place around the rebar and spalling will occur. By applying a layer of ECC, which has very good crack control properties and high tensile capacity relative to regular concrete, spalling can be prevented. Research conducted (Kanda, Saito, Sakata, & Hiraishi, 2003) shows that sprayable ECC is an effective retrofit measure to prevent spalling of concrete. The mix design of ECC can be seen in Table 2-5, with some important notes. The air content has been neglected for the mix proportions even though it makes up 15 to 25% of the mix due to the viscosity enhancing agent used. The quantity of the viscosity enhancing

agent was not provided, and it was used to prevent segregation between the matrix and the fibers. For mix C, low heat of hydration cement was used due to the potential use of the sprayable ECC in hot conditions. Using a tapered pin load test, which is in conformance with Japanese Industry Standard B 1353-1988, it is possible to simulate the expansion of rebar due to corrosion. After performing tests on sprayed ECC, the tests showed that 3.5 mm of pin displacement was required to cause corrosion cracking. This value is higher than the typical value of 0.5 to 1.0 mm for regular concrete, which corresponds to a rebar diameter increase of 0.01 to 0.02 mm. The implications of having a corrosion crack is that as the crack forms, more harsh chemicals can infiltrate the concrete cover to the rebar causing accelerated corrosion. By having a protective layer of ECC, which exhibited a higher tolerance for expansive forces, it is possible to mitigate the ingress of harsh chemicals through crack width control.

Table 2-5: Mix design for sprayable ECC (Kanda, Saito, Sakata, & Hiraishi, 2003)

Mix	Water/Binder Ratio	Sand/Binder Ratio	Water Content (kg/m^3)	Fiber Volume Fraction (%)	Cement:Fly Ash Weight Ratio
A, B, D	0.32	0.41	382	2.1	7:3
C (low heat of hydration cement)	0.32	0.42	382	2.1	7:3

2.5.2 Flexural Applications

Tests were also performed on flexural and tensile members. Both sprayed and placed ECC were examined, and the differences were quantified. The fiber orientation within the matrix contributes to the flexural and tensile strength of the ECC. If the fibers are normal to the crack direction, they will provide more capacity. Given this it was observed that during the

spraying process, since thin layers were applied repeatedly to the specimen resulting in a compounded layer of ECC, the fibers were oriented parallel to the substrate. For a mass placement using traditional concrete placement techniques, the orientation of fibers was observed to be more random thus resulting in less tensile capacity and less deflection/straining in flexural beam tests, compared to the previously mentioned case where fibers are all oriented normal to the expected crack direction in a beam (Kanda, Saito, Sakata, & Hiraishi, 2003).

2.5.3 Earthquake Applications

Columns constructed with ECC were tested in (Li V. C., On Engineered Cementitious Composites (ECC) A Review of the Material and Its Applications, 2003). Through cyclic loading up to a drift of 10% the column that was constructed using ECC exhibited a multitude of cracking but no spalling of concrete or visible signs of failure relative to the regular concrete. Conventional concrete was shown to spall around the vertical column reinforcement and stirrups at the base of the column. This is a testament to the vastly increased toughness of ECC over conventional concrete. Given ECCs ability to absorb energy it makes it a viable material to provide better response of structures to earthquake loading.

2.5.4 Masonry Strengthening Applications

Concrete masonry blocks are made from zero slump concrete that is compressed and vibrated into steel molds and then steam cured. The blocks are laid in a wide range of patterns using mortar as a joint material. The mortar consists of general use cement, free lime, sand, and water, mixed to a consistency that allows for the mason to progressively lay blocks. Given that there is a cold joint between the concrete block and the mortar joint there is a plane of weakness, and if the composite system is subjected to tension a

debonding failure will likely occur here. By providing an overlay of ECC it is possible to increase the tension capacity of the system due to the high tensile capacity of the strengthening material. A weakness that must be addressed is the interface between the masonry wall and the parging material. A technique that can be utilized to improve the mechanical bond between the surfaces is to prepare the masonry block face by using a roughening technique, such as sand blasting. Wetting the masonry block surface prior to application of the ECC is also beneficial due to the masonry block absorbing water if it is not saturated. By absorbing water, the block would take some of the mixing water from the ECC causing a weak layer of ECC at the interface which could result in delamination.

Similar work performed by (Kyriakides, 2011) shows that by strengthening masonry with ECC the compressive strength and stiffness increases by 44 to 53% and that the flexural strength in bending increases by 35 times relative to plain masonry. The failures were reported to be more ductile. The work done in this research program will also address the effect of strengthening masonry using a form of ECC.

2.6 Review of Materials and Properties

2.6.1 Brick Properties

Bricks are the primary component that make up a brick masonry assemblage. They are stacked upon each other using mortar as a joint material. Bricks are typically the stronger and stiffer of the two materials. The material properties of interest when discussing bricks are weight, modulus of rupture, compressive strength, absorption, initial rate of absorption, void area in cored units, and breaking load. The testing procedures for bricks are outlined in C67-11 of the ASTM 2012 standard. Bricks can be composed of clay (with various additives), concrete, or calcium silicate. They can either be moulded or extruded. In present

day construction in Canada, bricks are typically used in veneer applications. In historic construction, bricks were used in multi-wythe wall systems that were load bearing. Older brick manufacturing consisted of pressing clay into a mold, and the bricks would sometimes have an indentation on the top face known as a "frog". The current type of manufacturing performed for clay bricks is an extrusion process, where the clay is extruded to have two dimensions required for the bricks. The extruded clay is then wire cut to have the correct third dimension. At this point, the bricks are baked/fired to harden the clay.

2.6.2 Concrete Block Properties

Concrete blocks are precast in manufacturing plants. They are made with a zero-slump concrete and are placed into forms using vibration and pressure. The blocks are typically steam cured at an elevated temperature to increase the rate of production. Various sizes and shapes of concrete blocks exist, but the most common block used in a structural application is the 190 mm x 190 mm x 390 mm (actual dimensions). This block is known as a 20 cm standard block. There are two different weights available for the previously mentioned block; the heavy weight block, which is 16.2 kg, and the light weight block, which is 12.7 kg (Expocrete, 2012). The light weight block also has a higher fire rating of 2.1 hours versus 1.6 hours for the heavy weight block. This can be attributed to the type of aggregate used.

2.6.3 Mortar Properties

Mortar is the joint material used to bond masonry units together. It consists of cement, lime, water and sand in varying quantities. The mixing of mortar is typically done on site by the masonry labourer. For small projects, mortar is typically mixed in pails or wheelbarrows using shovels and hand mixers. For larger projects, the mortar is mixed in a mortar or concrete mixer which contains an internal agitator system for uniform mixing.

The labourer uses his or her experience to get the mortar to the right consistency for workability when placing the mortar, this is usually achieved by adding water. The masonry bricklayer will also add additional water to retemper the unused mortar as the mix water evaporates to improve workability. Mortar has relatively lower strength and stiffness than that of masonry units. When performing compression tests on mortar cubes cast in non-absorbent steel moulds it is important to note that the resulting compression tests are much lower than in situ mortar due to a higher water cement ratio. The water in in situ mortar will absorb into the masonry units, resulting in a lower water cement ratio and thus a stronger mortar (Franklin, Lynch, & Abrams, 2001).

2.6.4 Prism Properties

A masonry wall assemblage is composed of masonry units connected by mortar bed joints (horizontal) and head joints (vertical), in various orientations, the most common of which is running bond, where the units are staggered by half intervals. Where concrete walls are typically cast by erecting vertical forms, tying reinforcement within the forms, and casting a monolithic pour of concrete within the formwork, masonry is built by laying the individual blocks one by one, placing vertical and horizontal reinforcement as the blocks are being laid, and then grouting the cores of the blocks after the blocks are complete. This results in a series of cold joints between the blocks and mortar joints, as well as the blocks and grout. Bricks are typically not grouted since their cavities are much smaller and do not allow for vertical reinforcement, although they may have horizontal wire reinforcement imbedded in the mortar joints.

A masonry prism assemblage is a small sample, typically 2 to 4 units high (meeting various aspect ratio requirements), constructed in stack bond for testing purposes (Canadian

Standards Association, 2004). The behaviour of a prism is a function of both the masonry unit properties, mortar properties, the interface between the masonry unit and mortar, and aspect ratio. In a compression situation, a masonry prism will have a higher compressive strength than an individual mortar sample and a lower compressive strength than an individual masonry unit. This is due to dissimilar lateral movement of the mortar and masonry unit, causing a triaxial compression force to be exerted on the mortar joint (Drysdale & Hamid, 2005). Given that mortar joints undergo a different loading condition to that of a regular mortar cube compression test, the overall strength of a prism is higher than that of the individual mortar strength. Also, due to the relatively thin mortar joints (typically 10 mm) instrumentation of these joints is very difficult (Franklin, Lynch, & Abrams, 2001).

The purpose of testing masonry prisms versus masonry walls is primarily due to the physical, financial or time constraints that are incurred when performing laboratory tests. To construct a full scale wall is at times impractical. Therefore, small scale prisms are utilized. If compression tests are performed on a prism, it is important to ensure that the surface of the prism does not deviate from the load plate as this can cause unwanted stress concentrations. The solution to this is to provide hard capping on the prism, in the form of mortar, sulphur or Plaster of Paris. Other research has assessed the suitability of other capping materials, such as foam, fiberboard, neoprene and gypsum (Fonseca & Ballard, 2013). Another thing to consider when performing compression tests is the height of the prism. If the prism is too short a conical shear-compression failure will occur, similar to a concrete cylinder compression test, this is due to the end constraints not allowing deformation (Drysdale & Hamid, 2005). If the prism is too tall, slenderness may become

an issue due to the possibility of eccentric loading. The preferred height-to-thickness ratio ranges from 2:1 to 5:1. The type of end restraint is also an important consideration. Using a brush steel platen can cause a reduction in frictional forces between the platen and the specimen. By performing compression tests with proper prism instrumentation it is possible to determine the stress strain curve of the prism, including the modulus of elasticity, ultimate stress and failure stress. Flexural strength can be measured through various loading conditions, such as bond wrench, three-point bending, four-point bending, and uniform bending; the focus of this thesis is on the four-point bending beam test. The bond wrench test consists of applying an eccentric load to a single mortar joint on a brick prism. This allows for the calculation of the modulus of rupture. The three-point bending beam test consists of setting a masonry beam up in a simply supported configuration with a point load applied at midspan. An issue that arises with the three-point bending test is that "it fails at the joint with the critical combination of high bending moment and low joint strength" (Drysdale & Hamid, 2005). Four-point bending alleviates this problem by providing a region of constant bending moment and zero shear (between applied loads).

There are various mortar joint curing techniques that can be performed on the prisms, as outlined by the National Concrete Masonry Association (NCMA) (National Concrete Masonry Association, 1994). Four different methods are investigated, including:

> Curing method A: Sprayed with water 1 day following construction; then cured in sealed plastic bags for 25 days; then cured in laboratory air for two days.
>
> Curing Method B: Cured in laboratory air for 28 days. Sprayed with water at 7 and 14 days after construction.

Curing Method C: Cured in laboratory air for 28 days.

Curing Method D: Cured outside for 28 days. Tops of prisms covered for protection from rain.

NCMA concluded that moist curing (Curing Methods A and B) more than triples the flexural tensile strength of the prisms, as this allows for sufficient moisture to hydrate the cement in the mortar. It was also observed that the coefficient of variance of flexural tensile strength of the prisms for Curing Methods A and B were much lower than that of Curing Methods C and D, indicating that a more consistent value of flexural tensile strength can be obtained by moist curing.

2.6.5 Modulus of Elasticity and Modulus of Rupture

A research evaluation of the flexural tensile strength of concrete masonry was conducted by the NCMA (National Concrete Masonry Association, 1994), where walls and prisms of various thicknesses were constructed and tested in flexure. The walls were simply supported and tested in out-of-plane bending using a uniformly distributed load applied with an air bag. The prisms were tested using the bond wrench test. For 4" thick concrete masonry walls the modulus of rupture was reported to be 285 psi (1.96 MPa) with a coefficient of variance of 11%, and for the 4" thick concrete masonry companion prisms the modulus of rupture was reported to be 231 psi (1.59 MPa) with a coefficient of variance of 16%. The mortar used for these specimens was type S. Interestingly, the researcher also indicated that for narrower specimens (4" thick, for example), a strain gradient appeared. Given that the researchers tested 4", 8" and 12" thick specimens they suspected that the gradient is present between the 4" and 8" specimens, resulting in larger modulus of rupture values for the 4" specimens. The researchers also reported that the mortar type, curing

method, unit tensile strength, and the unit manufacturing played important rolls in the modulus of rupture for a masonry assemblage.

2.6.6 Retrofit Material / Strengthened Masonry

Previous research has been done on various repair techniques, and some important lessons can be learned from the conclusions made. Franklin, Lynch and Abrams (Franklin, Lynch, & Abrams, 2001) employed numerous retrofit techniques of URM brick piers subjected to in-plane lateral cyclic load, but given the focus of this thesis two will be discussed. The first retrofit technique examined is the externally mounted rebar with a shotcrete overlay. In this test the shotcrete was poured into a form instead of using a spray gun application, similar to this study. The conclusion made on this repair technique was that the shotcrete and rebar did not behave compositely with the existing URM pier. This effectively means that the URM pier would be responsible for carrying the axial load while the reinforced concrete pier would resist the in-plane shear forces. The concluding thought on the retrofit technique is that "shotcrete is an effective rehabilitation method because of the large deformation capacity and the energy dissipated through steel yielding".

The second applicable retrofit technique performed was externally mounted steel hardware cloth coated with ferro-cement overlay. The ferro-cement overlay was applied using a trowel. This application is very similar to that of a scratch coat for manufactured stone veneers, so it would be familiar to masons. The tests showed that there was a "slight increase in strength of the initial linear portion of the force-deflection curve". Once the steel hardware cloth fractured the pier behaved as an un-retrofitted pier by rocking.

2.6.7 Prisms Retrofitted with ECC

Marios A. Kyriakides performed research involving retrofitting brick prisms and beams with an engineered cementitious composite (ECC) (Kyriakides, 2011). The bricks used were yellow clay bricks with dimensions of 94 mm x 58 mm x 196 mm, grade MW, type FBS, and manufactured to meet ASTM C216-10. The mortar was a custom by volume blend consisting of 1 part cement (Type I/II), 1 part lime (Type S), 5 parts sand (Oly 1 – a type of coarse masonry sand), and water added based on the professional masons experience, resulting in a similar mortar to type N as per ASTM C270-10. Compression tests were performed on plain tall prisms (PPT) consisting of 5 full size bricks, plain short prisms (PPS) consisting of 3 full size bricks and 2 cut bricks, and short prisms retrofitted with ECC (PUE). Tests were also performed on brick prisms strengthened with various configurations of welded wire mesh and stitch dowels, but these will not be reported here as they are outside the scope of this research program. The average brick strength was found to be 79.3 MPa along with an average elastic modulus of 16.5 GPa. It is important to point out that the elastic modulus of the bricks was measured using similar bricks at the University of Colorado. The average mortar strength was determined by performing compression tests on 50 mm x 100 mm mortar cylinders, with the results shown in Table 2-6, with the standard deviations given in brackets. Cylinders were cast using ECC as well, and the results of the compression test can be seen in Table 2-7. The results of the plain and retrofitted prism tests can be seen in Table 2-8. All standard deviations are given in square brackets.

Table 2-6: Compressive strength of mortar used for prisms (Kyriakides, 2011)

Group	$f'_{c\ mortar}$ (MPa)	Age (days)
PPS	11.3 [0.6]	122
PPT	11.3 [0.6]	122
PUE	8.5 [1.0]	122

Table 2-7: Compression strength and elastic modulus of ECC used for prisms (Kyriakides, 2011)

Group	$f'_{c\ ECC}$ (MPa)	E_{ECC} (GPa)	Age (days)
PP	-	-	-
PUE	54.7 [4.1]	12.5 [1.2]	68

Table 2-8: Average compressive strength and elastic modulus of masonry prisms (Kyriakides, 2011)

Group	f'_m (MPa)	E_m (GPa)	Age $_m$ (days)*	Age $_{ECC}$ (days)**
PPT	20.70 [1.00]	7.16 [1.11]	114	-
PPS	20.06 [2.37]	5.13 [0.65]	114	-
PUE	29.04 [2.87]	7.86 [0.67]	114	64

* from day of masonry fabrication

** from day of ECC application

It can be seen that a strength increase from 20.70 MPa and 20.06 MPa for the tall and short un-retrofitted prisms, respectively, to 29.04 MPa for the short prism retrofitted with 13 mm of ECC was measured. The failure modes for the un-retrofitted prisms "exhibited vertical cracks, namely face shell separations according to ASTM C1314-10". The retrofitted prisms exhibited vertical cracking in the ECC layer at peak load, followed by horizontal cracking in the ECC layer paired with a drop in load, and finally vertical cracking of the masonry surface and delamination of the ECC – masonry interface.

2.6.8 Beams Retrofitted with ECC

The beam component in (Kyriakides, 2011) consisted of building a brick prism using nine bricks of the same composition and dimensions as the compression tests. The resulting dimensions of the plain beams were 94 mm x 196 mm x 602 mm, and the layer of retrofit had dimensions of 13 mm x 196 mm x 602 mm. The plain brick specimens were denoted as (FP) and the strengthened beams were denoted as (FUE). The prisms were fabricated by the same professional mason that constructed the compression test prisms. The loading configuration used was a four-point bending technique to obtain a constant moment region, similar to that seen in Figure 2-1. It is interesting to note that this load configuration deviates from ASTM E518/E518M – 10, which specifies L/3 spacing of the load points, where L represents the clear span of the beam; this can be seen in Figure 2-1. Kyriakides selected to go with an L/2 spacing of the point loads. The test was performed using a 245 kN MTS hydraulic actuator with a loading rate of 0.005 mm/sec. The properties of the mortar and ECC used for the beams can be seen in Table 2-9 and Table 2-10.

Kyriakides reported that the FP beams failed below 0.7 kN, while the FUE beams ranged from approximately 3 kN to 18 kN, with deformation up to 2 mm at peak load also reported.

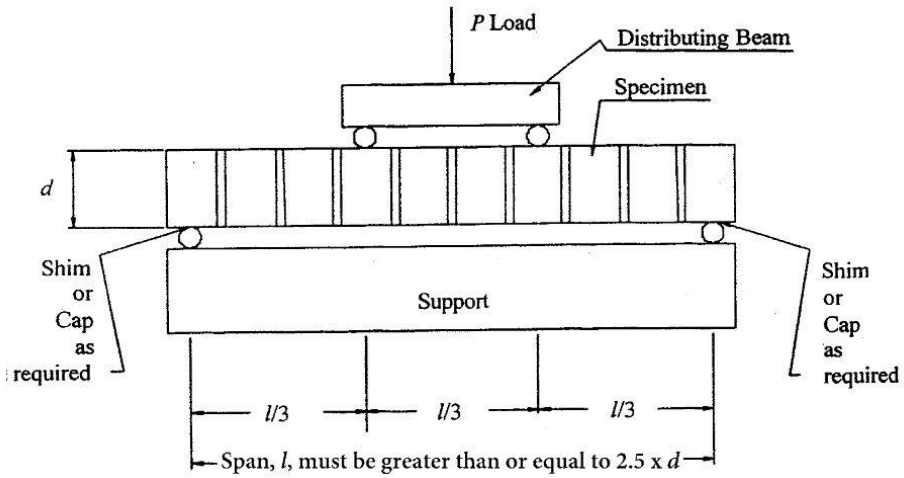

Figure 2-1: Four-point bending test from ASTM E518/E518M – 10 (ASTM International, 2010)

Table 2-9: Compression strength of mortar used for beams (Kyriakides, 2011)

Group	$f'_{c\ mortar}$ (MPa)	Age (days)
FP	11.3 [0.6]	122
FUE	11.1 [0.2]	122

Table 2-10: Compression strength and elastic modulus of ECC used for beams (Kyriakides, 2011)

Group	$f'_{c\ ECC}$ (MPa)	E_{ECC} (GPa)	Age (days)
FP	-	-	-
FUE	53.1 [1.7]	12.1 [0.9]	38

Work has been performed at the University of British Columbia and the University of Calgary in collaboration with this project, and a brief review of their results will be presented.

At the University of British Columbia bond tests were performed on EDCC overlay on concrete and clay masonry (Yan, 2016). The mixture of EDCC was varied in these tests, with the main variable being the presence of fibers. The workability of the EDCC was also

varied using additional high range water reducing admixtures. The curing methods were also varied between standard curing method and field curing method. Two different thicknesses of strengthening material were evaluated (20mm and 30mm). With all these parameters in mind it was possible for the researcher to encompass several variables which can contribute to the bond characteristics of an EDCC overlay and a masonry substrate. It was concluded that EDCC can achieve adequate bond through both standard and field curing techniques; fiber presence and orientation negatively impacted the bond strength; improved workability using HRWRA improved bond strength; 30mm EDCC thickness showed lower bond strength than the 20mm EDCC thickness; and the maturity age of EDCC was found to be 56 days. The researcher recommended that EDCC requires adequate workability (150 mm slump) to achieve adequate bond strengths with the masonry substrate; the thickness of EDCC used should not be a function of bond strength, given that it controls strength of the specimen, the bond should be improved based on application technique and surface preparation; and to reduce the impact the fiber presence has on bond proper fiber orientation and substrate surface preparation are required.

Durability was evaluated by (Du, 2016), specifically restrained shrinkage resistance, freeze and thaw resistance, and bond strength durability. All aspects of durability reported for EDCC outperformed plain mortar. Spraying versus hand casting EDCC, as well as fiber type and quantity in EDCC, were also evaluated within the testing program.

Work is also being done at the University of British Columbia involving optimizing the EDCC mix design, direct tension tests of EDCC at a static and dynamic rate, optimizing the spray gun application of EDCC, and diagonal shear tests of specimens strengthened with EDCC, among other things. (Soleimani-Dashtaki, Soleimani, Wang, Banthia, &

Ventura, 2017) and (Soleimani-Dashtaki, Ventura, & Banthia, Seismic Strengthening of Unreinforced Masonry Walls using Sprayable Eco-Friendly Ductile Cementitious Composites (EDCC), 2017) explores portions of this work further.

The work performed at the University of Calgary consisted of full scale wall tests done on plain and strengthened masonry walls constructed in running bond with 200mm standard weight concrete blocks (Kaheh P. , 2018). The additional published works consist of, but are not limited to, free vibration tests (Kaheh & Shrive, Effects of eco-friendly ductile cementitious composites (EDCC) on dynamic characteristics of hollow concrete masonry walls, 2016) and in-plane shear load tests (Kaheh & Shrive, Influence of eco-friendly ductile cementitious composites (EDCC) on in-plane behaviour of hollow concrete masonry walls, 2016). The researcher varied the number of sides being strengthened with 20mm of EDCC to find an optimal strengthening configuration. It was concluded that the presence of EDCC increased the stiffness of the wall; the failure changed from a rocking failure for unstrengthened walls to block failure and in one occurrence EDCC failure; no debonding was observed; the drift capacity and ductility were improved; the strength increased significantly; the researcher also commented that the strength increase relative to the cost increase to go from strengthening one side to two sides was not justified, so the most optimal strengthening configuration was one side only. This lends itself to the idea that to retrofit existing buildings the façade would likely need to be kept intact architecturally, as well as the ease of application for long corridor walls would be much higher than individual rooms where set up and tear down would be required. It was observed that strengthening one side only introduced torsion into the specimen during in-plane loading due to asymmetry. The researcher commented that at this time more tests are

being performed. The free vibration tests performed showed that the presence of EDCC in the uncracked state impacted the natural frequency more than in the cracked state. Torsion was present in the in-plane vibration test for one side strengthened, and the damping ratio of the wall was decreased by the presence of EDCC in the uncracked state, and increased it in the cracked state.

3 Experimental Program

3.1 Test Specimens

The concrete blocks utilized were the 10 cm standard weight concrete blocks (measuring 90 mm deep x 190 mm high x 390 mm long) produced by Expocrete in British Columbia. Light weight blocks are the most common in structural use in the provinces of British Columbia, Alberta, and Saskatchewan, based on conversations with the Saskatchewan branch of the masonry subcontractor Brxton (formerly Gracom). In Manitoba, heavy weight blocks are most prevalent, possibly due to the cost of the special aggregate used in light weight blocks. The goal of this project was to limit the variability between the samples, meaning that the same type of mortar, block, and brick was used to construct the samples. The same mason were used to limit workmanship discrepancies. The bricks used were new clay bricks (measuring 92 mm deep x 57 mm high x 193 mm long).

The mortar used in the construction of both brick and concrete block prisms and beams was Portland lime and sand masonry mortar type S "Specialty QC Pre-Mix Mortar" manufactured by Steels, which meets CSA A179M for type S mortar. The 80 lb bags contained Portland cement, hydrated lime, pulverized limestone, and dried masonry sand and were pre-blended, meaning they only required the addition of water to make mortar. The mix design is in adherence with ASTM C 270, which outlines mortar used for unit masonry. The reason for selecting spec mix mortar was to ensure the consistency of mortar used not only for samples tested in this thesis, but also those being tested by other members of the NSERC CRD. As per the mixing instructions provided by the supplier, the mortar was to be mixed in a mechanical batch mixer no less than five minutes and water is to be added until the mortar becomes sufficiently workable. The mortar should be used within

2.5 hours after initial mixing takes place, and retempering is permitted if it is required due to evaporation of the initial mixing water. The mortar was mixed in small batches by the Brxton laborer in a pail with a mixing drill to provide the batches required for the two masons constructing the specimens.

3.2 Construction of Specimens

All specimens were constructed by Brxton using typical masonry construction practices over the course of two days. Levels and string lines were used to ensure plumbness. Mortar, which consisted of pre-mixed mortar and water, was mixed in a bucket using a mixing drill by the laborer, as seen in Figure 3-1. The mortar was mixed to a consistency deemed appropriate by the laborer and masons based on their knowledge of typical masonry construction practices, which worked out to approximately 7 parts spec mix to 1 part water by weight. The samples were built in a stack bond pattern. After each line of samples was constructed, it was covered with poly to protect the specimens from evaporation. The samples were left covered for several months and were surface saturated using water in a pail or spray hose every one to two days. 30 mortar cubes were cast during both days of sample construction. Figure 3-2 shows the typical mortar used for construction and Figure 3-3 shows the construction process, complete with covered specimens in the back.

Figure 3-1: Mixing mortar for masonry prism and beam construction

Figure 3-2: Fresh mortar on board

Figure 3-3: Construction of masonry prisms and beams by masons

The strengthening material under consideration in this project is an eco-friendly ductile cementitious composite that will ultimately be applied to the exterior face of a masonry wall via a spray gun application. Due to the ongoing study of the spray gun application by other members of the NSERC CRD, and for the sake of time effectiveness of this research program, a hand application method was employed for this study. Hand application is also beneficial given that small masonry prisms and beams are to be strengthened, not full walls.

Once the benchmark specimens were designated, meaning that they would not receive EDCC strengthening material, the remainder of the specimens that were to receive EDCC could be strengthened. This process involved laying the specimen down flat on the ground, ensuring that the specimen was handled gently and supported along the edges to prevent

premature cracking at the mortar-masonry interface. The edges of the specimens were ground down prior to formwork application to ensure that there was a true edge to apply the formwork to. This also ensured that the top and bottom surfaces of the prisms were ground flat for the compressive load test. Oriented strand board was then glued to the sides of the specimen, with an offset of the desired overlay thickness as seen in Figure 3-4. Prior to strengthening, the surface of the specimen to be strengthened was air blasted to remove dust and then wiped with a wet cloth to further prepare the surface and to ensure that the specimen had some surface moisture to help facilitate a stronger bond. No surface roughing was done to the specimen based on conversations with the collaborators on the NSERC CRD.

Figure 3-4: Offset of formwork for EDCC overlay

The EDCC was mixed in a 5-gallon Hobart Mixer, seen in Figure 3-5 and Figure 3-6. Initially, the dry constituent materials, consisting of cement, fly ash, silica fume, sand, and fibers were weighed out and bagged. At the time of mixing, the water was weighed and a high range water reducing admixture (HRWRA) was measured out. Batch sizes ranged from 5 L to 6.5 L.

Figure 3-5: Mixer used for EDCC mixing

Figure 3-6: Mixer information plaque

The wet ingredients were added to the mixing bowl, followed by the cement, fly ash combined with silica fume, sand, and fibers, as seen in Figure 3-7 and Figure 3-8. The mixing time and speed was controlled throughout the process. After the mixing was complete, the EDCC was hand applied to one side of the specimen, as seen in Figure 3-9. The EDCC was then trowelled smooth, and the formwork was used as a guide to better achieve consistent thickness. EDCC cylinders and beams were also cast using a vibrating table and manual compaction. No vibration was done on the masonry specimens, although some manual compaction took place through the hand placement technique.

Figure 3-7: Adding HRWRA to the mixing bowl

Figure 3-8: EDCC in mixing bowl

Figure 3-9: EDCC application

Three thicknesses of EDCC are used in testing; 10mm, 20mm and 30mm. The specimens are named using the following convention; the first letter represents whether the specimen is constructed of concrete masonry units (C) or bricks (B), the second letter represents if

the specimen is a prism (P) for compression or beam (B) for flexure, and the third letter represents if the specimen is unstrengthened (U) or strengthened (S). If the specimen is strengthened, the following number represents the EDCC thickness (10, 20 or 30), followed by a dash and the specimen ID number (1 through 8 for prisms or 1 through 6 for beams). For example, BPU-4 would be the fourth brick prism unstrengthened specimen tested in compression and CBS10-3 would be the third concrete masonry unit beam strengthened with 10mm of EDCC tested in flexure. The outline of number of specimens constructed can be seen in Table 3-1.

Table 3-1: Specimen construction

	EDCC Thickness				
	0mm	10mm	20mm	30mm	Total
CMU Prism	8	8	8	8	32
Brick Prism	8	8	8	8	32
CMU Beam	7	6	6	6	25
Brick Beam	7	6	6	6	25
					114

The water/binder ratio for the EDCC was 0.27. No viscosity enhancing admixture is used in EDCC, although the stiffness of the mix does not allow for segregation so it is likely not needed. HRWRA was added to the mixes, and it was indicated by the mix designer that to improve workability of the mix the amount of HRWRA should be increased, opposed to adding water. The HRWRA used in this mix design was Grace ADVA 195, which contained polyoxyalkyleneamine, 5-chloro-2-methyl-2H-isothiazol-3-one, proprietary polyacrylate aqueous solution, proprietary component for WASHO, sodium gluconate, and water. The Grace ADVA 195 had a density of 1.08 g/cm^3 and was in liquid form (W.R. Grace & Co., 2011). For a 6L batch 12.7 mL of HRWRA was used, for example, as indicated through the mix designers notes, and to remain in accordance with other

researchers in the NSERC CRD. This was measured using a syringe to ensure accurate volume measurement and was dispersed in a portion of the mixing water to ensure that all intended HRWRA made it into the mix. The cement used was a Lafarge Type GU hydraulic cement, that contained Portland cement, limestone, gypsum, calcium oxide, magnesium oxide, and quartz. The cement was grey and in powder form and had a density of 3.15 g/cm^3 (Lafarge North America Inc., 2014). The fly ash used was Lafarge Type Cl fly ash which contained fly ash, crystalline silica, and particulates not otherwise regulated. The fly ash was grey in colour, in powder form and had a density ranging from 2 to 2.9 g/cm^3 (Lafarge North America Inc., 2009). This mix design included silica fume, which helps with strength, durability, permeability but also increases the amount of curing water required due to limiting the amount of bleed water that could escape from the concrete during setting. The silica fume was a BASF Rheomac SF 100, which is now known as BASF MasterLife SF 100, and is a densified silica fume material admixture. The silica fume contained silica and crystalline silica. It was grey and in powder form and had a density of approximately 2.2 g/cm^3 (BASF Canada Inc., 2016). The mix design for EDCC can be seen in Table 3-2.

The batch sizes were typically kept the same at 5 to 6.5 L. Specimens were strengthened, then the remaining EDCC from the batch would be cast into cylinders or prisms, or discarded. The cylinders were initially cast by compacting the EDCC by hand and rodding. After discussion with various collaborators on the project it was determined that the EDCC cylinder mold should be placed on a vibrating table to help reduce the amount of entrapped air. The EDCC was placed in the cylinder mold in three lifts and allowed to vibrate on the table, as well as being compacted by hand and rodding. Once the EDCC had filled the mold

it was trowelled smooth at the top and covered. After several days the EDCC cylinder was demolded through use of pressurized air and was placed in a plastic bag with water in it directly adjacent to the masonry specimens. At the time of testing for the compression cylinders, sulphur capping was used to ensure a uniform top and bottom surface for loading.

Table 3-2: EDCC mix design*

Mixture	Cement	Water	Sand	Fly Ash	Silica Fume	HRWRA	Vfiber**
EDCC	1	0.86	1.21	1.99	0.20	.0052	2%

*Mass ratios of cement, Vfiber is volume fraction
**Composed of 1% PVA + 1% PET fibers

The fibers selected for use in the EDCC mix were a combination of polyvinyl alcohol (PVA) and polyethylene terephthalate (PET) fibers. The PVA fibers were purchased from Kuraray, and are called Kuralon RECS15 8mm, the properties can be seen in Table 3-3. The PET fibers were purchased from Reliance Industries Limited, from the Recron 3S category (Reliance Industries Limited, 2017), and had a bag marked 1.7DTEX 6mm. The properties can be seen in Table 3-4. These fibers were applied at a dose of 1% PVA and 1% PET by volume. The PVA fibers have a higher structural capacity and higher cost relative to the PET fibers. The reason for utilizing both fibers was to find a balance of structural performance and cost economics. The fibers were taken straight from the bag and mixed in, with no washing done prior to use. The fibers were monofilament and dispersed in the mortar matrix upon mixing.

Table 3-3: Kuralon RECS15 8mm fiber properties (Kuraray Co Ltd, 2017)

Type	Fiber diameter (μm)	Length (mm)	Specific Gravity (g/cm3)	Tensile Strength (MPa)	Elongation (%)	Young's Modulus (MPa)
RECS 15 PVA Fibers	40	8	1.3	1600	6	41

Table 3-4: Recron 3S 6mm PET fiber properties (Yan, 2016)

Fiber Type	Diameter (um)	Length (mm)	Specific Gravity (g/cm3)	Tensile Strength (MPa)
Recron 3S PET Fibers	40	6	1	588

Once the EDCC was applied to the specimens they were covered with plastic and left to set. Covering with plastic right after placement allowed for any bleed water present to be trapped under the plastic and reserved for curing, helping to prevent plastic shrinkage cracks from forming. After approximately 12 to 16 hours the specimens would have water placed on them and would be re-covered with plastic to wet cure them, the specimens would have water applied to them daily from this point on for 28 to 56 days to cure the EDCC. Given that the masonry specimens were in a horizontal position it allowed the curing water to pond on top of the EDCC. This is a variation of the "Curing Method A" outlined in (National Concrete Masonry Association, 1994) which indicated that using this curing method improved the flexural performance of masonry prisms. The compression specimens, their cylinders, and the EDCC beams were moved into the wet curing chamber to allow for automated wetting of the EDCC once space became available in the curing chamber. They were placed in a horizontal configuration to allow for ponding of water. The masonry beams strengthened with EDCC were placed in the curing chamber in a vertical position due to space limitations. The curing chamber operated by spraying twice a day for approximately 15 minutes, and was not capable of providing more frequent

spraying. The doors were kept shut to allow the humidity to remain high in the chamber between spray cycles. The specimens were removed from the curing chamber several days before testing to allow the surfaces to dry, this allowed for marking lines on the specimens for instrumentation and positioning in the test apparatus. It also ensured that the specimens would not be saturated during testing which may provide a change in test results, as it was not the purpose of these tests to quantify the effects of saturation on the properties of EDCC strengthened masonry.

3.3 Test Setup, Instrumentation, and Test Procedures

The following tests were performed utilizing various load frames, actuators, instrumentation and data acquisition systems, as described in this section:

- Plain and strengthened masonry prisms in axial compression
- Individual concrete masonry units (CMUs) and bricks in axial compression
- Mortar cubes in axial compression
- EDCC cylinders in axial compression
- Plain and strengthened masonry beams in four-point bending
- EDCC cylinders in split tension
- EDCC beams in four-point bending
- EDCC ultrasonic modulus of elasticity measurements

3.3.1 Plain and Strengthened Masonry Prisms in Axial Compression

Initially, a practice test was performed using a specimen constructed in the lab using locally sourced materials, which consisted of a 140mm x 190mm x 390mm 2 course concrete block prism and spec mix mortar. The specimen was constructed by the researcher. The setup, as seen in Figure 3-10, for the practice compression test consisted of a 5000 kN MTS load

frame capable of 356mm of displacement, complete with a spreader plate at the top and bottom of the sample to help prevent load concentrations on the sample. Plaster of Paris was cast in plastic bags and placed on the top and bottom of the sample while still fresh to better conform to the uneven masonry surface to further promote the reduction in stress concentrations. The samples were not loaded until the plaster had hardened sufficiently. It was found to be troublesome to ensure that the plaster was adequately forming to the top and bottom faces of the sample and to wait for the plaster to set, given the large number of tests being performed. Fiber board will be used for future tests due to its ease of installment.

Figure 3-10: Practice concrete block prism compression test

The practice compression samples were instrumented with various types of surface mounted strain gauges and 200 mm pi gauges to measure the compressive strains in the sample during loading. This allowed for the comparison of results between the pi gauges and strain gauges. Given that the number of samples being tested would call for the installation of many strain gauges, if reusable pi gauges could be used for the tests it would be a preferable option, assuming that the test results were adequately close between the two instruments. The strain gauges were mounted on both the face shells of the concrete masonry units and the mortar joints. 70mm strain gauges were used for the face shells and 6mm strain gauges were used on the mortar joints. All strain gauges were mounted parallel

to the load direction. The strain gauges and pi gauges were mounted on both the short and long face of the masonry prisms. The pi gauges were left on for the duration of the test, as protective metal plates with slotted holes were attached to the pi gauge mounting screws to protect the gauges from debris during testing. The failure mode during testing was also observed to be gradual, therefore no debris contacted the gauge. The spreader plate that was placed above the test specimen was chained to the cross head to prevent it from slipping off the specimen during testing. The actuator was equipped with a load cell to record the load applied to the specimen. The actuator was run in load control at a loading rate of approximately 1 kN/s.

The remainder of the compression tests for both the plain and strengthened brick and concrete block prisms were performed using a 600 kip Baldwin load frame that was load controlled. The universal testing machine had a baseplate that displaced vertically, and a reaction head on a swivel located above the specimen. Steel plates and fiber board were placed above and below the specimens to adequately distribute the load to the specimen, and to not damage the load frame. An example of a specimen in the load frame can be seen in Figure 3-11.

Figure 3-11: Strengthened masonry specimen in compression load frame

200 mm pi gauges were glued to the specimens at mid height of the centre of each face of the specimen. Normally the bolts used to mount pi gauges are glued and epoxied onto the specimens, but this was not applicable in this case due to the need to remove the pi gauges during testing. Therefore, only hot glue was used to mount the bolts. Given that the test was relatively short and no impact was expected on the gauges during testing it was deemed acceptable to only use glue. The specimens were loaded to approximately 70% of ultimate load, at which point the load was held for approximately 1 minute to remove the pi gauges from the specimen. The specimen was then loaded to failure. One of the specimens was instrumented with a vertical 70mm strain gauge to verify that the pi gauges were giving accurate strain readings. Two of the CPS30 specimens were instrumented with horizontally mounted LVDTs to capture any lateral movement of the specimens during loading. This is discussed further in the Experimental Results section.

For the compression tests, axial load is applied by a hydraulic testing machine to specimens capped with fiber board, as per (Fonseca & Ballard, 2013). ASTM 1314-12, which is the standard test method for compressive strength of masonry prisms, was followed for these

tests, except for capping and failure time requirements. The failure time requirement was violated due to needing to hold the load constant for approximately one minute while removing the instrumentation prior to failure. The centroid of the strengthened specimens did not coincide with half of the thickness of the specimen due to the different stiffness properties of the EDCC compared to the concrete masonry units and bricks. Calculations were performed to adjust the EDCC to an equivalent block of masonry with the same thickness as the EDCC, therefore the width of the EDCC was adjusted for calculation purposes. This was done to attempt to determine the true centroid of the specimen prior to positioning the specimen in the test setup. The positioning of the specimens in the test setup was influenced by these calculations. This would aid in loading the specimens through their true centroid to help alleviate axial load applied eccentrically which would induce bending in the specimens.

After the tests were completed, the EDCC thickness was measured using calipers at 4 points along the cross section of the EDCC. Taking these measurement helped to provide a more accurate stress calculation given that the EDCC thickness could not be cast exactly the same for each specimen.

3.3.2 Individual CMUs and Bricks in Axial Compression

An individual CMU block was tested in the same 600 kip Baldwin load frame as the one used for the plain and strengthened masonry prism axial compression tests outlined above. The only difference was the instrumentation used for this test. The bricks were tested using a concrete cylinder compression machine that allowed for the control of load rate and recorded the maximum load applied. The base of the machine displaced upwards during loading and a top plate on a spherical seat allowed for even distribution of load. One of the bricks in the test setup can be seen in Figure 3-12.

Figure 3-12: Individual brick in compression test machine

For the concrete block compression test, the recorded values were the time and the load. The actuator was run in load control. The output from this test was test duration, load, and ultimate load.

The brick compression test recorded loading rate and ultimate load. An example of the machine output can be seen in Figure 3-13, where the left number represents load rate in pounds force per second, and the right number represents the maximum load applied so far by the specimen. Once failure occurred and the loading rate went negative the maximum applied positive load was displayed on the screen.

Figure 3-13: Example of brick instrumentation output

3.3.3 Mortar Cubes in Axial Compression

The mortar cubes were tested in a 300 kN Instron 300DX Universal Testing Machine and had a steel top plate placed on them prior to loading, as seen in Figure 3-14. The head was mounted spherically to avoid stress concentrations and allow for an even distribution of load. The machine had load and displacement outputs, which could be saved to the computer connected to the testing machine. ASTM C109/C109M – 13 was followed for the testing of 2 inch mortar cubes.

Figure 3-14: Mortar cube compression test in Instron 300DX Universal Testing Machine

3.3.4 EDCC Cylinders in Axial Compression

The EDCC cylinders were tested in three different machines. The first machine was the same machine used for the bricks tested in axial compression, as seen in Figure 3-15. The second machine was the same one used for the mortar cubes in axial compression, as seen in Figure 3-16. The third machine used was an MTS actuator mounted vertically, positioned to apply loads downwards, seen in Figure 3-17. The reason for using the second and third machines was to allow for instrumentation of the cylinders with vertical and horizontal strain gauges to measure additional properties besides ultimate strength. ASTM

C39/C39M – 14a was followed for compression tests of cylinders, with the loading rate typically falling into the middle of the allowable rate (35 psi/s).

Figure 3-15: EDCC cylinder mounted in Cylinder Machine

Figure 3-16: EDCC cylinder mounted in Instron 300DX machine

Figure 3-17: EDCC cylinder tested using an actuator and DAQ

3.3.5 Plain and Strengthened Masonry Beams in Four-Point Bending

Two practice flexural specimens were tested, one of which was a plain brick beam (Figure 3-18) and the other was a concrete block beam strengthened with an early version of EDCC (Figure 3-19). The flexural test setup consisted of steel load and reaction frames with a horizontally mounted actuator. The samples were positioned vertically on a base support which allowed for translation and rotation. A horizontal loading scheme was selected to eliminate self-weight from the out-of-plane horizontal loading. It was expected that the unstrengthened samples may fail prematurely during placement in the test setup if the vertical loading configuration was used. A combination of linear variable differential transformers (LVDTs) and pi gauges were used during the practice tests to verify the performance of the gauges for the test configuration, as seen in Figure 3-20. The failed CMU practice specimen can be seen in Figure 3-21.

Figure 3-18: Practice unstrengthened brick flexural test setup

Figure 3-19: Practice strengthened CMU flexural test setup

Figure 3-20 Practice strengthened CMU flexural test instrumentation

Figure 3-21: Practice strengthened CMU flexural test

For the flexural specimens, the actuator was equipped with either a 22 kN or 44 kN load cell to measure the applied load on the sample, depending on the type of specimen being tested. Select specimens were instrumented with strain gauges, and all the specimens were instrumented with two 125 mm stroke LVDTs and one 3 mm stroke LVDT, all of which were spring loaded to help alleviate slack in the measurements. The 3 mm LVDT was used to capture the initial displacement profile and was removed once it reached its minimum stroke position.

The flexural tests were performed on strengthened and unstrengthened specimens. For each test, the specimens were instrumented with two 125mm LVDTs mounted at mid height at each lateral edge of the specimen and a 3mm LVDT mounted at mid height and mid width. For each specimen type a single specimen was instrumented with a 70 mm concrete strain gauge at mid height and mid width on the tension face to capture strains during testing up until failure. The load cells were switched during testing depending on the type of specimen being tested. For the unstrengthened specimens, a 22 kN S shaped load cell was used, for the strengthened specimens (except for CBS30 specimens) a 44 kN S shaped load cell was

used, and for the CBS30 specimens the actuator controller load output was used due to the high capacity of the specimens. Figure 3-22 and Figure 3-23 show the CMU and brick unstrengthened beams in the testing configuration.

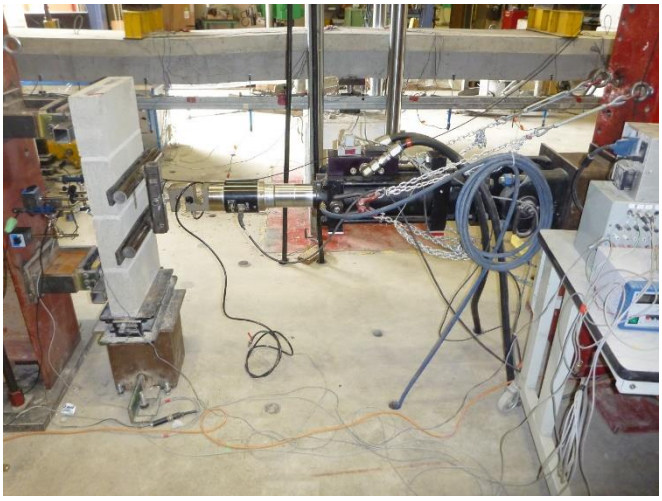

Figure 3-22: CBU flexural test setup

Figure 3-23: BBU flexural test setup

Based on the positive performance of the specimens in the practice tests, the flexural tests were performed with the flexural specimens positioned vertically on a base roller, with two supports mounted horizontally to a steel reaction frame. The actuator, which applies two point loads, was mounted horizontally to a load frame. This put the specimen in a four point loading configuration. The reason for placing the specimen vertically is to remove the self-weight of the specimen from the flexural stress developed between the supports and help reduce the occurrence of failure prior to loading due to self-weight. Figure 3-24 shows a schematic view of the flexural test setup. Other than modifying the orientation, ASTM E518-10 was followed for this testing.

After the tests were completed, the EDCC thickness was measured using calipers at 4 points along the cross section of the member. The measurements were taken along the failure plane. This is not necessarily the thinnest or thickest location of EDCC on the specimen, since the failure likely occurred in this area due to the presence of the mortar joint in the masonry beam. Taking the measurement at this location helps to provide a more accurate thickness for the EDCC given that the EDCC thickness could not be cast exactly the same for each specimen.

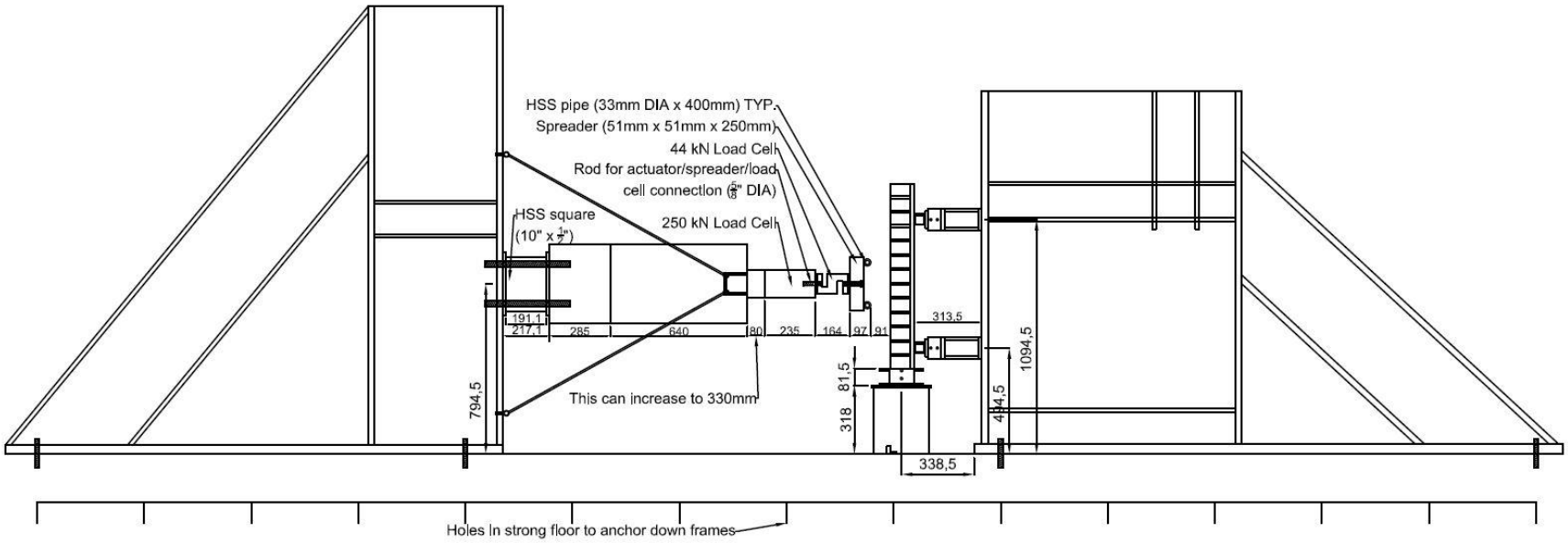

Figure 3-24: Schematic view of flexural test setup

3.3.6 EDCC Cylinders in Split Tension

The EDCC cylinders tested in split tension were loaded in the same machine used for the axial compression tests for the bricks, seen in Figure 3-25. It involved some additional framing to properly impart the load on the specimen. The bottom plate displaced upwards, with a manual control valve controlling the oil pressure used to displace the piston. The meter mounted to the machine allowed for control of the pounds force per second applied to the specimen. The machine also recorded the maximum load in pounds-force that was applied to the specimen before the load dropped. The head was mounted spherically to help minimize stress concentrations on the cylinder.

Figure 3-25: EDCC cylinder mounted in split tension cylinder configuration

3.3.7 EDCC Beams in Four-Point Bending

EDCC beams were tested in four-point bending using the MTS Instron 300DX machine and a custom load frame. The base supports of the frame were rounded bars, fixed in place and spaced 254mm apart. The load was applied to the top of the beam by a spreader plate with two rounded bars welded to it, spaced 85mm apart. The beam overhung the supports

by approximately 25mm to ensure that it did not slip off the supports during testing. A bent steel angle was epoxied and glued to the top of the beam, mounted horizontally to allow for installation of instrumentation without interfering with the cross-head of the machine. A threaded rod was screwed into the base of the machine to accept the LVDTs. The configuration can be seen in Figure 3-26. ASTM C1609/C1609M – 12 was followed for the testing of EDCC prisms in four-point loading. A beam in the testing configuration is shown in Figure 3-27.

Figure 3-26: EDCC beam and instrumentation in four-point bending test apparatus

Figure 3-27: EDCC beam in four-point bending test apparatus

3.3.8 EDCC Ultrasonic Modulus of Elasticity Measurements

Ultrasonic modulus of elasticity measurements were taken using Proceq Pundit Lab Ultrasonic Equipment, as seen in Figure 3-28, Figure 3-29, and Figure 3-30 . The process for performing this testing involved first calibrating the machine using a cylinder which was provided with the equipment. This allowed for verification that the equipment was working properly. The machine was equipped to two transducers, one of which transmitted a signal and the other acted as a receiver for the signal. Given that the surface may not be completely flush and free of voids, and that the measurement is sensitive to voids, a lubricant was used on the points of contact between the sensors and the specimen. By placing the concrete cylinders on their side and measuring across the flat faces of the cylinder a measurement was achieved, as seen in Figure 3-31 and Figure 3-32. Following taking a measurement using the ultrasonic equipment, the cylinders designated for this testing were tested in compression. These cylinders were also the ones which had another means of measuring their modulus of elasticity, two of which were instrumented with vertical and tangential strain gauges and one which was equipped with expansion rings. This was done to compare the measurements taken between the ultrasonic measurement

and the previously mentioned measurements. ASTM E494 – 10 was followed for the ultrasonic measurement of modulus of elasticity for EDCC cylinders.

Figure 3-28: Proceq equipment in case

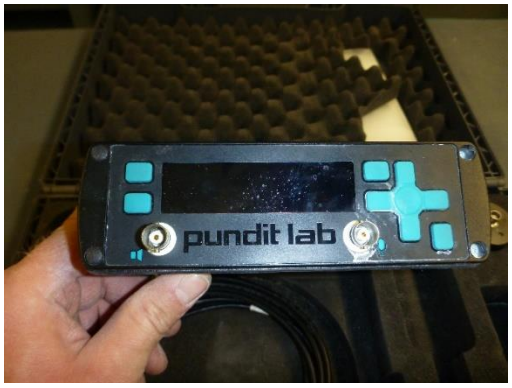

Figure 3-29: Proceq Pundit Lab front view

Figure 3-30: Proceq tranducer

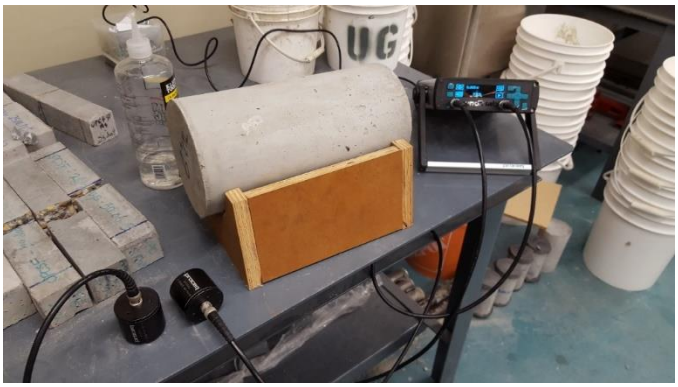

Figure 3-31: EDCC Cylinder in test setup for ultrasonic modulus of elasticity measurement

Figure 3-32: EDCC Cylinder being tested for ultrasonic modulus of elasticity measurement

The results of these tests were not included in the published work, although it does pose an interesting option for future researchers to quantify the modulus of elasticity through non-destructive testing.

4 Experimental Results

4.1 Compression Test

4.1.1 Practice Compression Test

A practice compression test was conducted to quantify the effectiveness of the testing procedure and the instrumentation. The test method worked effectively, and the resulting specimen can be seen in Figure 4-1 below. It was observed that crushing directly under the load plate took place, likely due to the sample discontinuity at the corners. Vertical cracking also took place, likely due to the transverse tensile stresses developed due to the Poisson effect. Refer to Figure 4-2 for the failed practice specimen. This is further reinforced by masonries inherent weakness in tension relative to its compressive capacity. The only method available for measuring total sample shortening (displacement) was the stroke values from the actuator, which included deformations in the Plaster of Paris capping material as well as the sample. The vertical displacement was measured using the stroke reading from the actuator. The load displacement curve observed during the test was not representative of the actual displacement in the sample due to the influence of the Plaster of Paris. Therefore, using machine stroke to measure strain is not acceptable due to the influence of the capping material.

Figure 4-1: Practice compression test specimen before test

Figure 4-2: Practice compression test specimen after test

While the practice test was performed with both strain gauges and pi gauges it was determined that for actual sample testing only pi gauges would be used to capture an average strain value across both the masonry unit and the mortar joint. Due to the number of tests being performed and the closeness in results between the strain gauges and pi gauges the actual tests were performed with only pi gauges. The purpose of the instrumentation was to capture the initial stiffness of the specimens, therefore the pi gauges could be removed during testing to prevent damage to the gauges.

4.1.2 Compression Tests on Plain and Strengthened Specimens

The compression specimens were placed in the testing machine with fiber board on the top and bottom to minimize the impact of surface imperfections. Steel plates was placed above and below the fiber board to spread the load from the spherical head of the actuator to the full cross-sectional area of the specimen. Marks were placed on the specimen at various heights to shoot a laser level along the vertical axis of the specimen to ensure that the specimen was placed level in the test setup. The top and bottom of the EDCC overlay was ground flush with the top of the substrate material to avoid stress concentrations on the EDCC and to attempt to share the load compositely between the masonry and the EDCC.

200 mm pi gauges were mounted on each face of the sample at mid height to capture strains in the samples during loading. The test setup can be seen schematically in Figure 4-3, the instrumentation can be seen in Figure 4-4, and an actual specimen can be seen in Figure 4-5. To prevent the gauges from being damaged, they were removed at approximately 70% of the ultimate load, after which the specimen was loaded to failure. One specimen, CPS10-6, seen in Figure 4-6,was instrumented with an additional 70mm concrete strain gauge on the East (strengthened) face. This gauge recorded strain until specimen failure. CPS30-7 and CPS30-8 (Figure 4-7) were instrumented with a single LVDT at the bottom, mid-height, and top of the East (strengthened) face. The LVDTs were mounted horizontally to measure any lateral movement exhibited by the specimen during loading. All three LVDTs were spring loaded to help reduce noise in the readings.

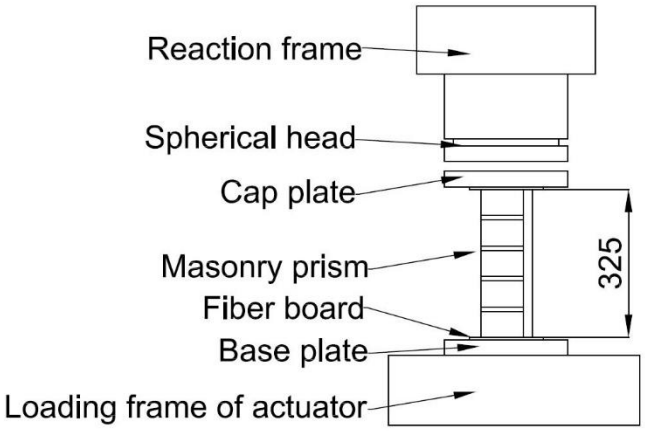

Figure 4-3: Schematic drawing of compression test

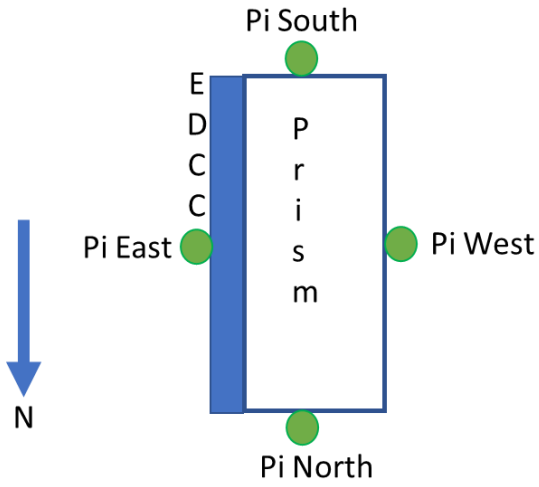

Figure 4-4: Schematic plan view of compression test instrumentation

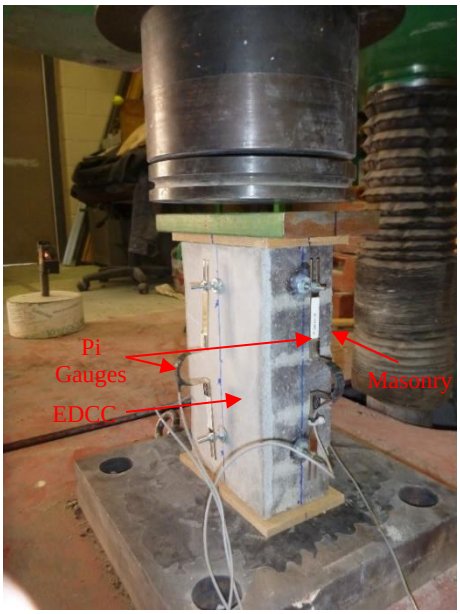

Figure 4-5: BPS10 in compression testing configuration

Figure 4-6: CPS10-6 strain gauge instrumentation

Figure 4-7: CPS30-7 LVDT instrumentation

Compression test results are presented below in Figure 4-8 to Figure 4-16. The instrumentation scheme allowed for the capture of strain on each side of the specimen. It is important to note that the stress-strain curves on each graph do not represent the ultimate stress that the specimens failed at, rather, it represents the point at which the Pi gauges were removed from the specimens. The purpose of the graphs are to measure stiffness.

During the testing, it appeared that the strengthened concrete block samples experienced some initial bending under axial loading, as displayed in Figure 4-10. This may be attributed to a shift in the centroid due to lack of cross-sectional symmetry of the specimen. If the load was not applied directly through the centroid, this eccentricity would create a moment, causing initial tension on the East (strengthened) side and compression on the West (unstrengthened) side. If there was in fact a moment imposed on the specimen, the ultimate compressive load is expected to be lower due to the theoretical axial load – moment interaction in compression members. Two CPS10 specimens have been shown (Figure 4-9 and Figure 4-10). It appears that there was less initial bending developed in CPS10-1 versus CPS10-6. It should also be noted that the top and bottom of the EDCC layer were ground down prior to testing to reduce stress concentrations on the EDCC. This likely caused the cap plate to impart load directly on the masonry, as opposed to a combination of the EDCC/masonry.

Deviations in gauge readings for each sample can possibly be attributed to the Pi gauges capturing mortar joints. It is not realistic to expect identical behaviour between each face of the specimens due to the possibility of imperfections in the mortar joints, the masonry – mortar interface, and the possibility of differential shrinkage cracks between each specimen face. In Figure 4-10 the positive jump in strain for Pi 28 (East) on CPS10-6 was due to an instantaneous error where the gauge was physically disturbed during the test, the compressive strain pattern is still followed after the error. The modulus of elasticity was taken as the chord modulus measured along an effectively linear portion of the stress strain curve.

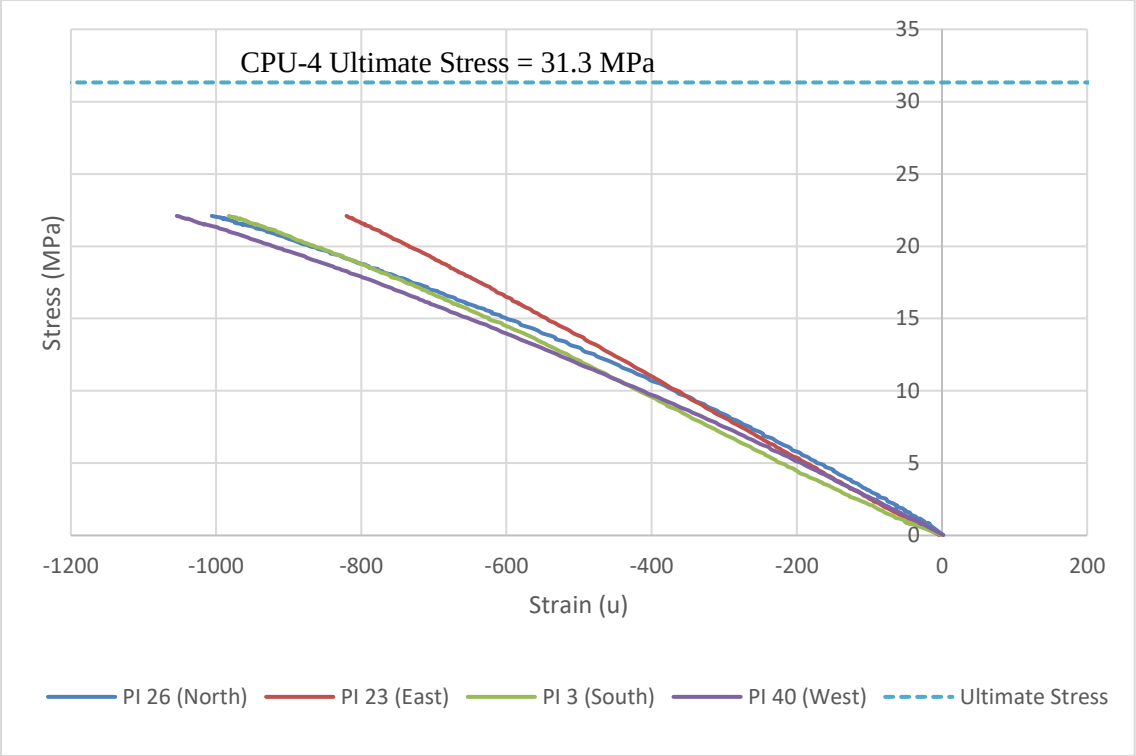

Figure 4-8: CPU-4 stress-strain plot

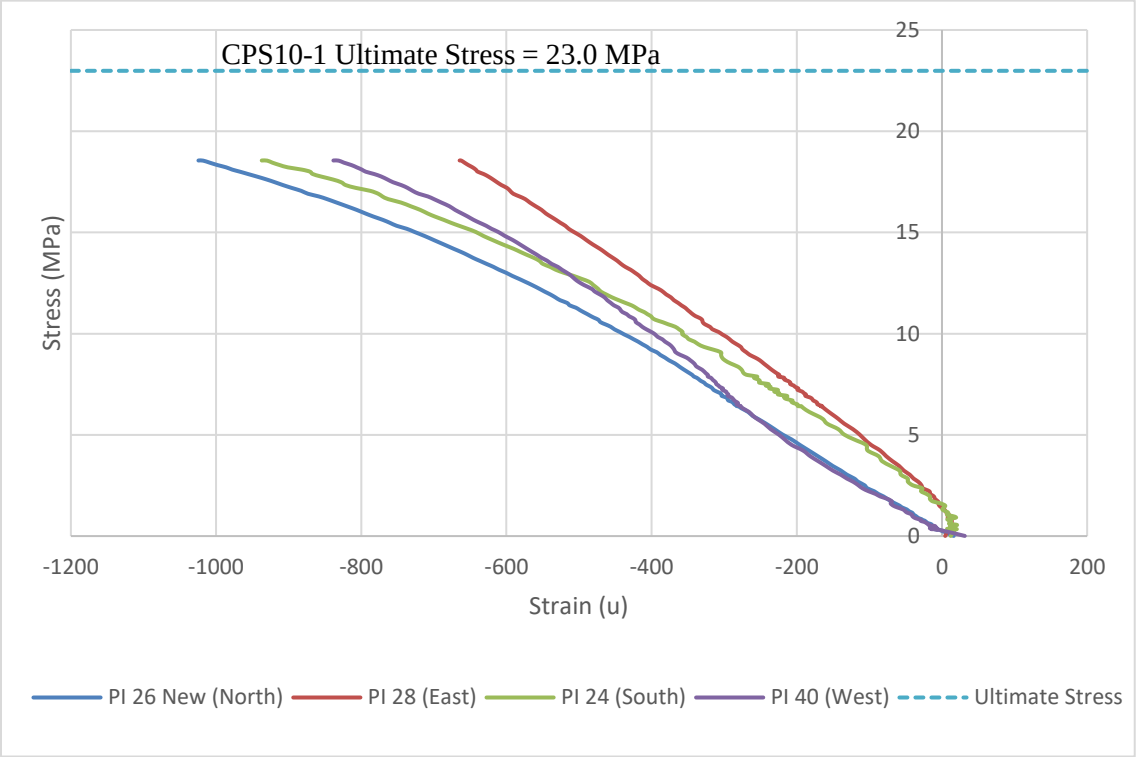

Figure 4-9: CPS10-1 stress strain plot

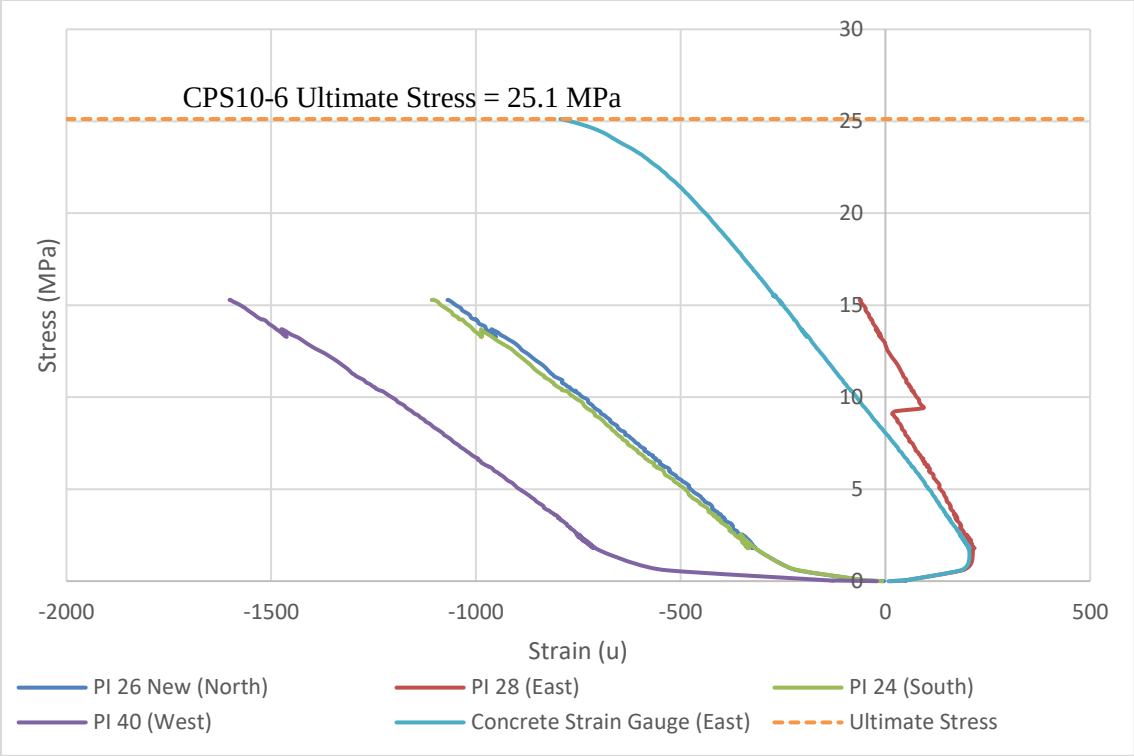

Figure 4-10: CPS10-6 stress-strain plot

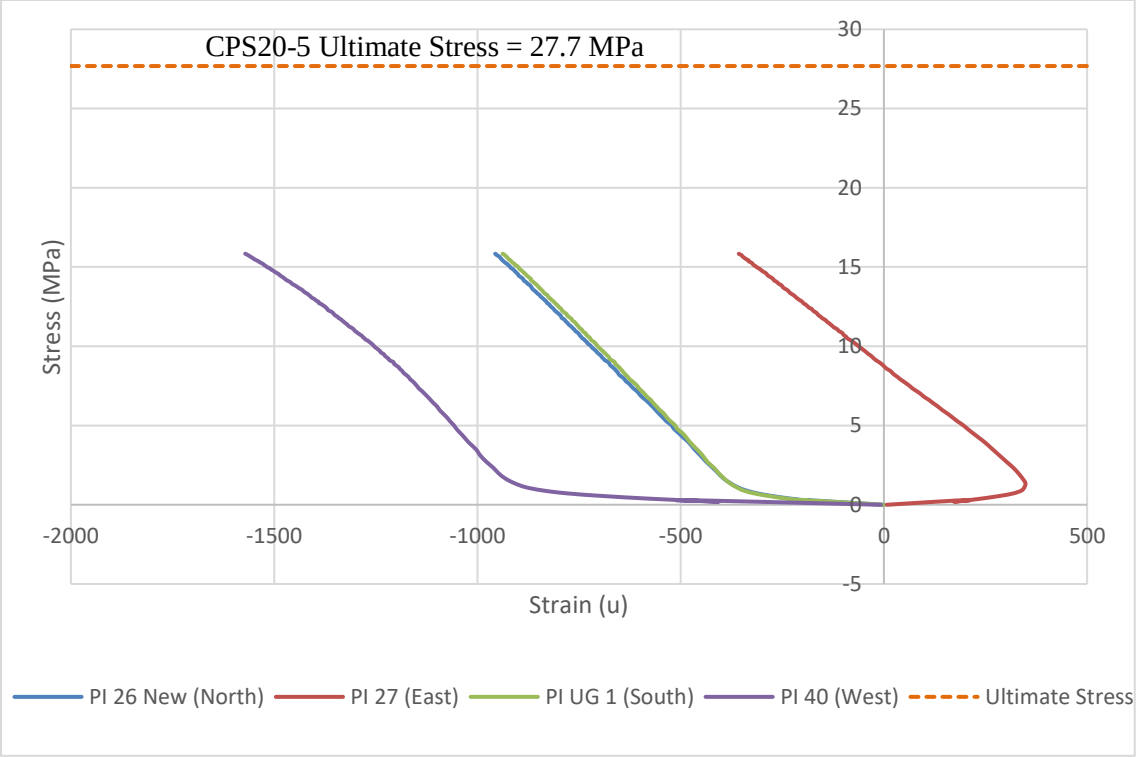

Figure 4-11: CPS20-5 stress-strain plot

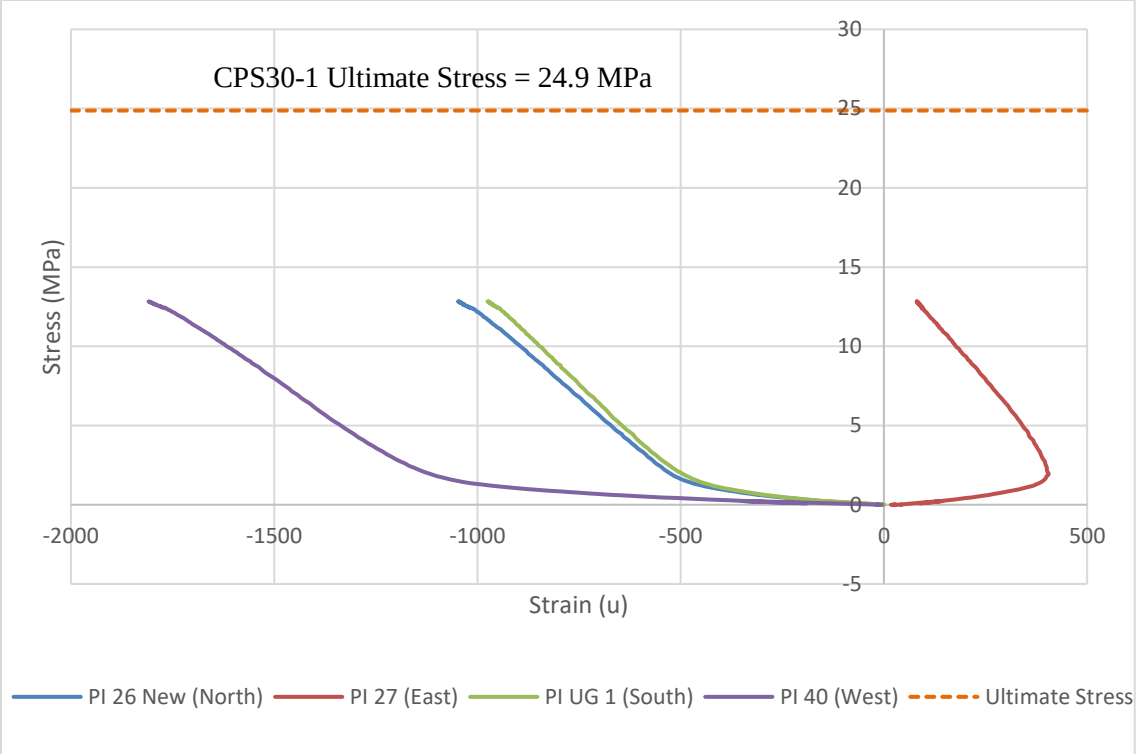

Figure 4-12: CPS30-1 stress-strain plot

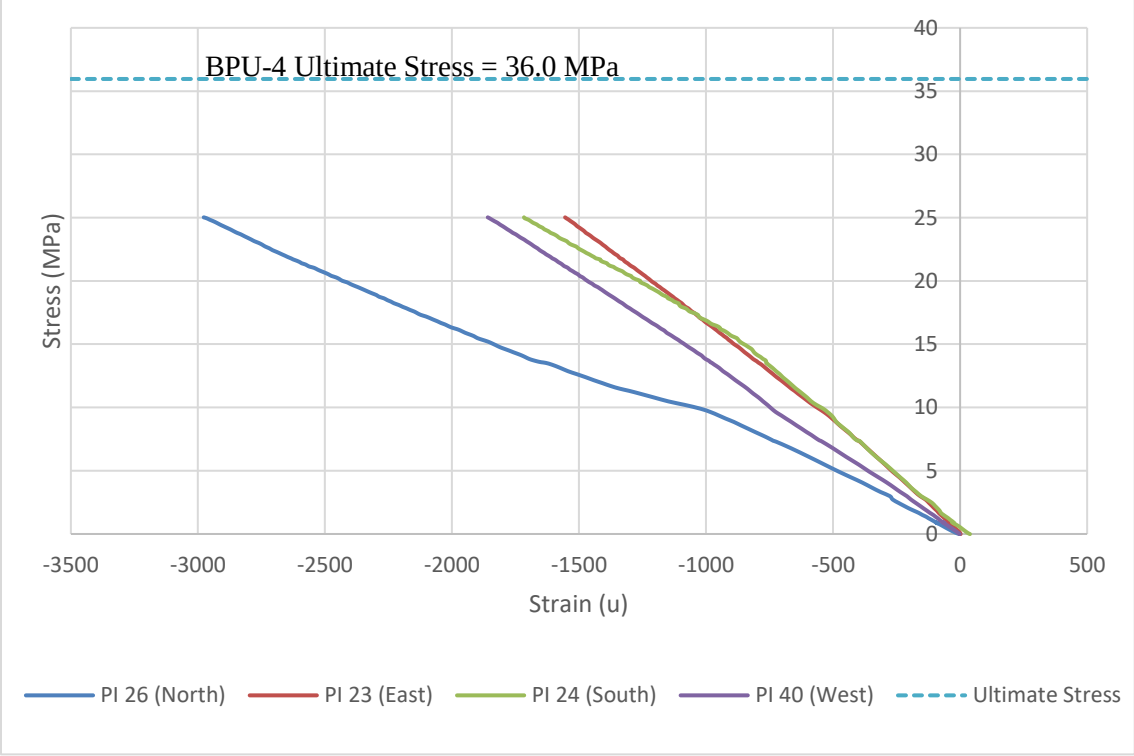

Figure 4-13: BPU-4 stress-strain plot

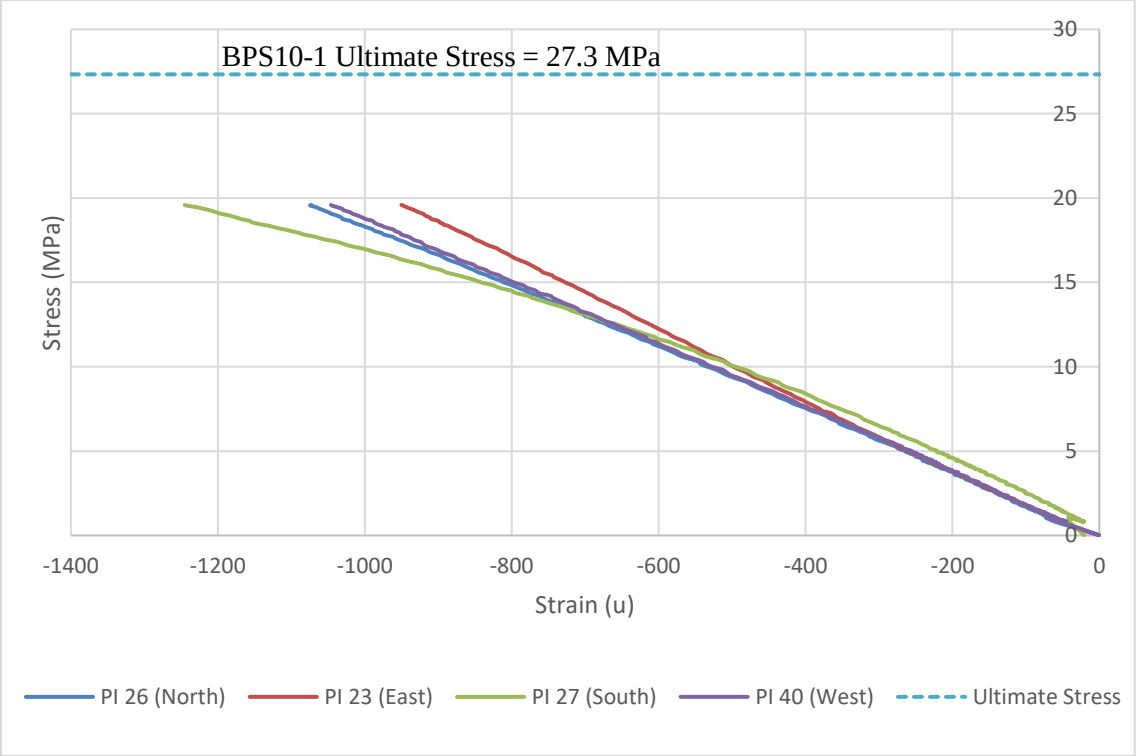

Figure 4-14: BPS10-1 stress-strain plot

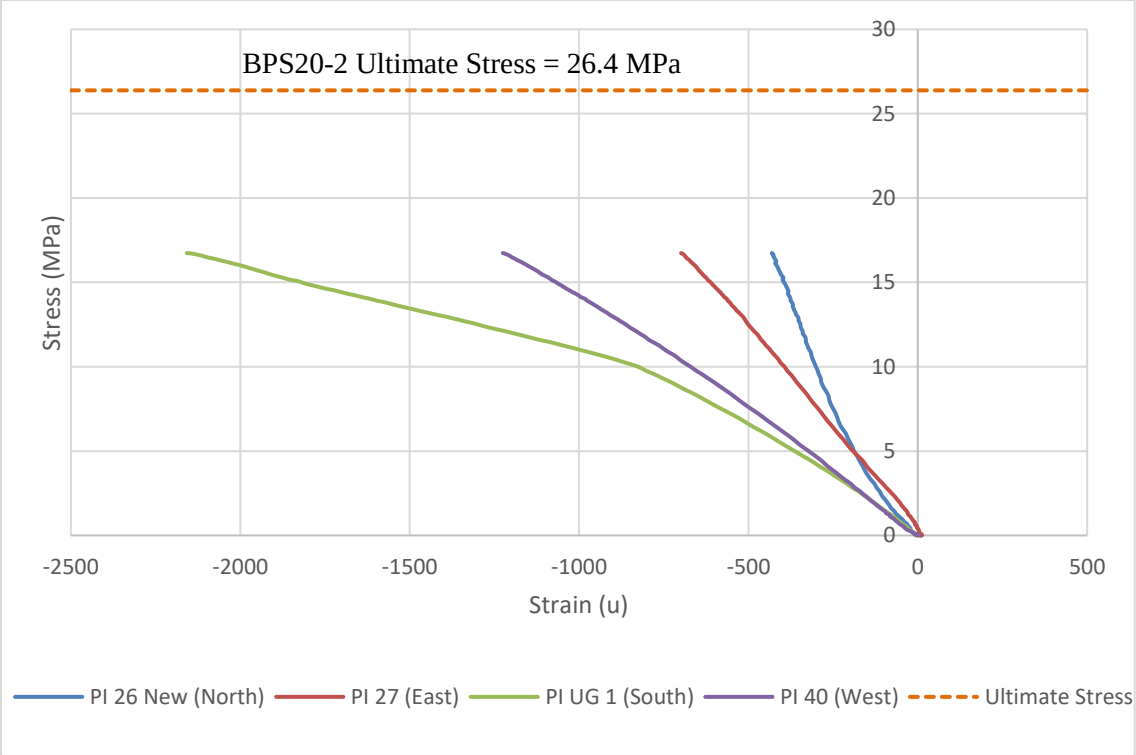

Figure 4-15: BPS20-2 stress-strain plot

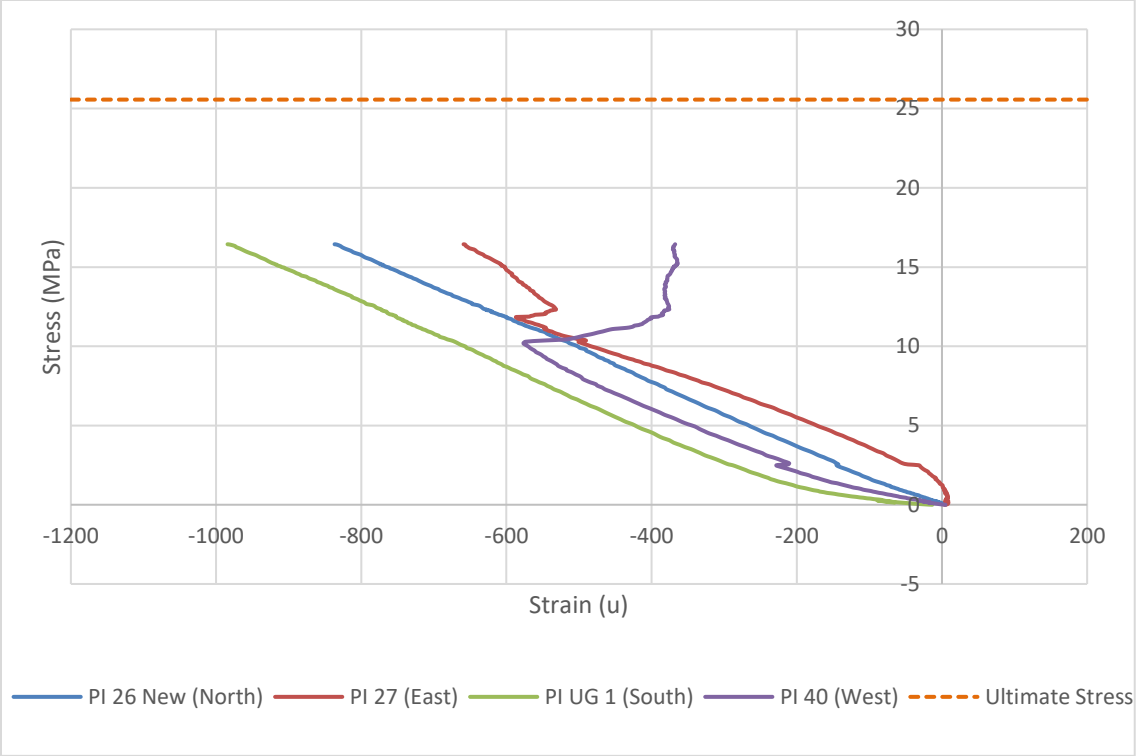

Figure 4-16: BPS30-5 stress-strain plot

The results from the strengthened masonry tests indicate that delamination of EDCC is occurring at failure. A technique that can be utilized to improve the mechanical bond between the surfaces is to prepare the masonry face by using a roughening technique, such as sand blasting. This may have negative effects on the mortar joints however, which may not have as high of abrasion resistance as the masonry. Wetting the masonry surface prior to application of the EDCC is also beneficial due to the masonry absorbing water if it is not saturated. By absorbing water, the masonry would take some of the mixing water from the EDCC causing a weak layer of EDCC at the interface which could result in delamination.

The failure of most the specimens consisted of crushing of the masonry and delamination of the EDCC from the face of the masonry. An example of this can be seen in Figure 4-17. Some minor deposits of brick and mortar can be seen on the EDCC layer, indicating areas

of increased bond, but the majority of the EDCC has delaminated. No visible deposits of EDCC are present on the brick face.

Figure 4-17: Typical delamination of EDCC from brick prism

In Table 4-1, average values for ultimate load and ultimate stress are shown. These results are also shown graphically in Figure 4-18 and Figure 4-19. The ultimate load carried by the unstrengthened and strengthened CMU specimens was approximately the same. However, the stress carried by the strengthened CMU specimens was lower, due to the inclusion of the EDCC in the area calculation. The unstrengthened brick specimens had a lower average load, but a higher ultimate stress compared to the CMU specimens. The strengthened brick specimens carried more load than the unstrengthened brick specimens, but the stress remained approximately the same for each EDCC thickness.

Table 4-2 shows the average modulus of elasticity results for each type of tested specimen. The column noted as “E” was prepared by using only the pi gauges that seemed to remain linear and show an increase in compressive strain throughout the testing. The column noted as “E (N/S)” shows the modulus of elasticity determined with only the North and South pi gauges. The column noted as “E (N/S/W)” shows the modulus of elasticity determined with only the North, South and West pi gauges. The reason for showing three different

values is that for the strengthened specimens it was typical to see the East (strengthened) face of the masonry exhibit little to no compressive stress. This could possibly be attributed to the EDCC restraining the deformation in the East face of the masonry, resulting in the bending of the specimen (larger compressive strains recorded on the West face). The decrease in modulus of elasticity of the brick specimens, when compared to the CMU specimens, may be attributed to the capture of four mortar joints by the pi gauges versus only one mortar joint on the CMU prisms, assuming the mortar joint is less stiff than the masonry.

Table 4-1: Compression test results

	Pult (kN)	St.Dev (kN)	σult (MPa)	St.Dev (MPa)	Number of Specimens
CPU	703.5	80.4	28.7	3.3	8
CPS10	701.7	59.9	24.1	2.0	8
CPS20	780.2	61.4	24.2	2.0	8
CPS30	738.9	78.6	20.3	2.1	6
BPU	652.3	63.0	35.6	3.4	8
BPS10	508.2	47.9	24.6	2.2	8
BPS20	557.1	37.5	24.9	1.8	8
BPS30	611.2	39.0	24.9	1.7	7

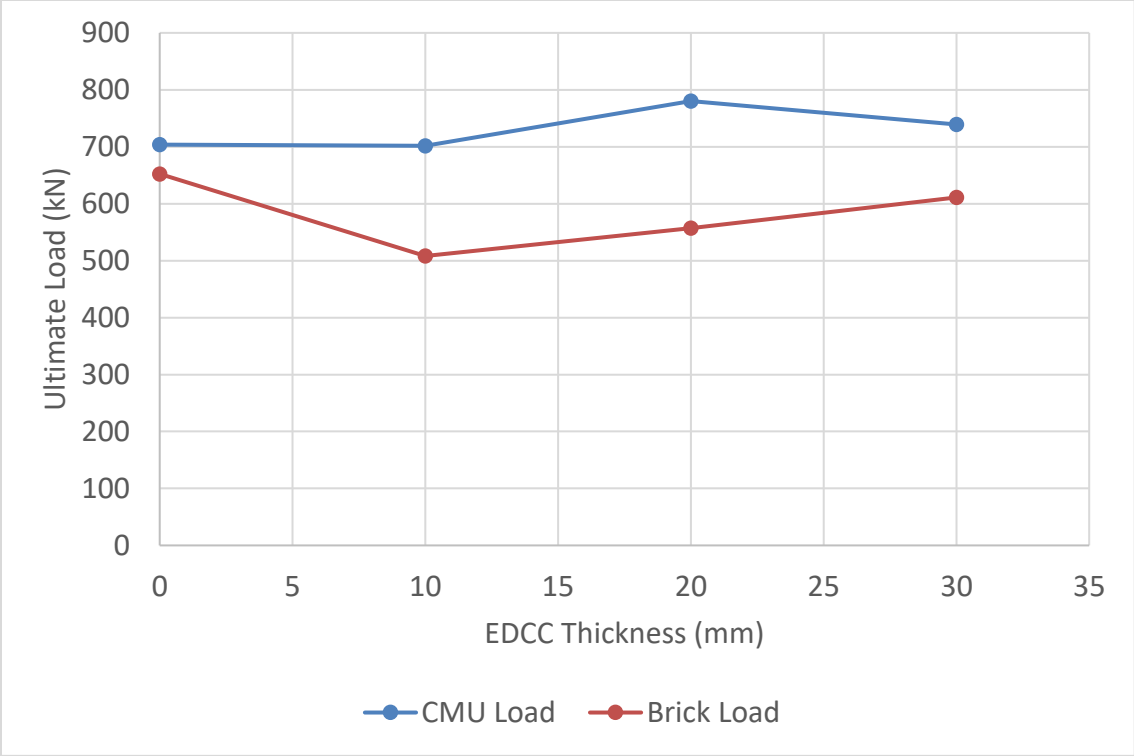

Figure 4-18: Ultimate load compression test results

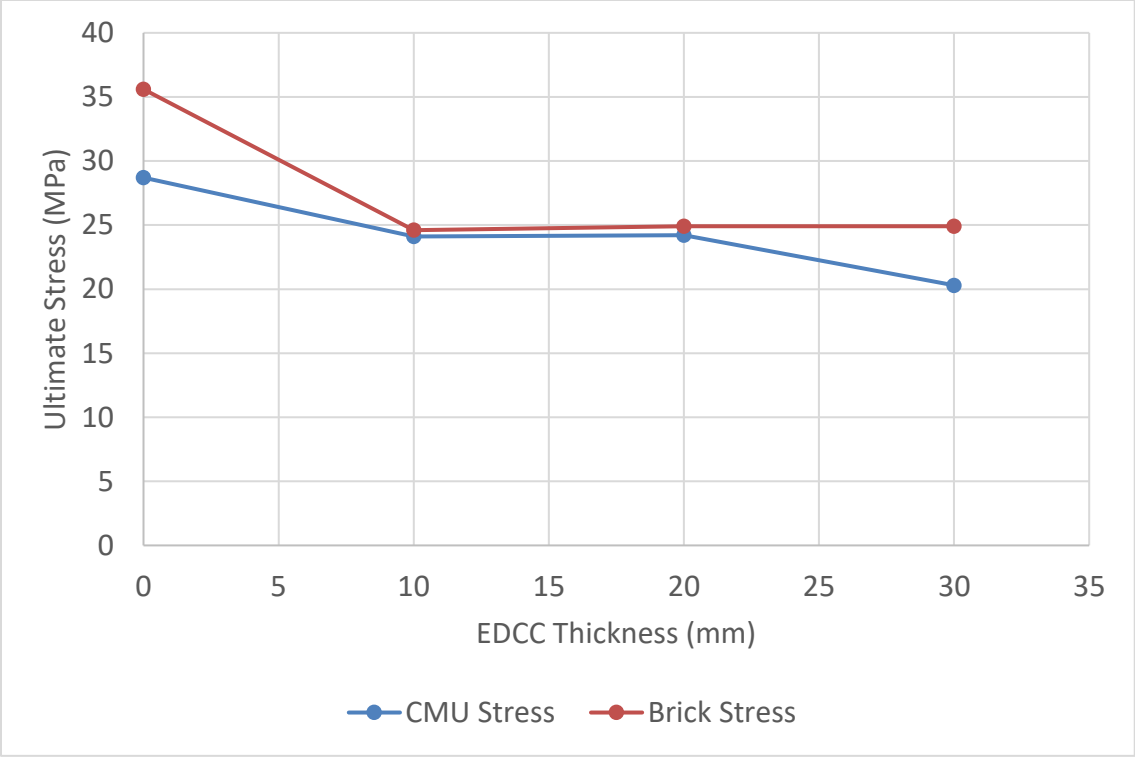

Figure 4-19: Ultimate stress compression test results

Table 4-2: Compression test modulus of elasticity results

	E (MPa)	St.Dev (MPa)	E (N/S) (MPa)	St.Dev (MPa)	E (N/S/W) (MPa)	St.Dev (MPa)	Number of Specimens
CPU	28386	2745	25923	3273	27891	3742	7
CPS10	23126	1722	21042	3409	21747	2957	8
CPS20	25551	3932	21874	3359	20929	4498	8
CPS30	30091	7023	21756	781	19582	358	6
BPU	18842	2450	19377	2699	18076	2953	7
BPS10	21277	4309	26280	12847	23660	9437	8
BPS20	16900	2356	18061	1581	16583	1792	8
BPS30	15653	4063	14831	2977	14564	2816	7

Special compression tests were performed on CPS30-7 and CPS30-8. CPS30-8 was instrumented with the typical pi gauge configuration, one on each respective face, but was also instrumented with three LVDTs, two of which were spring loaded 50mm LVDTs and one spring loaded 3mm LVDT. These were placed along the vertical centreline of the EDCC strengthened side of the prism. The 3mm LVDT was placed approximately 50mm from the top, one of the 50mm LVDTs was placed at mid-height, and the final 50mm LVDT was placed approximately 50mm from the bottom of the prism. This was done to capture the lateral movement of the specimen during the loading. Given that some of the strengthened specimens exhibited some bending due to their cross section the LVDTs were placed to determine if the specimen was displacing laterally during testing. Figure 4-20 and Figure 4-21 show the stress-strain plot and the stress-displacement plot respectively.

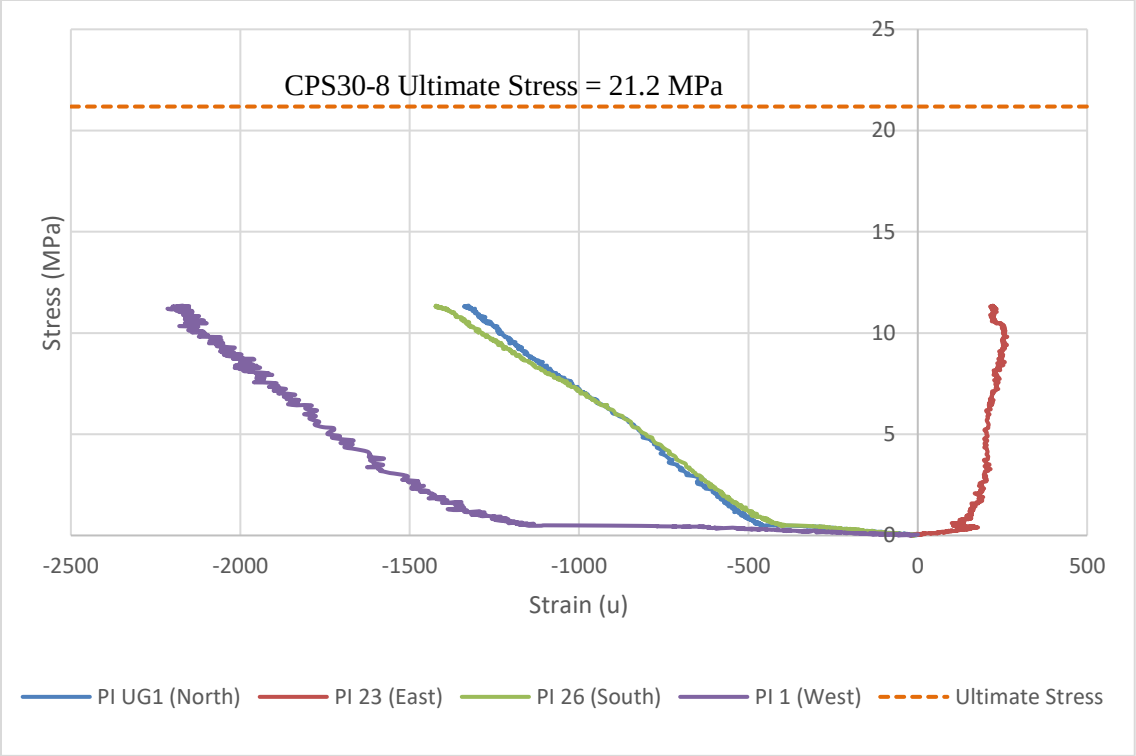

Figure 4-20: CPS30-8 stress-strain plot

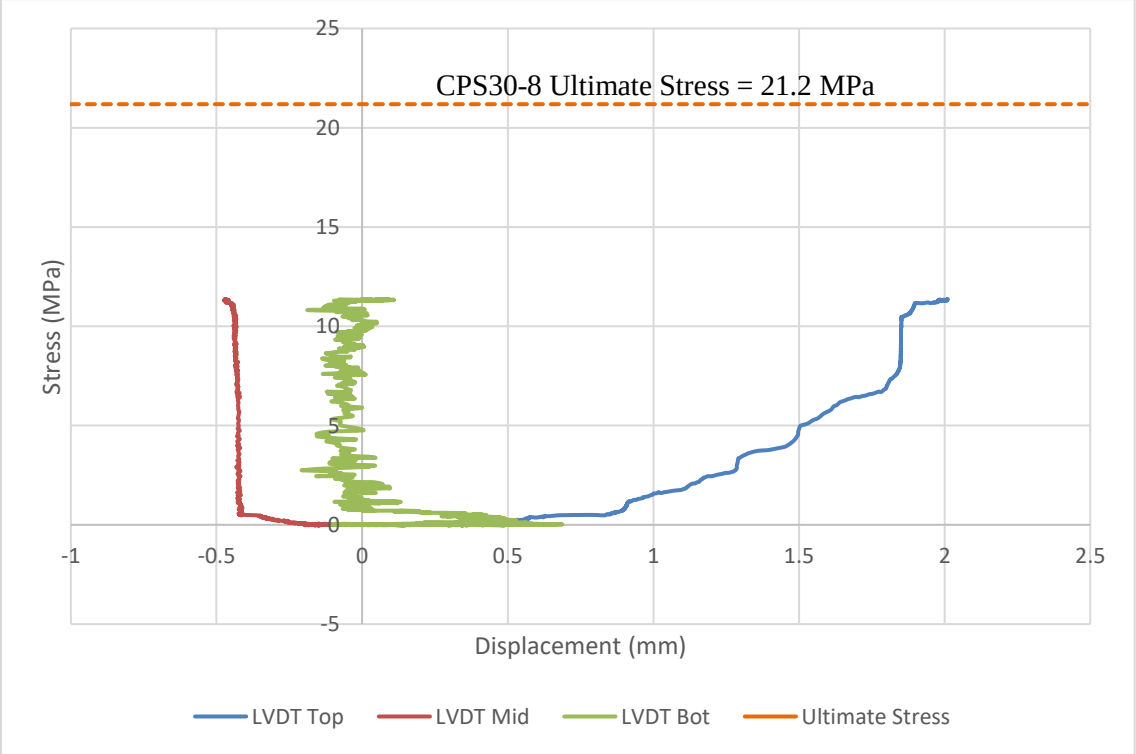

Figure 4-21: CPS30-8 stress-displacement plot

CPS30-7 was strengthened on both sides to make the specimen doubly symmetric. This specimen was also instrumented with LVDTs and pi gauges to capture the vertical straining and lateral displacement. The strengthening and instrumentation can be seen in Figure 4-22. It appeared that delamination occurred between the EDCC and the substrate at approximately 3.9 MPa. Figure 4-23 and Figure 4-24 show the stress-strain plot and the stress-displacement plot respectively. The failure shown in Figure 4-25 shows that the strengthening material delaminated from the substrate on both faces.

Figure 4-22: CPS30-7 in compression test setup

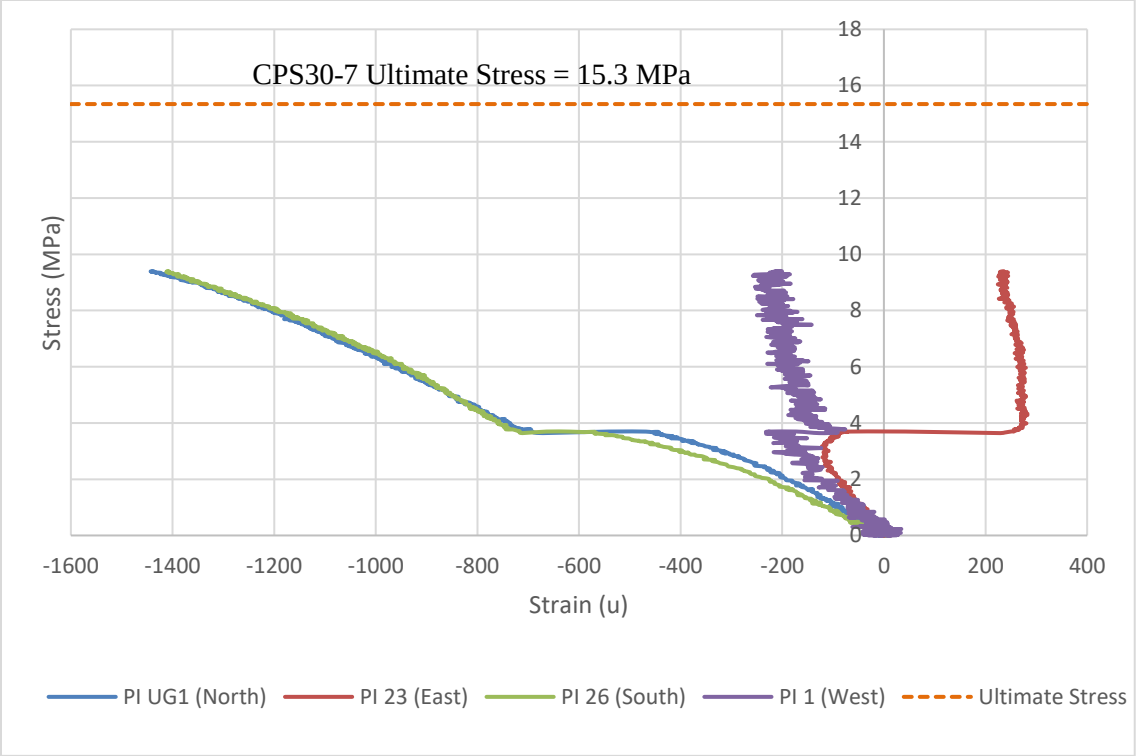

Figure 4-23: CPS30-7 stress-strain plot

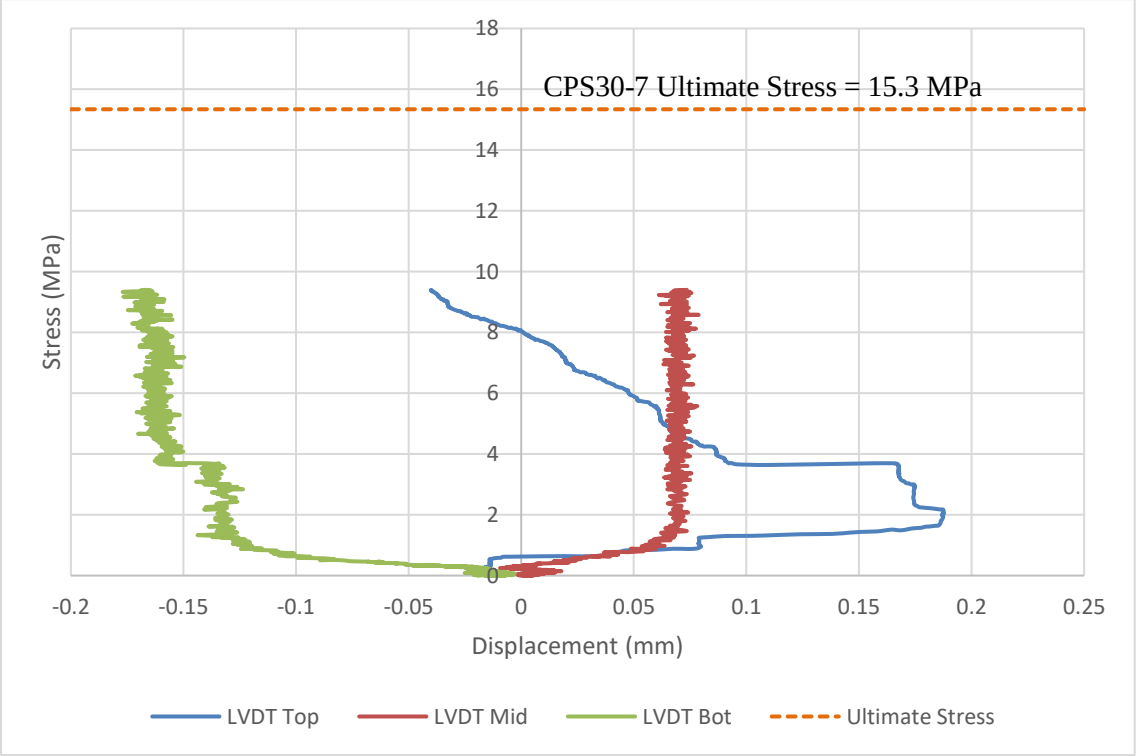

Figure 4-24: CPS30-7 stress-displacement plot

Figure 4-25: CPS30-7 after testing

By applying EDCC to one side only of the specimen the cross section becomes singly symmetric, resulting in a change in the location of the centre of mass. This means that by imposing an axial load if it was not through the centroid an additional moment would be imposed on the specimen. An additional moment imposed on the specimen would induce compression and tensile forces on the extreme fibers of the specimen, which would cause premature failure relative to failure occurring from pure axial load.

It was observed for the specimen that was strengthened on both sides that both sides strengthened with EDCC experienced delamination. The EDCC did not fail in these tests, yet the masonry crushed.

4.2 Flexure Test

The flexural tests were performed on strengthened and unstrengthened specimens. For each test, the specimens were instrumented with two 50mm LVDTs mounted at mid height at each lateral edge of the specimen and a 3mm LVDT mounted at mid height and mid width. The LVDTs were all configured to be spring loaded to remove slack from the gauge

reading. For each specimen type (CBU, CBS10, CBS20, CBS30, BBU, BBS10, BBS20, BBS30) a single specimen was instrumented with a 70mm concrete strain gauge at mid height and mid width on the tension face to capture strains during testing up until failure. For the unstrengthened specimens, a 22 kN S shaped load cell was used, for the strengthened specimens (except for CBS30 specimens) a 44 kN S shaped load cell was used, and for the CBS30 specimens the actuator controller load output was used due to the high capacity of the specimens. It was verified through the tests with the load cell that the actuator controlled load output was in good agreement with the load cell outputs.

The tests were conducted by first placing the specimen on the baseplate and positioning the roller to allow for proper base rotation during testing. The specimen was then clamped to the supports to position the load spreader properly against the specimen. Neoprene pads were used between the load spreader and the specimen to better distribute the load to the compression face of the masonry beam. The actuator was displaced until the spreader was flush against the specimen with only minimal load on the specimen. At this point the clamps were removed from the specimen, then the test program was run.

The actuator was run in displacement control at a displacement rate of 1 mm/min until the specimen failed (indicated by a significant drop in load), at which point the loading rate was increased to 6 mm/min to adequately displace the specimen prior to stopping the test. Despite the actuator running in stroke control, at the time of failure a significant crack occurred nearly instantaneously in some cases with only minor cracking visible along the mortar-masonry interface and laterally along the tension face of the EDCC, this resulted in a large deformation and a significant drop in load almost instantaneously at failure. It is for this reason that the load-deflection curves have been terminated at the time of sudden

failure, as the deformation observed is not representative of the amount of available deformation in the specimen.

The typical failure mode observed was cracking at the masonry-mortar interface and a lateral crack forming in the EDCC at approximately the same height as the masonry-mortar crack. An example of a strengthened brick beam can be seen in Figure 4-26, and the failure at midspan of the beam can be seen in Figure 4-27. In some instances, vertical delamination occurred along the EDCC-substrate interface. All the failures occurred between the applied loads in the maximum bending moment region. It was observed that the crack in the masonry substrate would always occur at the unit-mortar interface. Occasionally the crack would propagate from one brick-mortar interface to the other brick-mortar interface in the same mortar joint. The crack that formed in the EDCC would be near the mortar joint but would not always occur at the same height. This can possibly be attributed to the weak interface bond between the EDCC and the masonry substrate. If a weaker section of EDCC was near the mortar joint the crack may have propagated through the interface to the plane of EDCC weakness. Improving the bond strength would help alleviate this issue.

Figure 4-26: Strengthened brick beam in test setup

Figure 4-27: Example of brick beam failure at mortar joint and EDCC

Table 4-3 shows the average loads recorded for each specimen type, taken as the average of the ultimate loads applied to each specimen type. Figure 4-28 shows these results graphically. The theoretical loads are also reported, which have been calculated using the material properties determined from the materials testing performed during this testing program. The calculation for the theoretical load is shown in Appendix A: Theoretical Analysis of Flexural Specimen. It is important to note that both the split cylinder tensile test performed on the EDCC cylinder and the flexural test performed on the EDCC prism both reported high ultimate tensile stress in the EDCC, which yielded higher theoretical load calculations. In corresponding with researchers at the University of British Columbia, who

performed direct tension tests on EDCC (discussed further in 4.3.2), it was determined that the direct tension ultimate strength would yield theoretical flexural capacities in agreement with the testing program. Given that the failure in the beam occurred at the mortar joint, it is possible that the EDCC in that area experienced direct tension due to the bond remaining between the masonry and the EDCC directly above and below the mortar joint.

Table 4-3: Flexural test results and theoretical loads

Specimen	Average Load (kN)	Theoretical load (kN)	Number of Specimens
CBU	1.35	-	4
CBS10	15.12	12.30	5
CBS20	27.47	25.10	6
CBS30	36.16	38.80	6
BBU	2.18	-	7
BBS10	8.77	6.20	6
BBS20	12.83	12.50	6
BBS30	17.77	19.20	6

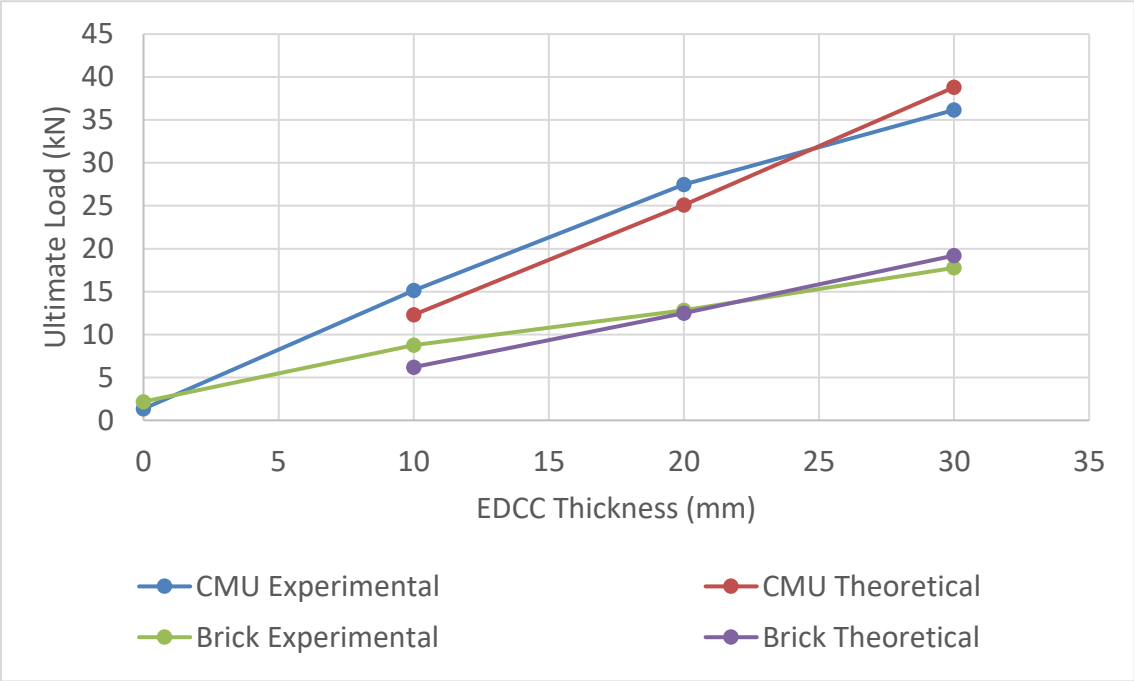

Figure 4-28: Flexural test results and theoretical loads

Table 4-4 shows the ratio of strength increase as the thickness of EDCC increases. The ratio values have been corrected by subtracting the unstrengthened average load from the strengthened average loads prior to calculating the ratio.

Table 4-4: Flexural specimen relative load ratios

Specimen	Average Load (kN)	Ratio
CBU	1.35	-
CBS10	15.12	1.00
CBS20	27.47	1.90
CBS30	36.16	2.53
BBU	2.18	-
BBS10	8.77	1.00
BBS20	12.83	1.62
BBS30	17.77	2.37

It can be seen in Figure 4-29 that as the thickness of EDCC increased on the tension side of the specimen the average ultimate load carrying capacity rises. The ratio is taken with respect to the 10mm EDCC strengthened specimens to better see the impact of EDCC thickness. The ratios have also been corrected by deducting the unstrengthened specimen capacity to obtain a direct ratio for EDCC thickness. It may have been thought that the doubling of EDCC thickness would double the capacity but that was not the case. This could be attributed to flaws being present in the EDCC at larger volumes of material.

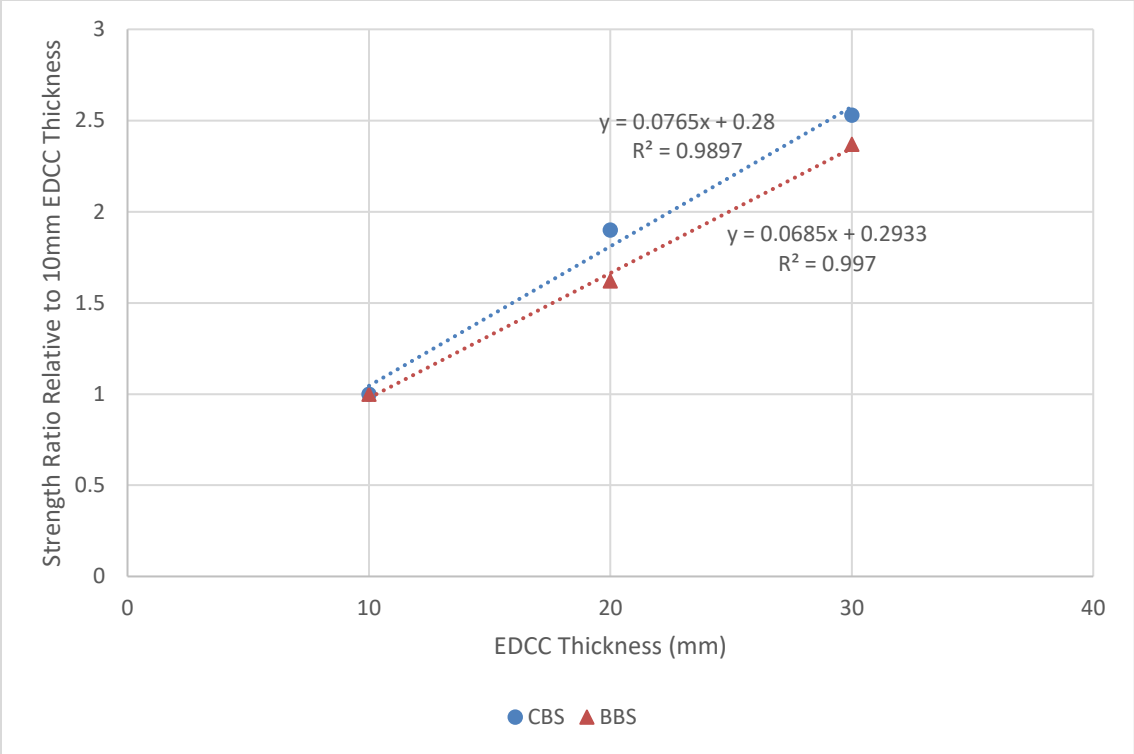

Figure 4-29: EDCC thickness vs strength ratio of strengthened masonry beams

For the CBS specimens (Figure 4-30 to Figure 4-35), it appeared that with an increase in thickness of EDCC there is an increase in the deformation that occurred prior to failure due to yielding, where the load is constant. It appeared that during the loading the stiffness increased in the specimen. This result was unexpected as the inertia of the specimen would most likely be decreasing during loading due to the presence of cracks forming in the EDCC and the tension side of the mortar-masonry interface. The materials tests performed on the EDCC did not show any signs of an increase in stiffness while loading. If the specimen was restrained at all from rotation at the supports experimental error may have been introduced into the results in the form of an increase in stiffness. The supports were constructed using hollow structural section pin supports, with the base support as a roller. If during testing the supports restrained the specimen from rotating the test results would be affected (Drysdale & Hamid, 2005).

For the setup of the masonry beams, once the sample was in place the neoprene pads were glued to the face of the sample that was to receive the actuator spreader. The sample was clamped to the supports to position it properly and to extend the actuator until it just started to read a small magnitude of load output, indicating that the actuator was in contact with the neoprene pads. Once the sample and actuator were in this position, the clamps were removed and the actuator load output was zeroed. It is possible that due to the tolerances in the pinned/roller supports the specimen would be able to displace as a rigid body prior/during rotational displacement. The way that the LVDTs were positioned, they would record both forms of displacement. This is one possible explanation for the change in slope of the load deflection curve. Initially, the curve shows a combination of specimen rotation and overall specimen translation up until the rigid body motion is terminated by the supports losing their slack. This is one potential drawback to performing the testing with the samples oriented in the vertical direction. There may have been other contributing factors aiding in the change in slope of the load deflection curve not indicated in this thesis.

The brick specimens showed a larger deformation at constant load relative to the CMU specimens. This is likely since the number of mortar joints intercepted by the constant moment region was three, compared to the one mortar joint intercepted for the CMU specimens. Given that all flexural specimen failures occurred by tensile failure of the mortar-masonry interface and tensile failure of the EDCC by having more mortar joints in the constant moment region there are more planes of potential weakness to allow for the EDCC to resist cracking, although stress concentrations in the EDCC are likely present at the mortar-masonry joint.

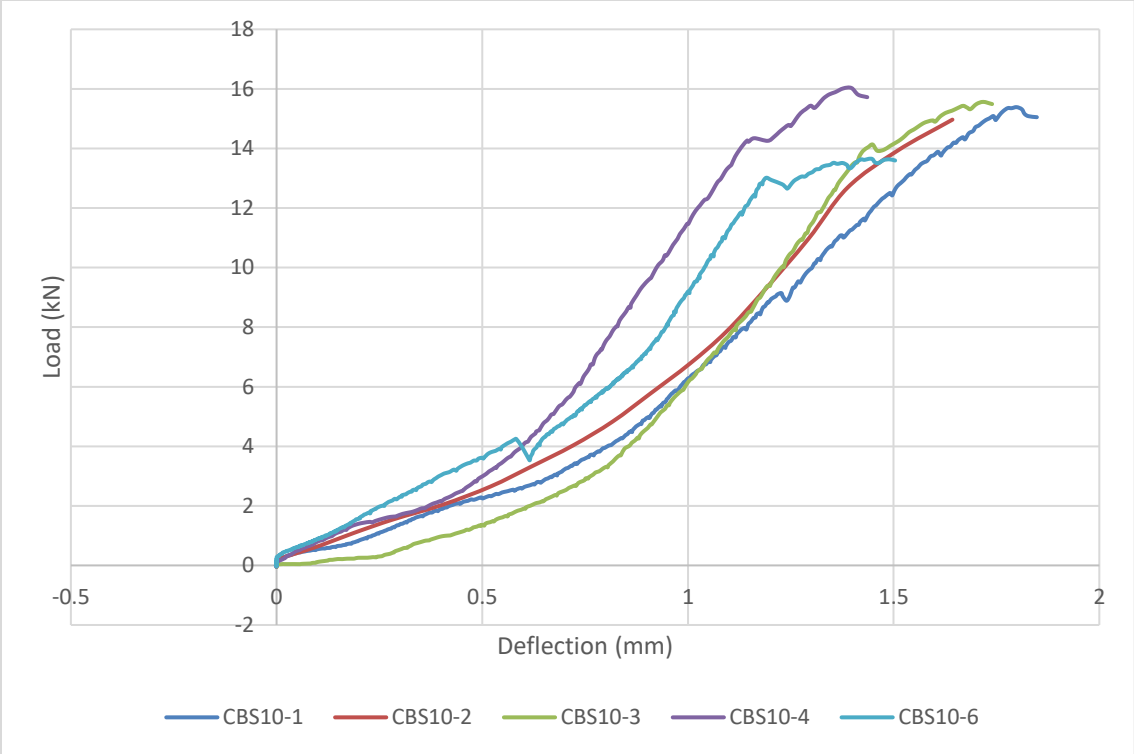

Figure 4-30: CBS10 load-deflection plots

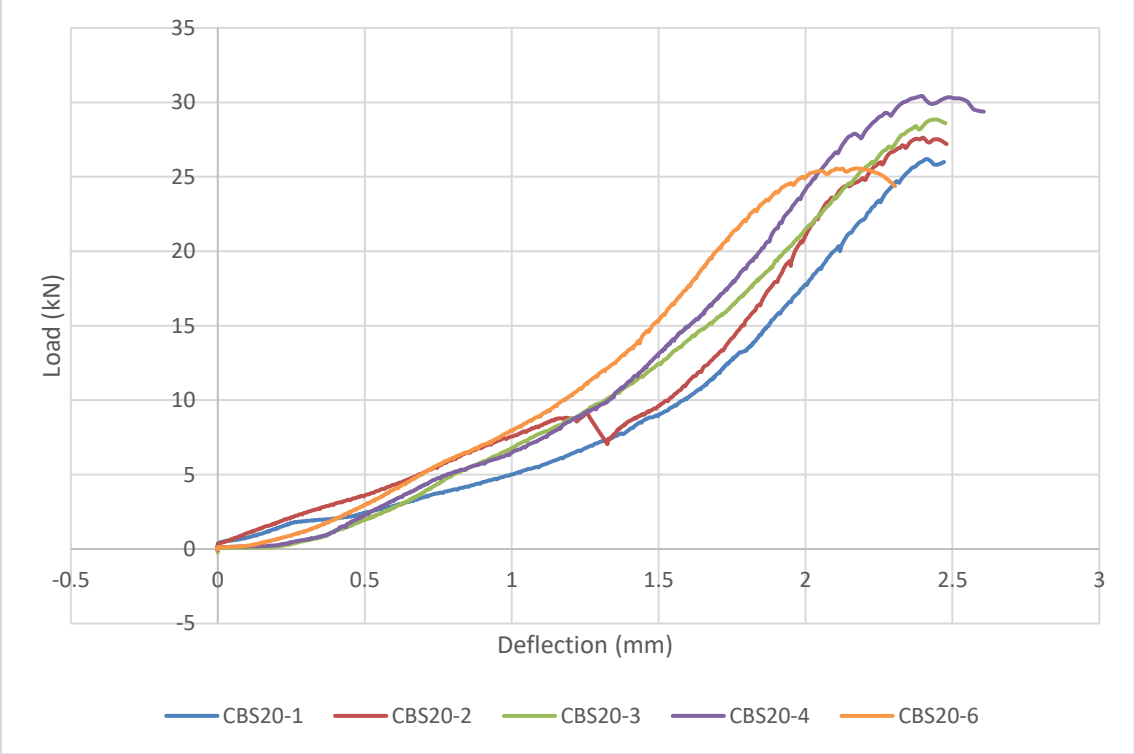

Figure 4-31: CBS20 load-deflection plots

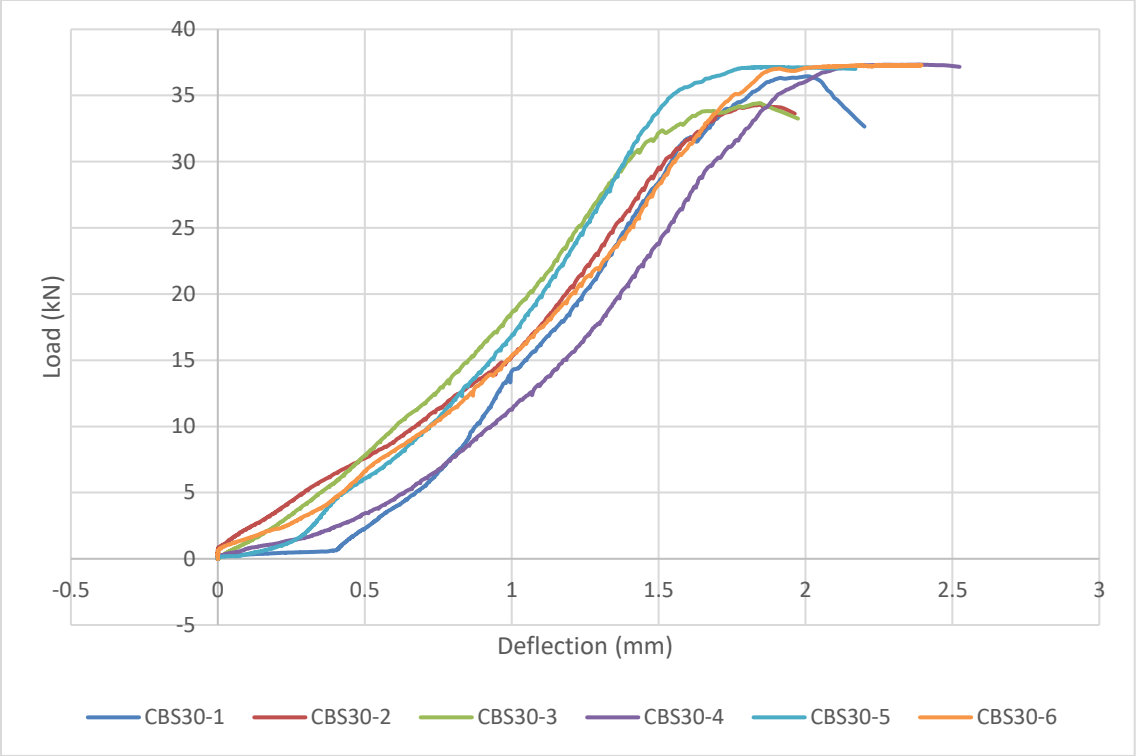

Figure 4-32: CBS30 load-deflection plots

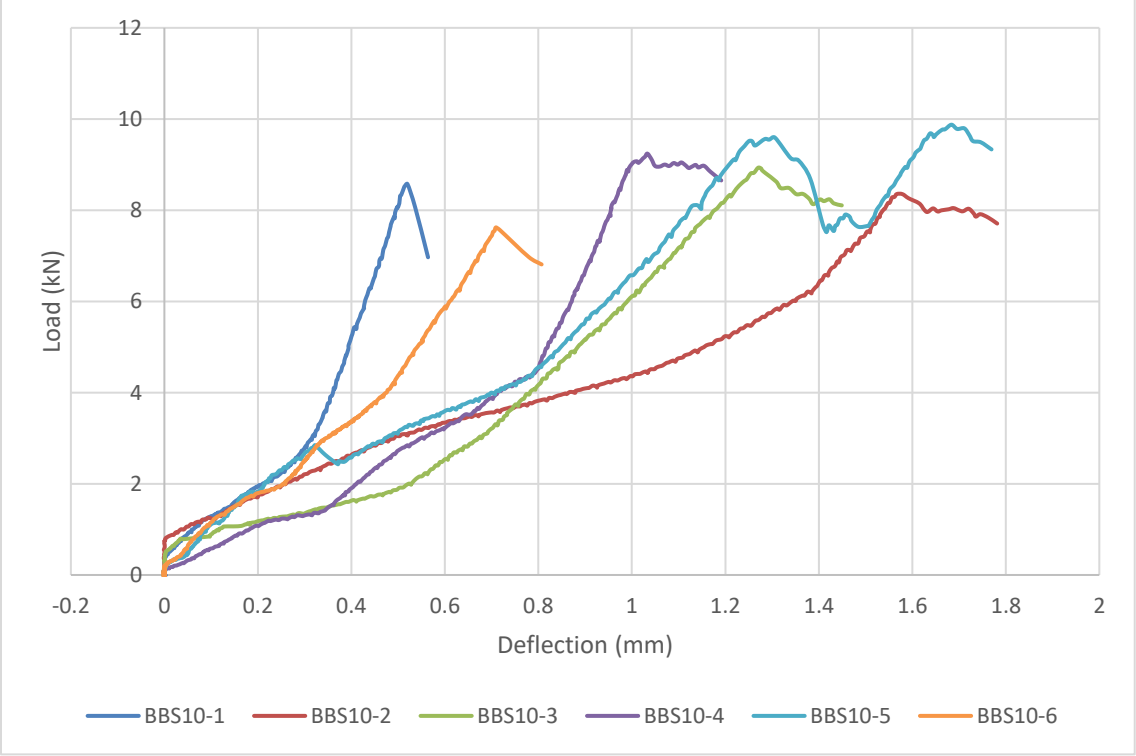

Figure 4-33: BBS10 load-deflection plots

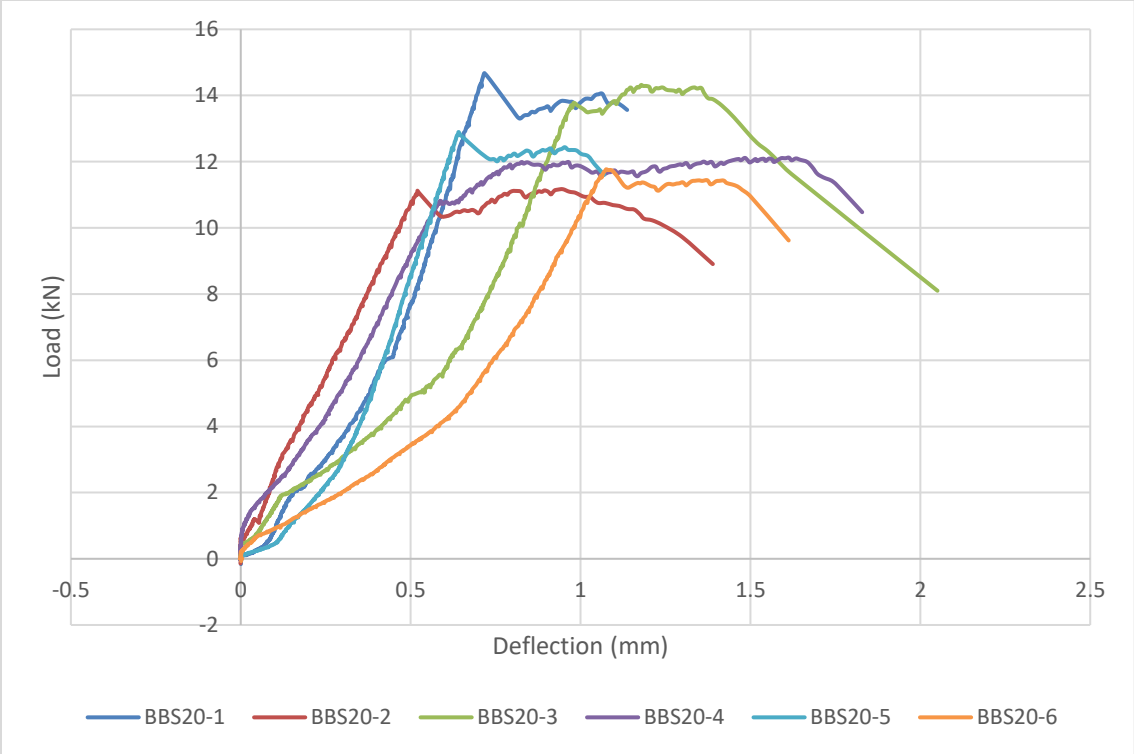

Figure 4-34: BBS20 load-deflection plots

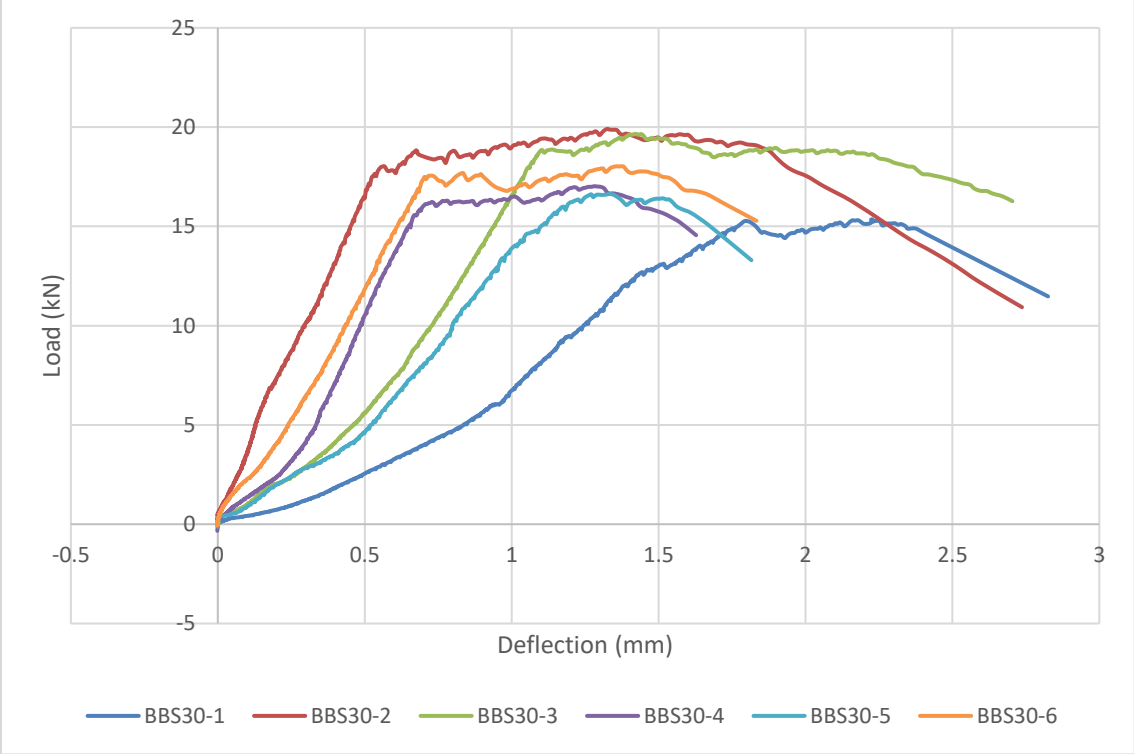

Figure 4-35: BBS30 load-deflection plots

4.3 Materials Testing

Individual materials tests were done to better quantify the material properties of the constituent materials. By doing this, the values could be used in the computer models to better predict the response and behaviour of the plain and strengthened masonry assemblages. It also allowed for hand calculations to be performed with accurate constituent properties to verify the assumed behaviour of the specimens.

4.3.1 Mortar Cubes

Individual mortar cubes were cast in steel molds at the time of unstrengthened specimen construction and tested periodically throughout the compression and flexural testing programs. The mortar cubes were tested in a 300 kN Instron 300DX testing machine at a loading rate of 1 kN/s, seen in Figure 4-36 and Figure 4-37. The cubes were placed atop a steel base plate and capped with a small steel plate. The load was applied with a spherical head mounted to the testing machine. The results of the mortar cubes can be seen in Table 4-5.

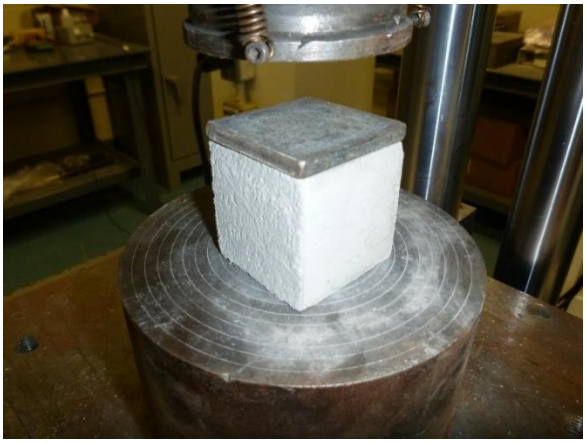

Figure 4-36: Mortar cube with steel cap plate

Figure 4-37: Mortar cube in test setup

Table 4-5: Mortar cube strength properties

Specimen Type	# of Specimens	Ultimate Stress (MPa)	Standard Deviation (MPa)
Mortar Cubes	29	28.0	4.8

4.3.2 EDCC Prisms

EDCC rectangular prisms were cast in steel molds during the specimen strengthening phase. The dimensions of the specimens were 75mm x 75mm x 300mm. These prisms were tested in a four-point bending configuration in the Instron 300DX testing machine, as seen in Figure 4-38. The actuator was run in displacement control to measure the descending branch of the load deflection curve. The supports were spaced 254 mm apart to allow for proper bearing and a slight overhang of the specimen. The distance from the supports to the nearest applied load was 83mm, and the distance between the point loads was 83 mm, yielding equal spacing. The prism was instrumented with a 3mm spring loaded LVDT and a 50mm spring loaded LVDT, as seen in Figure 4-39. Due to the space constraints it was not possible to mount the LVDTs directly to the specimen, therefore a bent angle spreader was hot glued and epoxied to the top of the EDCC beam at midspan. The displacement the specimen underwent would be matched by the angle. This allowed for the LVDTs to be

mounted to the angle and allowed for accurate displacement measurements. The load was applied via a spreader block made up of steel plates and rods welded together. A spherical head was mounted to the testing machine to prevent stress concentrations due to incorrect alignment between the loading equipment.

Figure 4-38: EDCC prism in test setup

Figure 4-39: EDCC prism instrumentation

Load was applied until the specimen was displacing under relatively small loads, indicating that the crack had formed in the tensile side of the EDCC and that the fibers had failed. It was observed that five of the six tests had flexural type failure, with a vertical crack forming in the middle third of the specimen. The sixth test had a diagonal shear crack form between

the support and the load point. The results are outlined in Table 4-6 and shown graphically in Figure 4-40.

Table 4-6: EDCC prism test results

Specimen	Ultimate Load (kN)	Standard Deviation (kN)	Deflection (mm)	Standard Deviation (mm)
EDCC Prism (Flexural Failure)	16.0	1.9	0.4	0.1
EDCC Prism (Shear Failure)	19.4	-	0.5	-

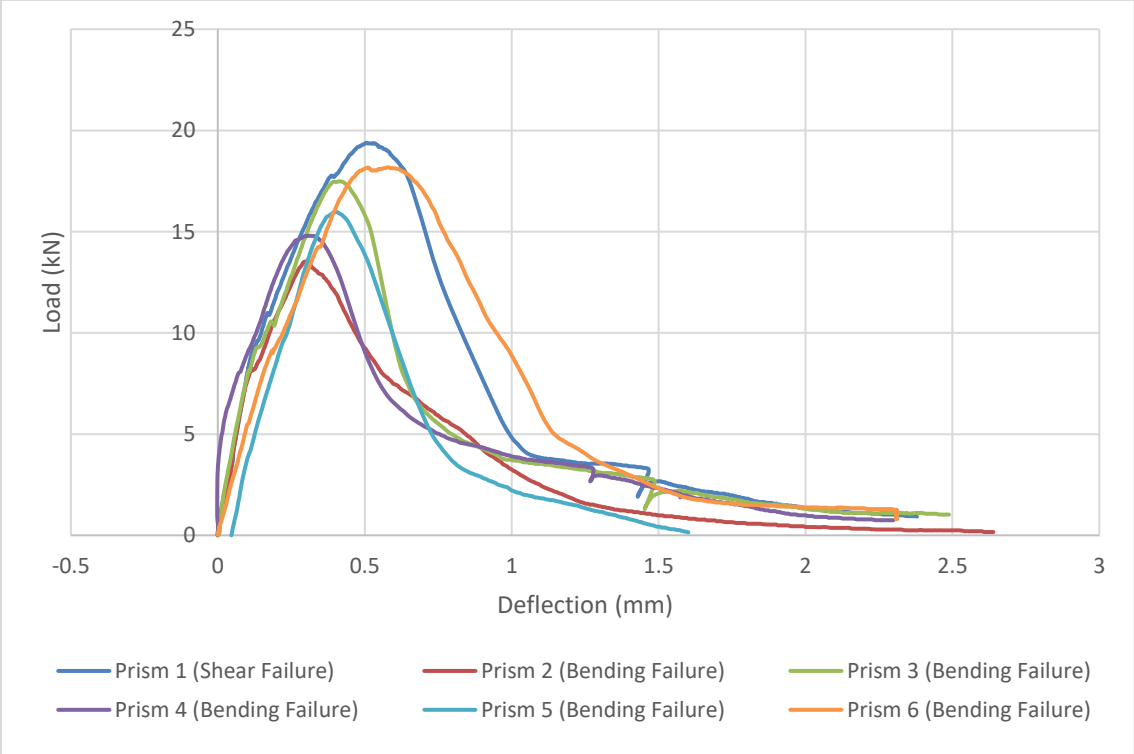

Figure 4-40: EDCC prism load-deflection plot (all samples)

Dog-bone direct tension tests were performed at the University of British Columbia (Soleimani-Dashtaki, Soleimani, Wang, Banthia, & Ventura, 2017). The EDCC specimens were prepared using the same mix design as that used in this research program. Figure 4-41

is a graph provided from those tests. It can be seen that at the lower strain rate which is similar to the tests performed at the University of Manitoba the peak tensile strength of EDCC appears to be approximately 3.7 MPa. This is much lower than the values determined through material testing in this research program and therefore will be used as a lower bound for calculation purposes.

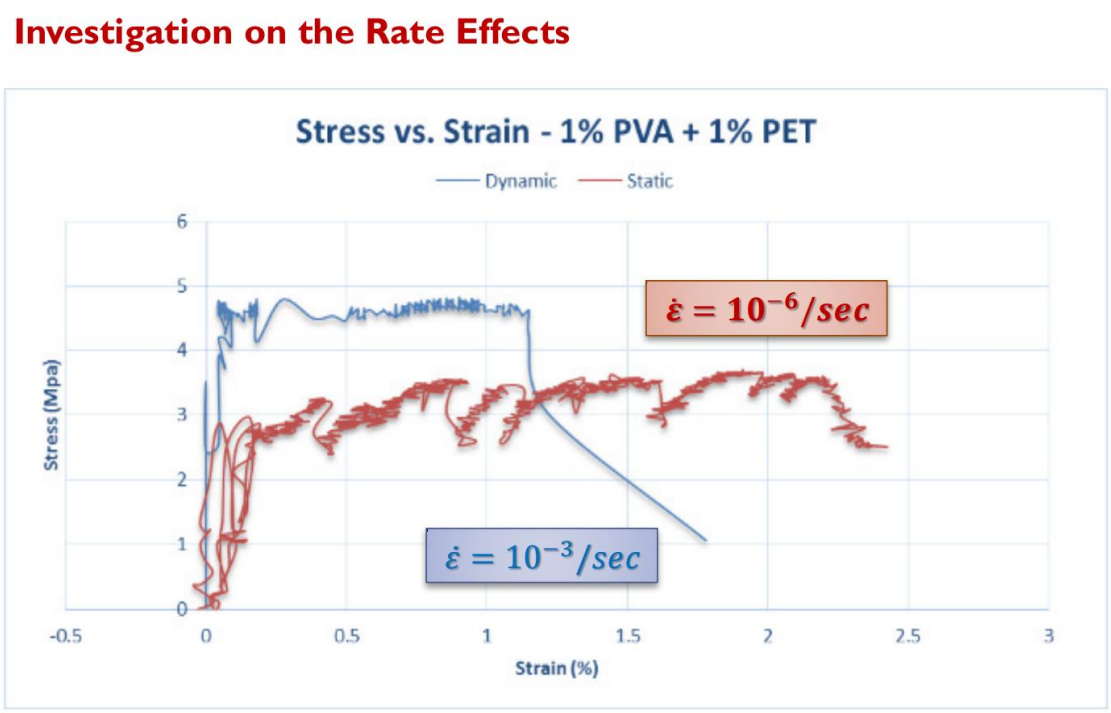

Figure 4-41: Direct tension dog-bone test on EDCC at University of British Columbia (Soleimani-Dashtaki, Soleimani, Wang, Banthia, & Ventura, 2017)

4.3.3 Bricks

Bricks were tested individually by saw-cutting the brick as seen in Figure 4-42. After saw-cutting, the brick was loaded in the cylinder testing machine which had a steel base plate and spherical head. The bricks were capped top and bottom using steel plates to help prevent stress concentrations due to non-planar surfaces, and to prevent damage to the testing equipment. The average ultimate stress recorded for the bricks was 62.8 MPa with

a standard deviation of 4.5 MPa, based on four tested specimens. A failed specimen can be seen in Figure 4-43.

Figure 4-42: Saw cut brick in test setup

Figure 4-43: Failed brick specimen

4.3.4 Concrete Blocks

A single concrete block was tested individually to determine the compressive strength. This was due to the number of specimens being constructed and that several blocks had to be discarded due to imperfections. Therefore, only the one block remained. The block was loaded in the same machine used for the prism compression tests and was capped top and

bottom with fiber board. No additional instrumentation apart from a load cell was used. The block was loaded at an average rate of 3.9 kN/s until failure, which can be seen in Figure 4-44. The ultimate stress recorded for this test was 22.7 MPa.

Figure 4-44: Failed CMU specimen

4.3.5 Sand

Sand gradation was done given that the NSERC CRD collaborators are using some local materials for their EDCC mixes. Figure 4-45 shows a comparison between the University of Manitoba sand and the University of British Columbia (UBC) sand used in (Yan, 2016). It is expected that as the fines increase in the sand gradation that the water demand will increase due to an increase in aggregate surface area. The mix design used in this research program was given by the researchers at UBC and was not changed to account for the

difference in sand gradation. A potential solution to future researchers is to modify the HRWRA dosage to account for the change in sand gradation, or to modify the sand gradation.

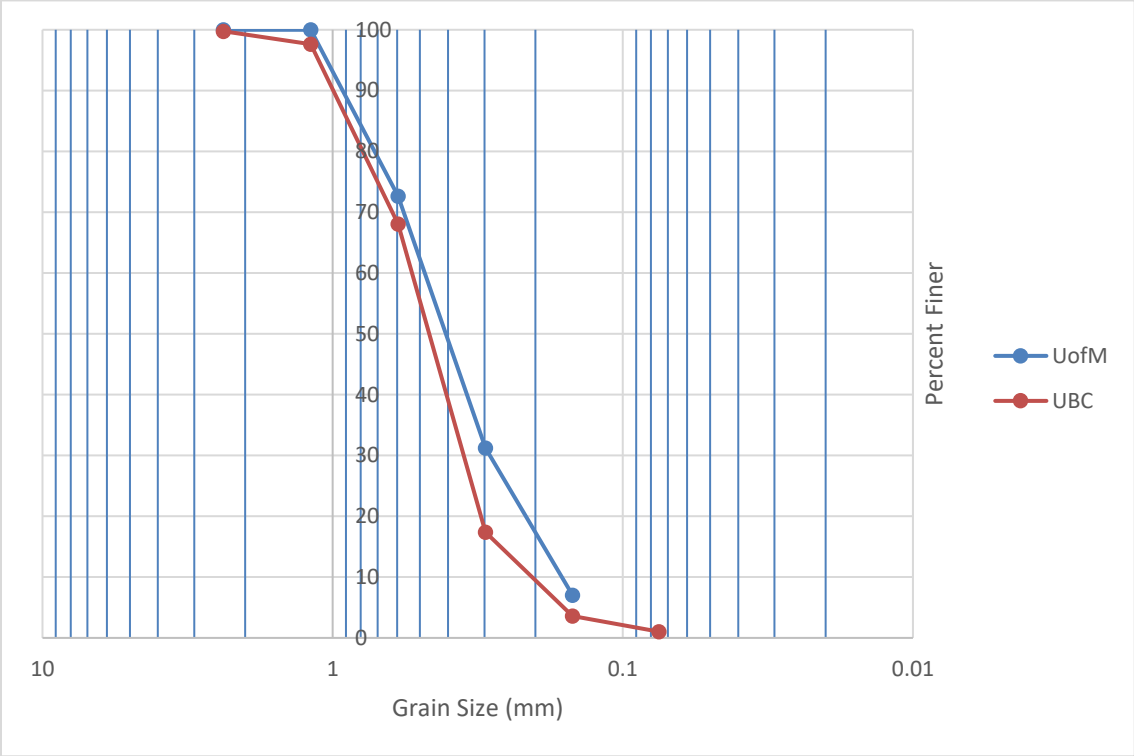

Figure 4-45: EDCC sand sieve gradation analysis

4.3.6 EDCC Cylinders

EDCC cylinders were tested to obtain their material properties. The EDCC cylinders were loaded in compression at a rate of 250 lbs/s (1.1 kN/s) as per ASTM C39/C39M – 14a; an example of which is shown in Figure 4-46. One 76 mm and two 102 mm diameter EDCC cylinders were instrumented with vertical and horizontal concrete strain gauges to capture strains up to failure, seen in Figure 4-47. A cylinder was instrumented with dial gauges to measure deformations during loading, as seen in Figure 4-48. Some of the EDCC cylinders were retained for split tensile loading, seen in Figure 4-49, which took place at a rate of 75 lbs/s (0.33 kN/s). The stress strain plots from the instrumented compression cylinders can

be seen in Figure 4-50, Figure 4-51, and Figure 4-52. The compression results of the cylinders can be seen in Table 4-7, and the results of the instrumented cylinders can be seen in Table 4-8. Split cylinder tension results are shown in Table 4-9. It was expected that due to the high fly ash content in the EDCC there would be additional strength gain from 28 to 56 days, although this was not evident in the results, apart from the gradual strength gain up to 120 days. The EDCC density was measured to be 1898 kg/m^3 with a standard deviation of 12.6 kg/m^3 by weighing three cylinders of known volume.

Figure 4-46: EDCC cylinder in typical compression setup

Figure 4-47: EDCC cylinder instrumented with strain gauges in large test setup

Figure 4-48: EDCC cylinder instrumented with dial gauges

Figure 4-49: EDCC split cylinder test

Table 4-7: EDCC cylinder compressive strength results

EDCC Cylinder Age	Number of Specimens	Strength (MPa)	Standard Deviation (MPa)
30	7	49.5	10.1
60	5	44.6	5.1
90	8	49.8	3.8
120	2	55.6	1.7

Table 4-8: Instrumented EDCC cylinder results

Cylinder	Stress (MPa)	E (MPa)	Poisson's Ratio	Age (days)	Diameter (in)
1	44.0	13623	0.18	28	3
2	71.4	19676	0.22	28	4
3	51.7	18770	0.22	28	4
Average	55.7	17356	0.21	28	-

Table 4-9: EDCC splitting tension cylinder results

Number of Specimens	Splitting Tensile Strength (MPa)	Standard Deviation (MPa)
4	6.71	0.80

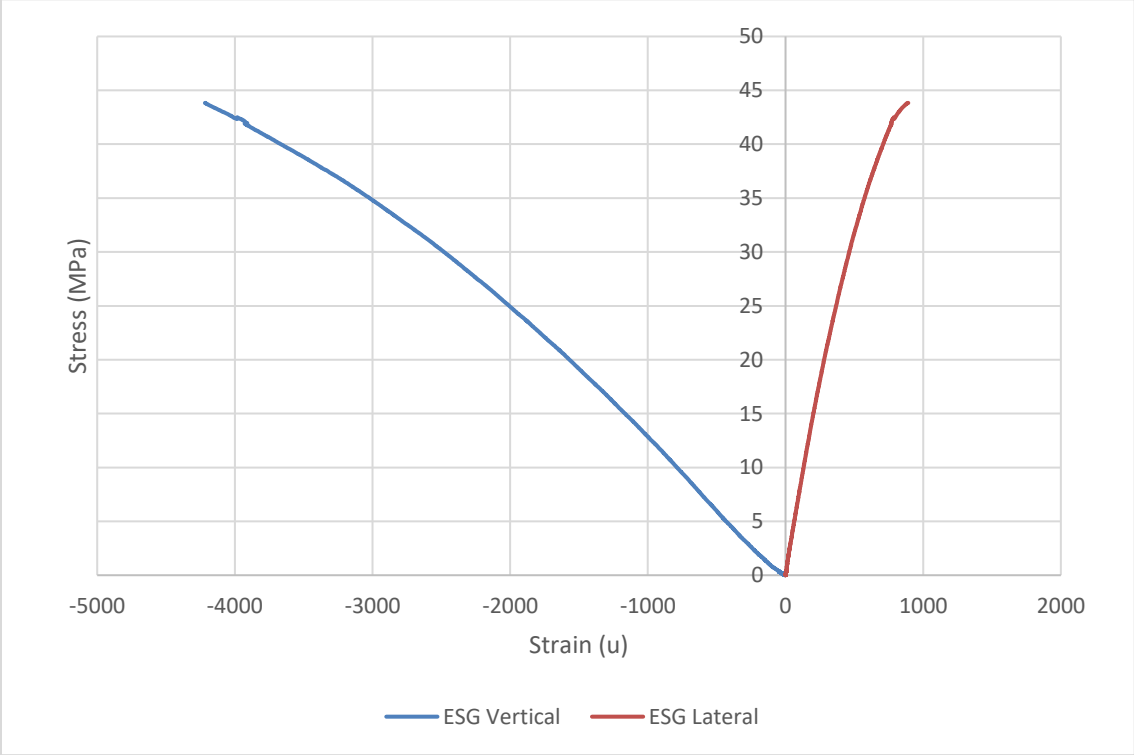

Figure 4-50: EDCC cylinder 1 stress-strain plot

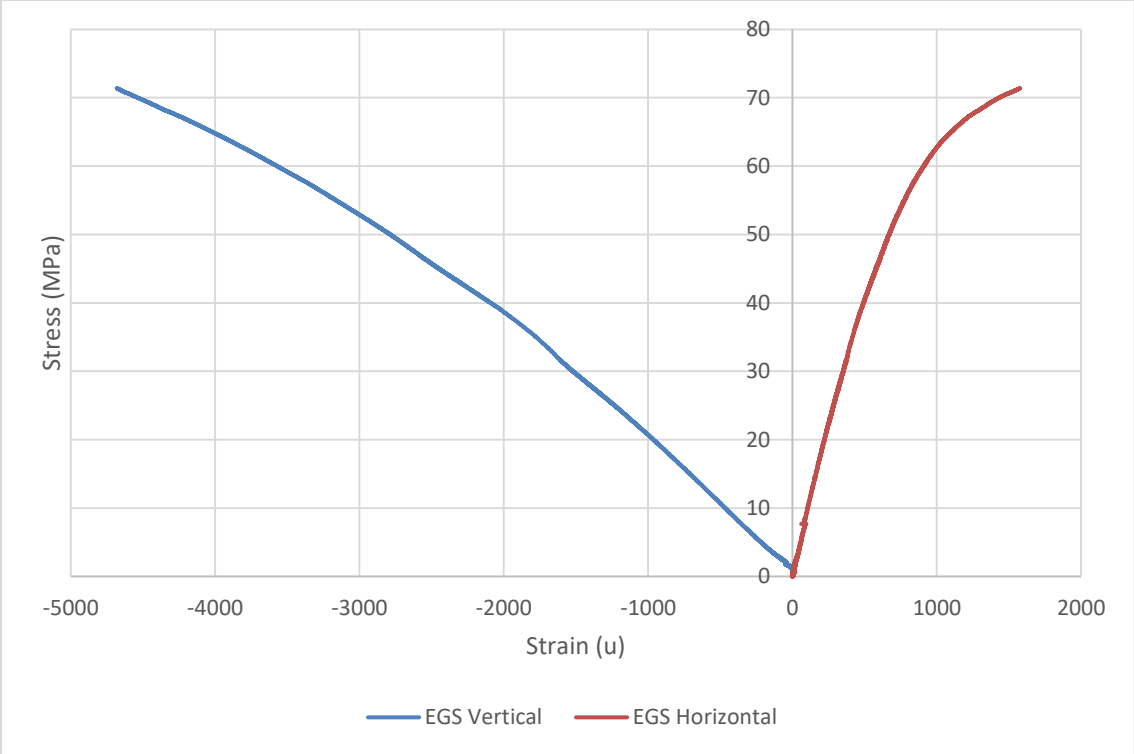

Figure 4-51: EDCC cylinder 2 stress-strain plot

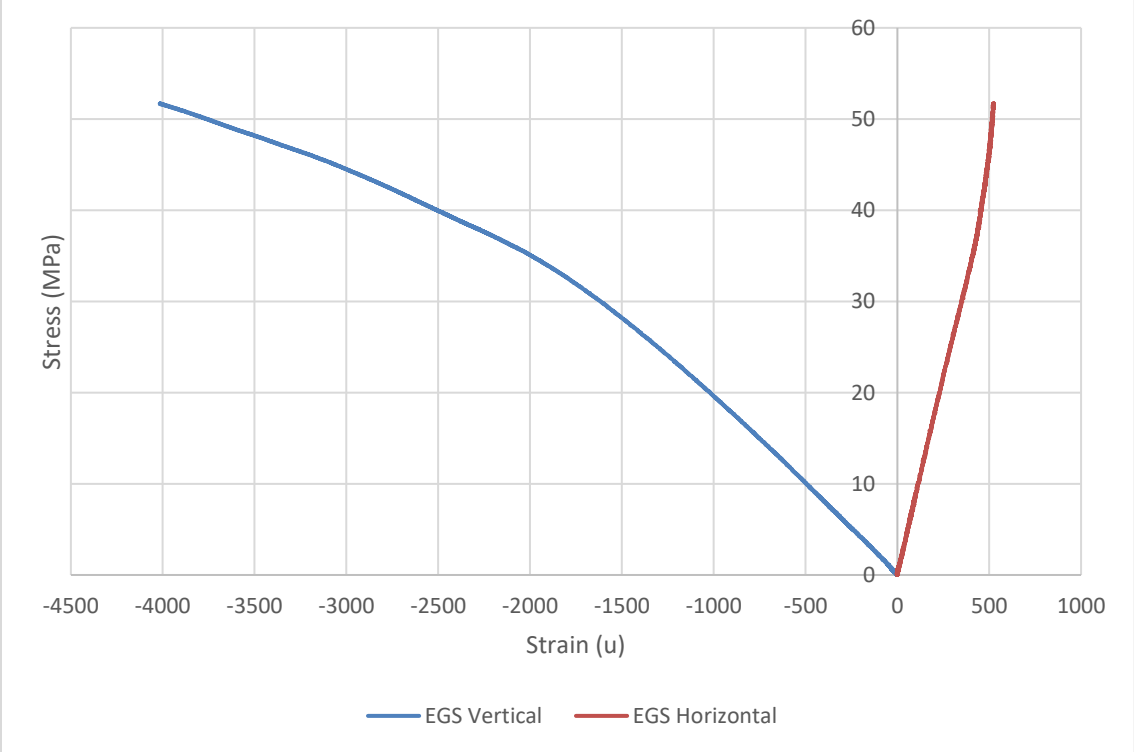

Figure 4-52: EDCC cylinder 3 stress-strain plot

5 Finite Element Modelling

Finite element modelling was carried out by a Dr. Basheer AlGohi using ABAQUS at the University of Manitoba, and the results are provided in the Appendix B: Finite Element Modelling of Flexural Tests section of the thesis. The author of this thesis did not perform the finite element modelling, therefore no information apart from the plotted software output and the experimental properties collected will be outlined. This work was deemed supplemental to the research, with the main focus of the research program focusing on quantifying experimental results as well as theoretical results using mechanics.

The following parameters were collected from the experimental work and used in the FEM program: Block compressive strength, mortar compressive strength, brick compressive strength, EDCC compressive strength, EDCC flexural strength, brick-mortar flexural bond strength, block-mortar flexural bond strength, EDCC modulus of elasticity, EDCC Poisson's ratio, EDCC split tension strength. The finite element modelling was done in such a way as to mimic the experimental setup. The model was done by modelling the masonry, the mortar, and the EDCC as discrete elements that interacted with one-another. Stress-strain curves from the various materials were used when available. For the flexural tests, the boundary conditions were set as pins and rollers to allow for rotation of the specimen during loading, which matched the test setup.

6 Data Analysis / Discussion

6.1 Compression Test Analysis

The compression tests indicated that the center of mass shifts in the strengthened specimens, resulting in flexural stresses being induced in the specimens during loading. This results in a drop in the maximum compressive stress achieved. Delamination was observed in the specimens at the time of failure through means of examining video recorded during testing as well as the bonded face of the masonry and the bonded face of the EDCC. Typically, little EDCC deposit was left on the face of the masonry aside from slight mortar deposits. It is likely that a weak interfacial layer formed between the EDCC and the masonry substrate resulting in delamination during loading. The pi gauges, which were measuring compressive strain on the face of the specimen, indicated that the EDCC face of the specimen went into tension during the initial loading, then began going into compression, this was paired with the opposite masonry face compressing rapidly until it began compressing at the normal rate until removal of the gauges. It is possible that these jumps in strain relative to load could be attributed to the specimen having shrinkage cracks at the location of the mortar joints. If this is the case, then by applying a compressive load to the specimen the mortar-masonry separation would close causing an inaccurate reading of strain. If the EDCC restrained the shrinkage crack from closing then the closing of the cracks on the other faces of the specimen would cause differential shortening in the specimen, possibly resulting in a tensile elongation being apparent in the EDCC face of the specimen. The use of strain gauges on certain specimens corroborated the results measured from the Pi gauges.

6.2 Flexural Test Analysis

It can be seen from the experimental work that the increase in strength as a function of EDCC thickness is effectively linear. The values plotted in Figure 6-1 have been corrected by subtracting the average strength of the unreinforced specimen from the strengthened specimens to remove the influence of the contribution of the masonry to the strength of the specimen. It is important to note that the slope of the lines show that there isn't a doubling of strength by doubling the thickness of EDCC. Rather, there appears to be a 76% strength gain for concrete beams strengthened with EDCC and a 68% strength gain for brick beams strengthened with EDCC.

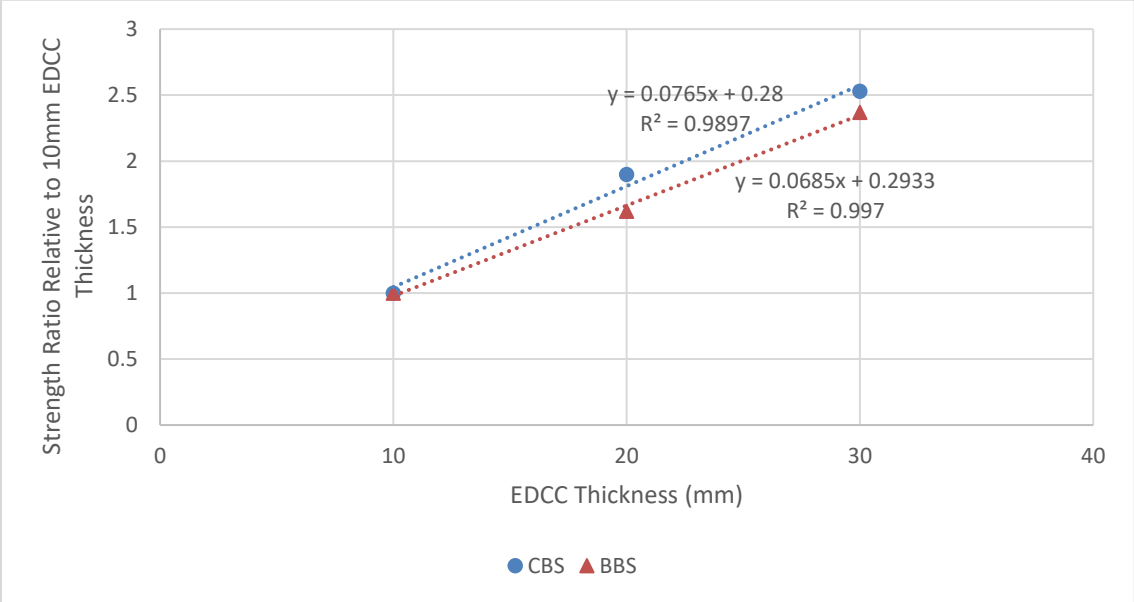

Figure 6-1: EDCC thickness vs strength ratio of strengthened masonry beams

Figure 6-2 and Figure 6-3 show a comparison between varying thicknesses of EDCC for a given masonry type. The trend appears to be that there is an increase in ultimate load carrying capacity, and subsequently a larger amount of energy dissipation, given that energy dissipation is related to the area measured under the load-deflection curve.

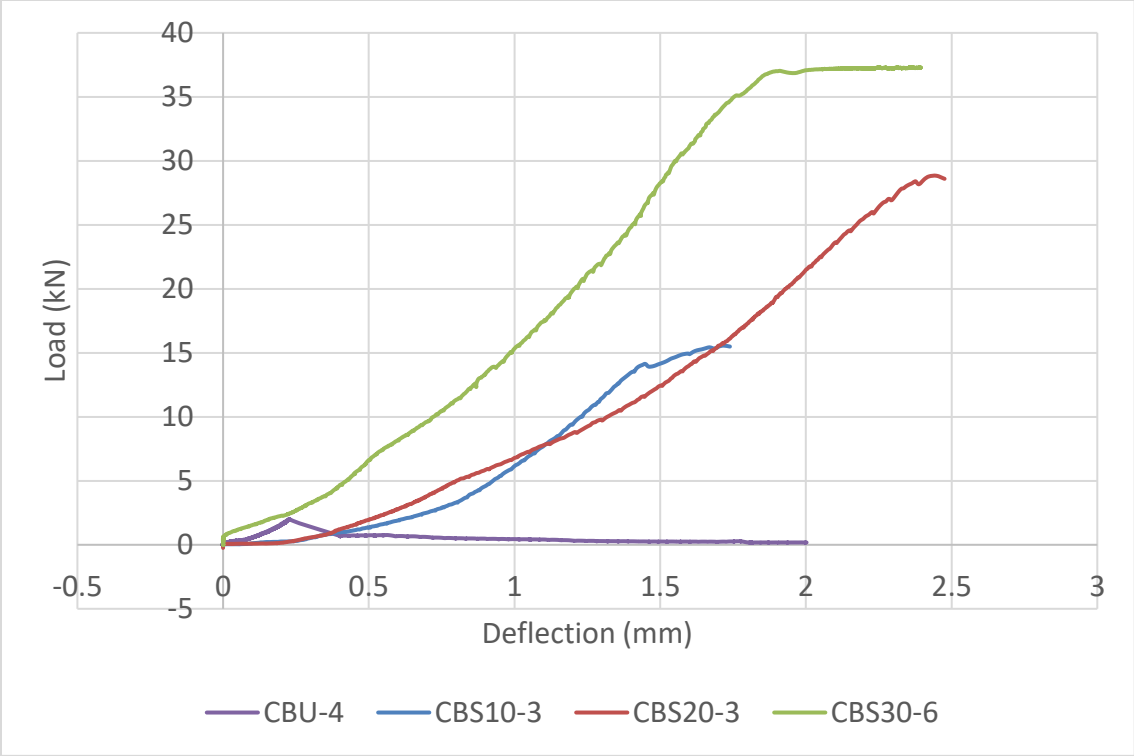

Figure 6-2: CMU load-deflection plot

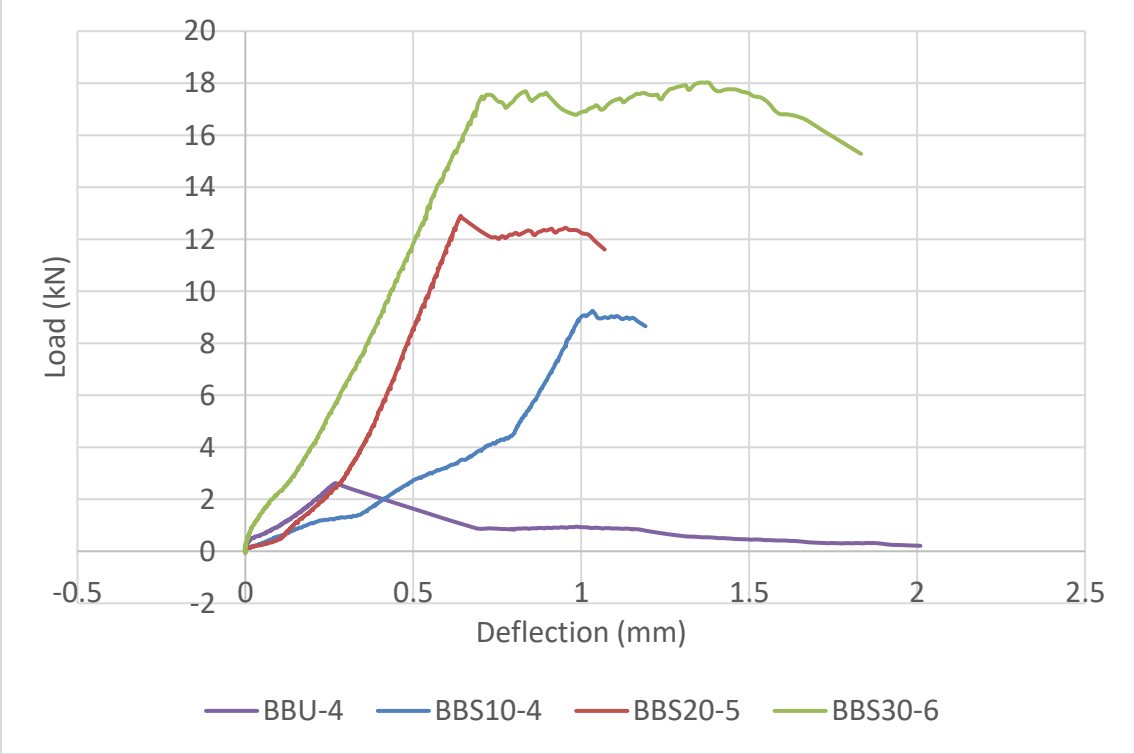

Figure 6-3: Brick load-deflection plot

7 Conclusion and Recommendation

This study observed the impact of engineered ductile cementitious composites (EDCC), which are a form of engineered cementitious composite (ECC) that utilizes supplementary cementitious materials that help reduce the environmental impact of the material, and how it impacts the strength of masonry prisms and beams in compression and flexure. Three different thicknesses of EDCC were tested, and plain specimens were tested to create a benchmark to measure improvements. By strengthening concrete block specimens, it appeared that a slight increase in load carrying capacity was achieved, although the ultimate stress was decreased (due to the increased cross-sectional area). The brick specimens appeared to have a decrease in ultimate load carrying capacity and ultimate stress. It is likely that the induced bending due to the restraining of one side of the specimen is the result of this. The increased number of mortar joints in the brick specimen likely caused a more observable decrease in ultimate stress versus the concrete block specimens.

The flexural performance of masonry strengthened with EDCC was quite high. The strengthened CMU showed an increase from 11 to 26 times that of plain CMU beams, while strengthened brick showed an increase from 4 to 8 times that of plain brick beams. The increase was dependent on thickness of EDCC, although doubling the thickness of EDCC did not double the strength. The strength increase was observed to be linear.

Various material properties were collected for plain bricks and concrete blocks, mortar cubes, EDCC cylinders and beams, and sand. By collecting these properties theoretical calculations as well as finite element modelling was able to be done to better understand the interaction and behaviour of the composite materials.

Overall, strengthening masonry with EDCC is a viable method to improve the performance of unreinforced masonry and poses many environmental benefits over traditional ECC strengthening options due to the reduction in cement required in the mix design.

Based on the research conducted the following recommendations for future works can be made. The mix design of the EDCC should be varied through a parametric study to find a balance between strength, stiffness, durability, bonding, and workability. It was found through this research that the workability of the current EDCC mix design was not desirable and required immediate placement after mixing, which may not be suitable for certain applications, such as situations requiring long transit times. Further research is being performed on seismic related applications for EDCC strengthened masonry by members of the NSERC CRD. Other structural materials may benefit from the strengthening applications of EDCC. Unreinforced concrete is a material that comes to mind. Evaluating the performance of materials strengthened with EDCC exposed to harsh chemical environments or variations in temperatures would be another area to investigate. It is likely that given the reduced permeability of EDCC relative to that of the porous masonry material that an external EDCC overlay would help prevent ingress of harmful chemicals. The performance in colder temperatures, specifically those in the freeze thaw range, would be of interest given that EDCC relies on bonding to the substrate material.

Given that delamination was observed in the compressive specimens, methods to improve the bonding of EDCC to its substrate should be explored. Site conditions may not be favourable, and the EDCC will likely need to be cast in a vertical orientation to existing structural members, therefore maintaining a cohesive material that allows for vertical surface application without sloughing while still bonding adequately to the substrate is

paramount. Strengthening specimens in a vertical orientation should be tested. Further investigation should also be done into the effects of strengthening only one side of a specimen, resulting in a singly symmetric specimen, as well as strengthening the compression face of a flexural specimen, given that load direction reversals typically occur in lateral loading.

References

ASTM International. (2010). *ASTM E518/E518M - 10 Standard Test Methods for Flexural Bond Strength of Masonry.* West Conshokocken: ASTM International.

BASF Canada Inc. (2016). *Safety Data Sheet - MasterLife SF 100.* Mississauga: BASF Canada Inc.

Canadian Commision on Building and Fire Codes, National Research Council of Canada. (2010). *National Building Code of Canada 2010 Volume 2.* Ottawa: National Research Council of Canada.

Canadian Standards Association. (2004). *CSA Standard S304.1-04 Design of masonry structures.* Mississauga: Canadian Standards Association.

Carnovale, D. J. (2013). *Behaviour and Analysis of Steel and Macro-Synthetic Fibre Reinforced Concrete Subjected to Reversed Cyclic Loading: A Pilot Investigation.* Toronto: University of Toronto.

Drysdale, R. G., & Hamid, A. A. (2005). *Masonry Structures Behaviour and Design Canadian Edition.* Ontario: Canada Masonry Design Centre.

Du, Y. (2016). *Durability performance of eco-friendly ductile cementitious composite (EDCC) as a repair material.* Vancouver: University of British Columbia.

Expocrete. (2012). *Concrete Masonry Products.* Saskatchewan: Expocrete.

Fonseca, F. S., & Ballard, J. R. (2013). Unbonded Capping of Masonry Prisms. *12th Canadian Masonry Symposium.* Vancouver.

Franklin, S., Lynch, J., & Abrams, D. (2001). *Performance of Rehabilitated URM Shear Walls: Flexural Behavior of Piers.* Urbana: Department of Civil Engineering, University of Illinois at Urbana-Champaign.

Kaheh, P. (2018). *Seismic Strengthening of Unreinforced Masonry Structures Using Eco-friendly Ductile Cementitious Composite Repair Material.* Calgary: University of Calgary.

Kaheh, P., & Shrive, N. (2016). Effects of eco-friendly ductile cementitious composites (EDCC) on dynamic characteristics of hollow concrete masonry walls. *Brick and Block Masonry - Trends, Innovations and Challenges* (pp. 2109-2116). Padova: Taylor & Francis Group.

Kaheh, P., & Shrive, N. (2016). Influence of eco-friendly ductile cementitious composites (EDCC) on in-plane behaviour of hollow concrete masonry walls. *Brick and Block Masonry – Trends, Innovations and Challenges* (pp. 2117-2125). Padova: Taylor & Francis Group.

Kanda, T., Saito, T., Sakata, N., & Hiraishi, M. (2003). Tensile and Anti-Spalling Properties of Direct Sprayed ECC. *Journal of Advanced Concrete Technology Vol. 1, No. 3; Japan Concrete Institute,* 269-282.

Kim, Y. Y., Kong, H.-J., & Li, V. C. (2003). Design of Engineered Cementitious Composite Suitable for Wet-Mixture Shotcreting. *ACI Materials Journal*, 511-518.

Kuraray Co Ltd. (2017, 11 11). *RECS15/RECS100L/RFS400.* Retrieved from Kuralon for non-asbestos products: http://kuralon-frc.kuraray.com/product-application/for-mortar/recs

Kyriakides, M. A. (2011). *Seismic Retrofit of Unreinforced Masonry Infills in Non-Ductile Reinforced Concrete Frames Using Engineered Cementitious Composites.* Stanford: Stanford University.

Lafarge North America Inc. (2009). *MSDS: Lafarge Fly Ash & Bottom Ash.* Reston: Lafarge North America Inc.

Lafarge North America Inc. (2014). *Lafarge Portland Cement (cement) - Safety Data Sheet.* Chicago: Lafarge North America Inc.

Li, V. C. (2003). On Engineered Cementitious Composites (ECC) A Review of the Material and Its Applications. *Journal of Advanced Concrete Technology - Japan Concrete Institute*, 215-230.

Li, V. C., & Kanda, T. (1998). Engineered Cementitious Composites for Structural Applications. *ASCE J. Materials in Civil Engineering. Vol 10, No. 2*, 66-69.

Li, V. C., & Wang, S. (2007). Engineered Cementitious Composites with High-Volume Fly Ash. *ACI Materials Journal*, 233-241.

Li, V. C., Fischer, G., & Lepech, M. D. (2009). *Shotcreting with ECC.* Lyngby: Spritzbeton-Tagung.

Li, V. C., Fukuyama, H., & Mikame, A. (1998). *Development of Ductile Engineered Cementitious Composite Elements for Seismic Structural Applications (T177-5).* Michigan: Elsevier Science Ltd.

Li, V. C., Lepech, M., Wang, S., Weimann, M., & Keoleian, G. (2004). *Development of Green Engineered Cementitious Composites for Sustainable Infrastructure Systems.* Beijing: International Workshop on Sustainable Development and Concrete Technology.

National Concrete Masonry Association. (1994). *Research Evaluation of the Flexural Tensile Strength of Concrete Masonry.* Herndon: National Concrete Masonry Association.

National Concrete Pavement Technology Center. (2014). *The Use of Ternary Mixtures in Concrete.* Washington: Federal Highway Administration - U.S. Department of Transportation.

Province of British Columbia. (2013, April). *Seismic Mitigation Program*. Retrieved May 17, 2013, from The Province of British Columbia: http://www.bced.gov.bc.ca/capitalplanning/seismic/

Reliance Industries Limited. (2017, 11 11). *Polyesters*. Retrieved from Reliance Industries Limited: http://www.ril.com/OurBusinesses/Petrochemicals/Polyesters.aspx

Soleimani-Dashtaki, S., Soleimani, S., Wang, Q., Banthia, N., & Ventura, C. E. (2017). Effect of high strain-rates on the tensile constitutive response of Ecofriendly Ductile Cementitious Composites (EDCC). *Proceedings of the 6th International Workshop on Performance, Protection & Strengthening of Structures under Extreme Loading* (pp. 93-104). Guangzhou (Canton): Procedia Engineering.

Soleimani-Dashtaki, S., Ventura, C. E., & Banthia, N. (2017). Seismic Strengthening of Unreinforced Masonry Walls using Sprayable Eco-Friendly Ductile Cementitious Composites (EDCC). *Proceedings of the 6th International Workshop on Performance, Protection & Strengthening of Structures under Extreme Loading* (pp. 154-164). Guangzhou (Canton): Procedia Engineering.

W.R. Grace & Co. (2011). *Material Safety Data Sheet - ADVA 195*. Cambridge: W.R. Grace & Co.

Wang, S., & Li, V. C. (2007). Engineered Cementitious Composites with High-Volume Fly Ash. *ACI Materials Journal*, 233-241.

Yan, Y. (2016). *Investigation into Bond Strength Between EDCC/Masonry*. Vancouver: University of British Columbia.

Zhou, J. (2011). *Performance of Engineered Cementitious Composites for Concrete Repairs*. Delft: Delft University of Technology.

Appendix A: Theoretical Analysis of Flexural Specimen

The following is a sample calculation of a 90mm CMU masonry beam strengthened with 20mm of EDCC:

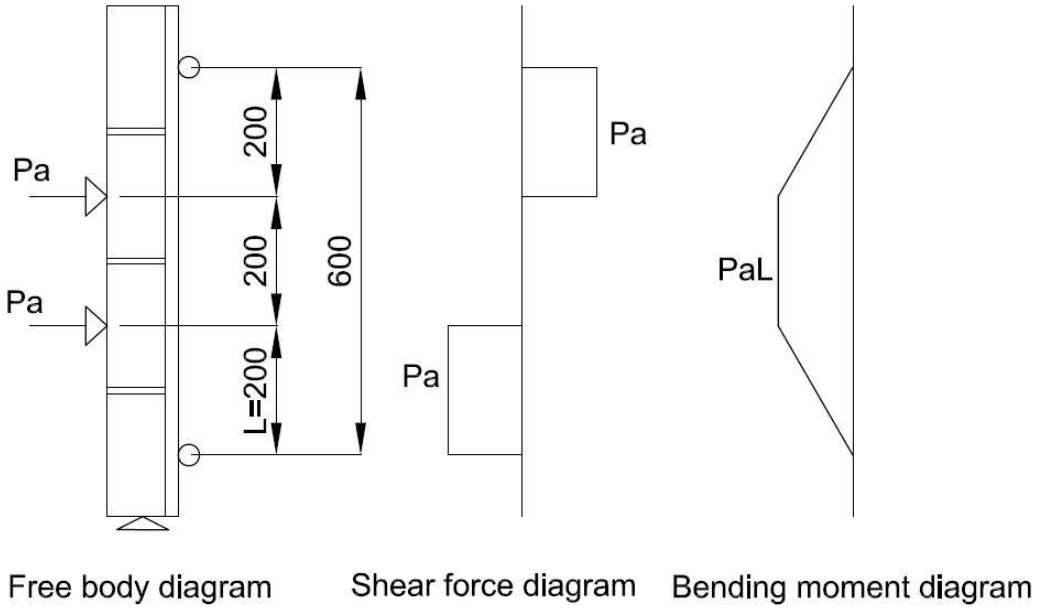

Figure A-1: Free body diagram, shear diagram, and bending moment diagram

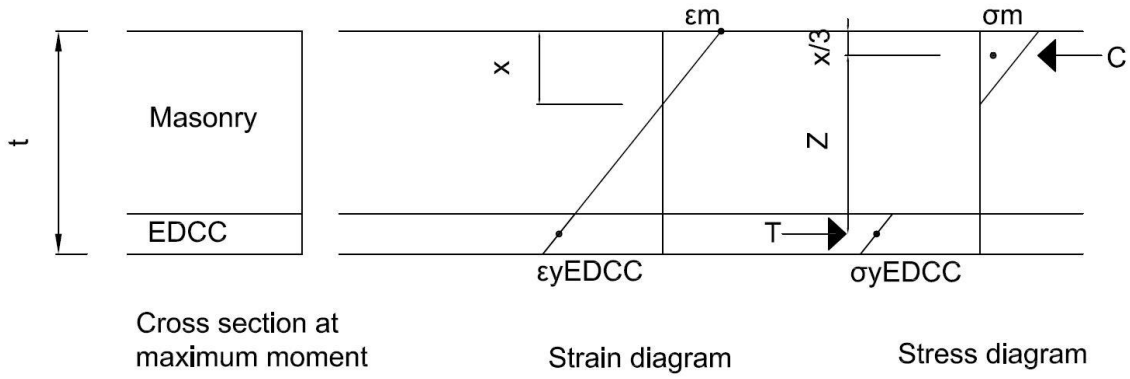

Figure A-2: Cross section of beam at mid-height in the maximum moment region

Note: Yielding strain has been taken at the center of the EDCC layer to simplify calculations. 100% composite action has been assumed between the EDCC layer and masonry.

σ_{mu} = Ultimate compressive strength of masonry (MPa)

σ_m = Stress in masonry at beam failure (MPa)

ε_m = Strain in masonry at failure

E_m = Modulus of elasticity of masonry (MPa)

σ_{yEDCC} = Stress in EDCC at failure (MPa)

Note: The yield and ultimate values for EDCC were similar therefore this value will be used interchangeably in the calculations.

ε_{yEDCC} = Strain in EDCC at yield

E_{EDCC} = Modulus of elasticity of EDCC

x = Distance from the extreme compression fiber to the neutral axis (mm)

t = thickness of beam (mm)

$t_{masonry}$ = thickness of masonry (mm)

t_{EDCC} = thickness of EDCC (mm)

b = width of beam (mm)

Note: It is assumed that the width of the masonry and EDCC are equal

Z = Moment arm (mm)

P_a = Applied third point loading (N)

P_t = Total applied load (N)

L = Third span length of beam (mm)

M_a = Applied moment to beam (N-mm)

M_r = Moment resistance of beam (N-mm)

C = Compression force in masonry (N)

T = Tension force in EDCC (N)

F = Force (N)

$$t = t_{masonry} + t_{EDCC}$$

$$\sigma_m = \varepsilon_m E_m$$

$$\sigma_{yEDCC} = \varepsilon_{yEDCC} E_{EDCC}$$

$$\varepsilon_{yEDCC} = \frac{\sigma_{yEDCC}}{E_{EDCC}}$$

$$C = \frac{\sigma_m x b}{2}$$

$$T = \sigma_{yEDCC} t_{EDCC} b$$

$$\sum F = 0 \quad therefore \quad T = C$$

$$\frac{\sigma_m x b}{2} = \sigma_{yEDCC} t_{EDCC} b$$

$$x = \frac{2\sigma_{yEDCC} t_{EDCC} b}{\sigma_m b} = \frac{2\sigma_{yEDCC} t_{EDCC}}{\sigma_m}$$

$$x = \frac{2\varepsilon_{yEDCC} E_{EDCC} t_{EDCC}}{\varepsilon_m E_m}$$

Using similar triangles from strain diagram:

$$\frac{\varepsilon_m}{x} = \frac{\varepsilon_{yEDCC}}{t - \frac{t_{EDCC}}{2} - x}$$

$$\varepsilon_m = \frac{\varepsilon_{yEDCC} x}{t - \frac{t_{EDCC}}{2} - x}$$

Substituting for x:

$$\varepsilon_m = \frac{\varepsilon_{yEDCC} \frac{2\varepsilon_{yEDCC} E_{EDCC} t_{EDCC}}{\varepsilon_m E_m}}{t - \frac{t_{EDCC}}{2} - \frac{2\varepsilon_{yEDCC} E_{EDCC} t_{EDCC}}{\varepsilon_m E_m}}$$

Note: It is assumed that at failure the masonry will still be in the linear elastic range. This can be verified by checking the strain in the masonry theoretically.

From the experimental tests:

$$\sigma_{mu} = 28.7\ MPa$$

$$E_m = 28386\ MPa$$

$$E_{EDCC} = 17356\ MPa$$

$$\sigma_{yEDCC} = 3.7\ MPa$$

$$b = 390\ mm\ for\ CMU, 193\ mm\ for\ brick, therefore:$$

$$b = 390\ mm$$

$$L = 200\ mm$$

Note: For brick σ_{mu} = 35.6 MPa and E_m = 18842 MPa

$$\varepsilon_{yEDCC} = \frac{3.7MPa}{17356\ MPa} = 2.13183x10^{-4}$$

$$t_{masonry} = 90\ mm\ for\ CMU, 92\ mm\ for\ brick, therefore:$$

$$t_{masonry} = 90\ mm$$

$$t_{EDCC} = Varies\ from\ 10\ mm, 20\ mm, and\ 30\ mm, therefore:$$

$$t_{EDCC} = 20\ mm$$

$$t = 90\ mm + 20\ mm = 110\ mm$$

$$\varepsilon_m = \frac{(2.13183x10^{-4})\dfrac{(2)(2.13183x10^{-4})(17356\ MPa)(20\ mm)}{\varepsilon_m(28386\ MPa)}}{110\ mm - \dfrac{20\ mm}{2} - \dfrac{(2)(2.13183x10^{-4})(17356\ MPa)(20\ mm)}{\varepsilon_m(28386\ MPa)}}$$

$$\varepsilon_m = 1.3467x10^{-4}$$

Note: The strain in masonry is well below the ultimate strain (assumed to be around 3000μ), therefore the assumption regarding the masonry being in the linear elastic range is correct

$$\sigma_m = 1.3467x10^{-4}(28386\ MPa) = 3.8227\ MPa$$

$$x = \frac{(2)(2.13183x10^{-4})(17356\ MPa)(20\ mm)}{(1.3467x10^{-4})(28386\ MPa)} = 38.716\ mm$$

$$M_a = P_a L$$

$$P_a = \frac{M_a}{L}$$

$$P_a = \frac{M_a}{L}$$

$$M_r = TZ$$

$$T = (3.7\ MPa)(20\ mm)(390\ mm) = 28860\ N$$

$$Z = t - \frac{t_{EDCC}}{2} - \frac{x}{3}$$

$$Z = 110mm - \frac{20\ mm}{2} - \frac{38.716\ mm}{3} = 87.095\ mm$$

$$M_r = (28860\ N)(87.095\ mm) = 2513561.7\ N - mm$$

Set $M_a = M_r$

$$P_a = \frac{2513561.7\ N - mm}{200\ mm} = 12568\ N$$

$$P_t = 2P_a$$

$$P_t = (2)(12568\ N) = 25136\ N$$

Therefore, the total applied load by the actuator to a 90mm CMU masonry beam strengthened with 20mm of EDCC would equal 25.1 kN.

Appendix B: Finite Element Modelling of Flexural Tests

Finite element analysis was performed at the University of Manitoba by Dr. Basheer AlGohi on the flexural specimens. The modelling was done using the ABAQUS structural analysis software suite. The individual material properties measured from the material experiments performed in this project were used as inputs for the finite element model. It can be seen through graphical comparison that there is some agreement between the finite element modelled specimens and the experimental results in terms of stiffness and ultimate strength. Comparing the amount of deformation that occurred under constant loading shows that there is some discrepancy between the modelling and the experimental work. It was observed in the experimental work that the amount of deformation was quite variable between specimens of the same type, therefore this discrepancy was expected. Each constituent material of the beam, including masonry, mortar, and EDCC, were modelled with their own individual material properties. The bond strength between masonry and mortar was calculated based on the plain masonry beams tested in flexure. The EDCC was assumed to have perfect bond to the masonry and mortar given the large surface area. During the testing little debonding was observed between the EDCC and the substrate materials. Having these finite element models allows for further simulation with varying material properties and dimensions to optimize the performance of strengthened masonry specimens.

Figure B-1 shows the idealization of the finite element model, given that the masonry, mortar, and EDCC were modelled as discrete elements. Figure B-2 to Figure B-7 show the comparison between the FEM results and the flexural experimental results. It can bee seen that there is some agreement between the FEM model and the experimental results with

respect to ultimate load capacity and stiffness. The experimental plots were terminated immediately after failure given the sudden crack propagation through the EDCC. This caused an overestimation of deflection given how the specimen deformed rapidly under little applied load. The rate at which the DAQ captured the displacement and load did not accurately depict the suddenness of the failure, and although the actuator was being run in displacement control the specimen's displacement at failure was larger than the designated displacement rate.

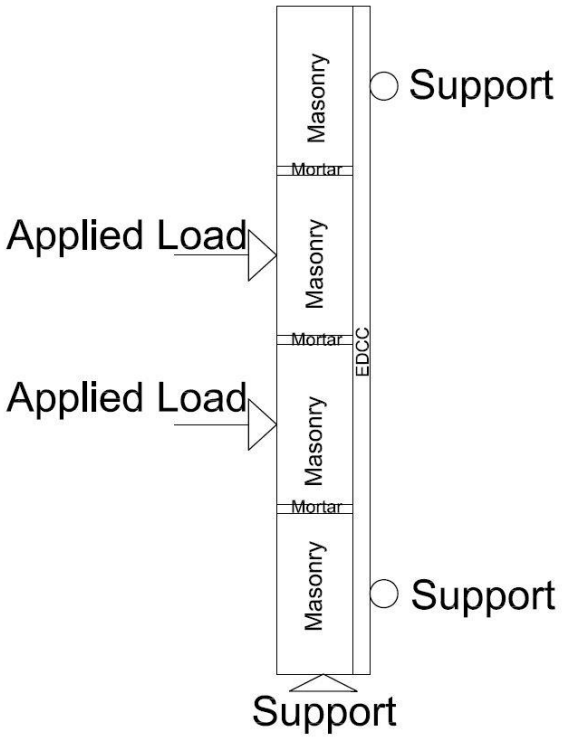

Figure B-1: Idealization of finite element model

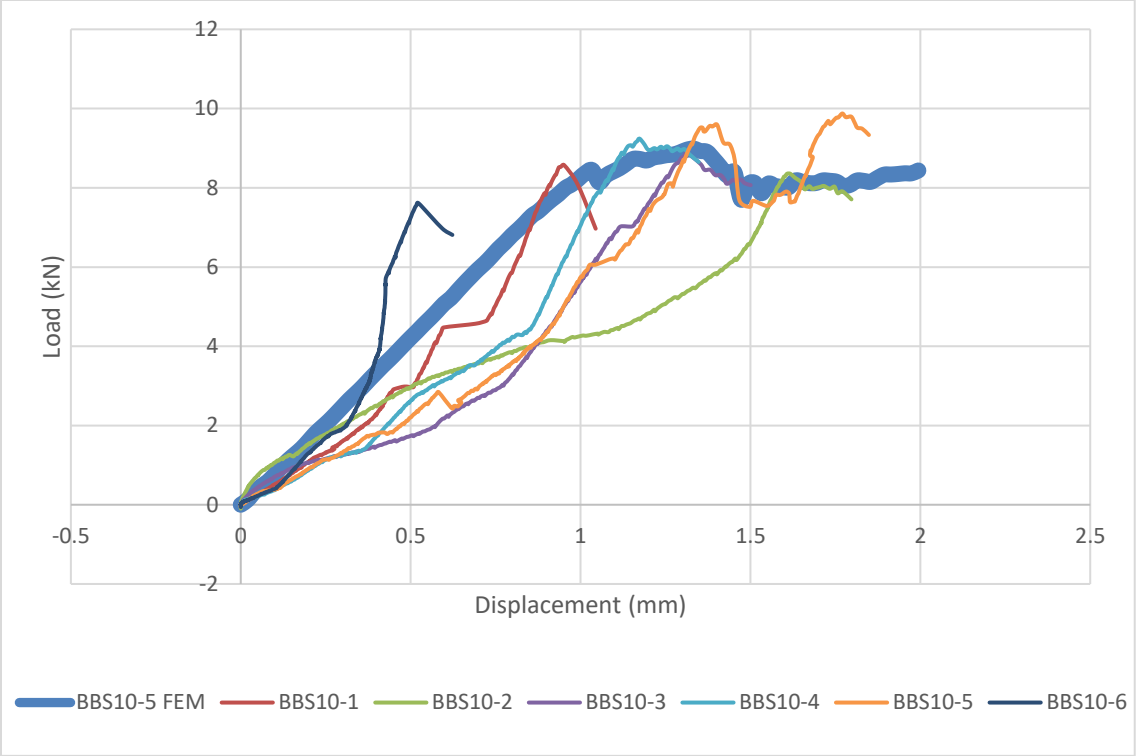

Figure B-2: BBS10 load-deflection plots with FEM results

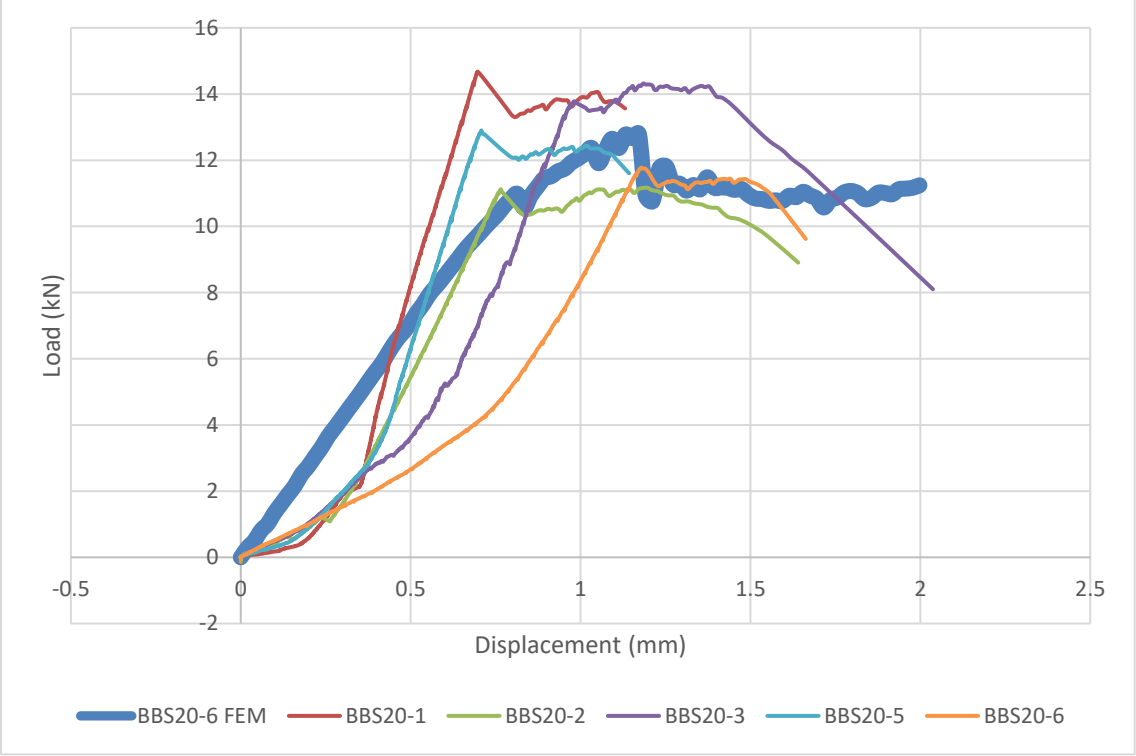

Figure B-3: BBS20 load-deflection plots with FEM results

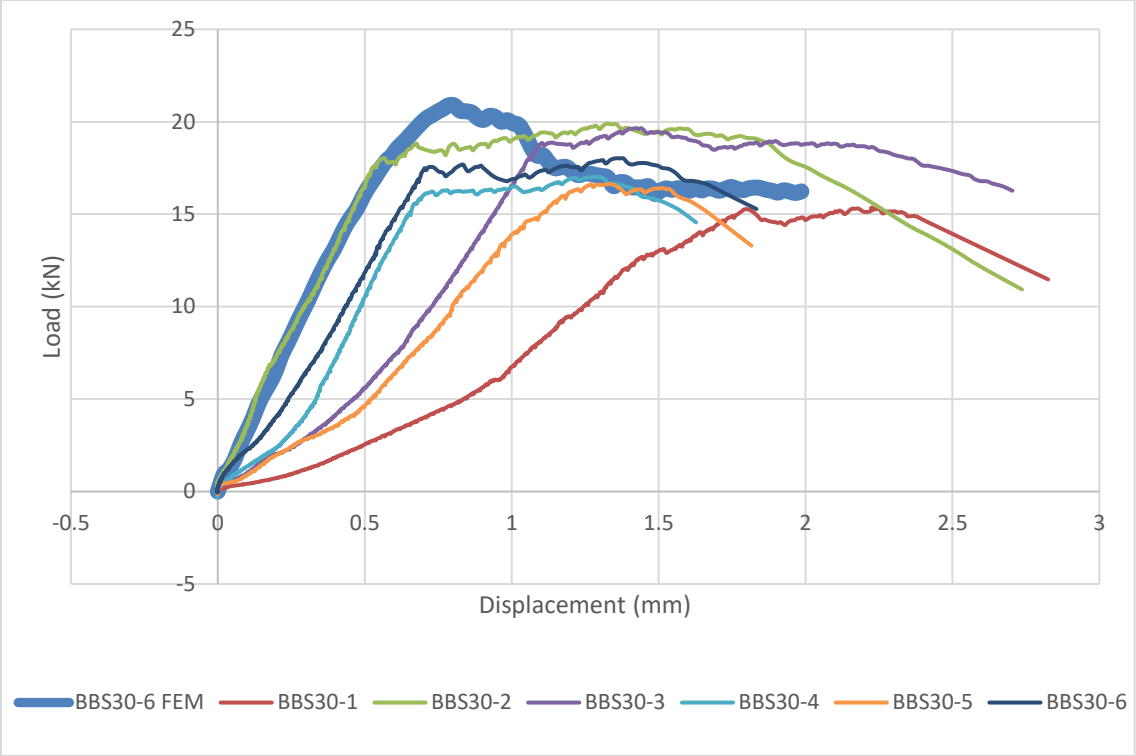

Figure B-4: BBS30 load-deflection plots with FEM results

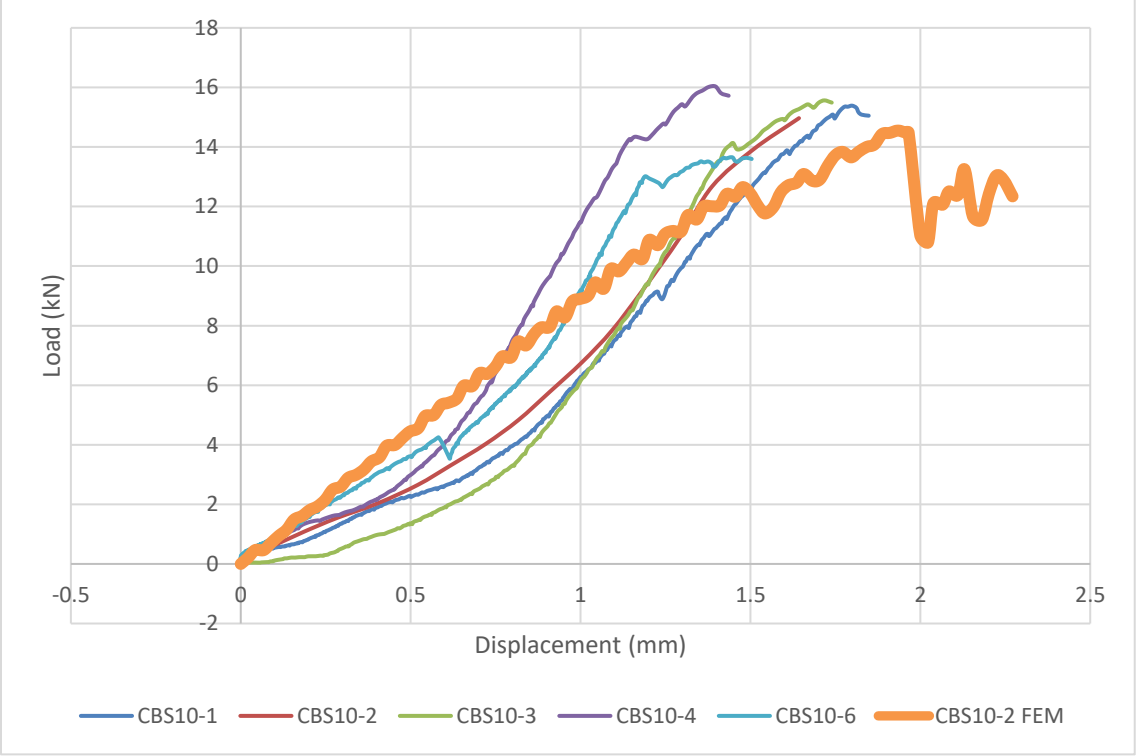

Figure B-5: CBS10 load-deflection plots with FEM results

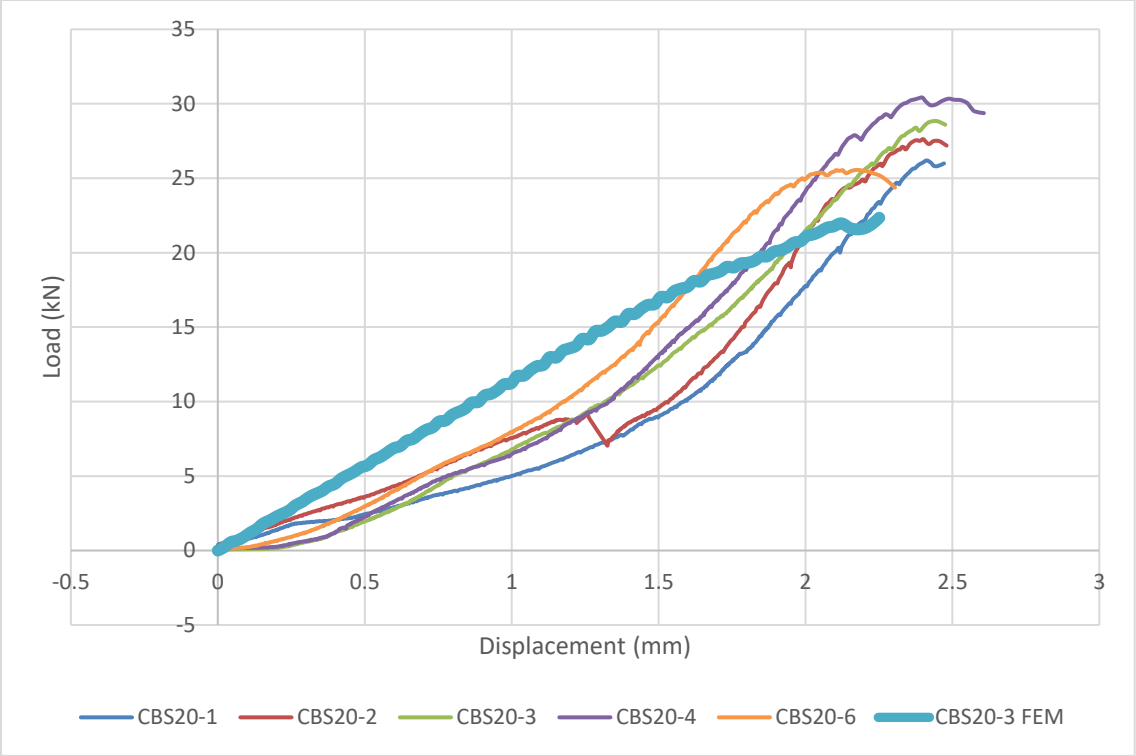

Figure B-6: CBS20 load-deflection plots with FEM results

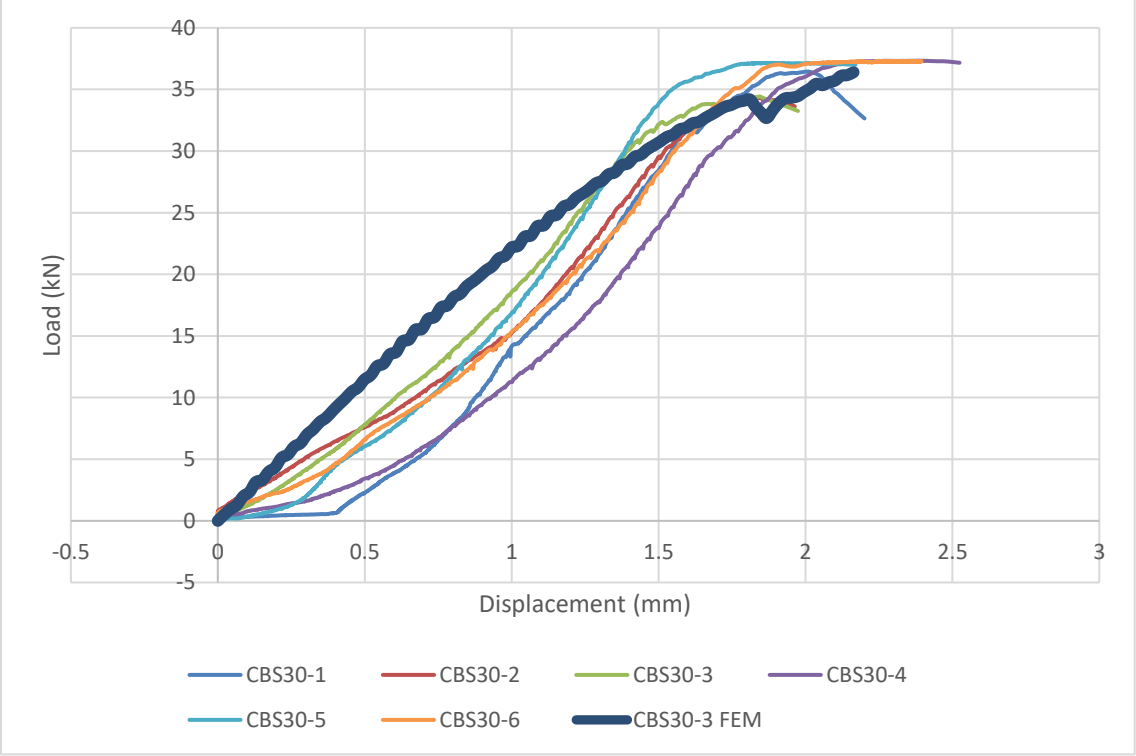

Figure B-7: CBS30 load-deflection plots with FEM results